VERY SMALL FIELD DOSIMETRY

Paul Henry Charles

B.App.Sc(Physics, QUT), M.App.Sc(Medical Physics, QUT)

Submitted in fulfilment of the requirements for the degree of

Doctor of Philosophy

(By publications)

School of Chemistry, Physics and Mechanical Engineering

Science and Engineering Faculty

Queensland University of Technology

2014

Keywords

Radiation oncology, medical physics, dosimetry, diode, Monte Carlo, small field dosimetry, very small field, disequilibrium dosimetry, air gaps, correction-less, correction-free.

Abstract

Advances in the precision of radiotherapy treatments have allowed the treatment of smaller tumour volumes to be more commonplace. However the treatment of small volumes necessitates the use of small radiation fields. A “small field” is generally defined as a field with lateral dimensions smaller than the lateral range of the electrons that contribute to dose. Under these conditions of lateral electronic disequilibrium, the measurement of dose to water becomes difficult. A primary reason is that most radiotherapy detectors are made of non-water equivalent material. This differing density exacerbates the effects of electronic disequilibrium by exaggerating it (density of detector less than water) or by undesirably compensating for it (density of detector greater than water).

The aim of this research was to investigate small fields, understand the physics behind them in a detailed manner, and improve on the accuracy of small field dosimetry. The concept of reporting the measured dosimetric field size for each small field output factor measurement (as opposed to reporting the nominal field size) was investigated to see if inter-machine consistency could be improved. The field size at which the dosimetric field size was required for accurate output factor measurements was quantified by introducing the concept of a “very small field”. The physics behind very small field dosimetry was investigated in detail, leading to a quantifiable theoretical definition of a very small field. The perturbations of non-water equivalent materials in very small fields were studied in detail, with a particular focus on air - which may be found intrinsic to certain detectors; as an imperfection in a solid phantom; or as a bubble lodged onto a detector in water. The subsequent detailed

understanding of these air perturbations led to the simulation based design of a new diode detector which, uniquely, responded the same in very small fields as in standard fields. These detectors were then physically constructed and tested to be accurate; and general recommendations for detector design for very small field dosimetry were established.

Using the dosimetric field to report small field output factor measurements significantly reduced the inter-machine variation of measured output factors (by up to 12 % for a 5 mm field size). It was found that measuring the effective field size was required for field sizes 15 mm or smaller to ensure output factors were consistent to within ±1 %. This formed the practical definition of a very small field. A detailed simulation analysis showed that electronic disequilibrium was the main reason for the large change in output factor as a function of field size. Electronic disequilibrium caused a significant change in dose below a field size of 12 mm (for a 6 MV photon beam). This was the theoretical definition of a very small field.

It was confirmed that very small amounts of air (up to 2 mm) did not perturb the radiation beam at normal field sizes, but did so at very small field sizes; with the size of perturbation increasing with decreasing field size. The introduction of air into the design of a diode successfully produced a detector that responded equivalent to water for output factors in very small fields. This was due to the under-response of the air cancelling out the over-response of the silicon in the diode at all field sizes. The experimental construction of the "correction-free" diode was successful and was the first diode detector in the world that did not require corrections for very small field output factors.

Table of Contents

Acknowledgements

I would like to thank my family – my wife Jacqueline and my daughters Emma and Elizabeth – for allowing me to embark on this PhD full time, when the more conservative option would have been to remain in full time employment. I am very grateful for this and all the support and encouragement that I received throughout the past 3 years.

I would like to thank my supervisor team who have always been extremely liberal and amazingly timely with their help and advice – no matter the magnitude of the advice requested.

I would also like to thank Gavin-Cranmer Sargison (Saskatchewan Cancer Agency, Saskatoon, Canada) and David Thwaites (University of Sydney) for a very successful collaboration, formed during this PhD.

Supervisory team

Dr Jamie Trapp (Primary)

Dr Scott Crowe

A/Prof Tanya Kairn

Prof Christian Langton

List of publications

G Cranmer-Sargison, **PH Charles**, JV Trapp and DI Thwaites (2013), A methodological approach to reporting corrected small field relative outputs. *Radiother. Oncol.* **109,** 350-355

PH Charles, G Cranmer-Sargison, DI Thwaites, SB Crowe, T Kairn, R Knight, J Kenny, C Langton and JV Trapp (2014), A practical and theoretical definition of very small field size for radiotherapy output factor measurements. *Med. Phys.* **41** (4), 041707

PH Charles, SB Crowe, T Kairn, J Kenny, J Lye, L Dunn, B Hill, R Knight, C Langton and JV Trapp (2012), The effect of very small air gaps on small field dosimetry, *Phys. Med. Biol.* **57** (21), 6947-6960

PH Charles, SB Crowe, T Kairn, R Knight, B Hill, J Kenny, C Langton and JV Trapp (2013), Monte Carlo-based diode design for correction-less small field dosimetry, *Phys. Med. Biol.* **58** (13), 4501-4512

PH Charles, SB Crowe, T Kairn, R Knight, B Hill, J Kenny, C Langton and JV Trapp (2013), The influence of Monte Carlo source parameters on detector design and dose perturbation in small field dosimetry, *J. Phys. Conf. Sers.* **489**, 012006

PH Charles, G Cranmer-Sargison, DI Thwaites, T Kairn, SB Crowe, G Pedrazinni, T Aland, J Kenny, C Langton and JV Trapp (2014), Design and experimental testing of correction-free diodes for small field dosimetry, *Med. Phys.* (accepted for publication**)**

List of Figures

List of Tables

Statement of Original Authorship

The work contained in this thesis has not been previously submitted to meet requirements for an award at this or any other higher education institution. To the best of my knowledge and belief, the thesis contains no material previously published or written by another person except where due reference is made.

Signature: QUT Verified Signature

Date: November 2014

Chapter 1: Introduction

1.1 RADIATION THERAPY

Radiotherapy is the medical use of ionising radiation to treat cancer [1]. The same radiation however not only harms cancerous tissue, but will also cause damage to healthy tissue. Therefore the radiation beam needs to be precisely targeted to maximise the dose to the cancer, and minimise the dose to surrounding healthy tissue [2]. The radiation dose delivered to both the cancer and the healthy tissue also needs to be measured accurately, to ensure that the dose that is delivered to the patient is the dose that is intended. Failure to do so will result in the patient receiving a radiation dose different to that prescribed. If the cancer was to receive less dose than prescribed, then tumour control would be compromised and the treatment may not be effective in removing the cancerous tissue. If nearby healthy tissues, including vital organs, receive more dose then prescribed, then the patient may have radiation induced complications. Thus, the accuracy of dose delivery becomes a vital part of radiotherapy treatments [3, 4].

1.1.1 X-ray interactions within a patient

A common source of ionising radiation for radiotherapy are X-rays from a medical linear accelerator [5]. Electrons produced from an electron gun are accelerated along a waveguide. Upon exiting the waveguide, the electrons are focused by bending magnets onto a high density tungsten target. The electrons interact in the target and produce Bremmstrahlung X-rays. It is these X-rays that form a radiotherapy X-ray beam. The peak energy of these X-rays is in the megavoltage energy range.

Megavoltage energy photons that are used in radiotherapy will interact with a patient's tissue predominantly by Compton interactions [1]. This occurs when a photon strikes an orbital electron with energy much greater than the binding energy of that electron, causing it to be ejected from the atom. The ejected electron is so highly energised that it will travel of the order of centimetres through the tissue before losing all of its energy. Along its path, the electron deposits its energy via ionisation and excitation of other orbital electrons. It is these reactions that contribute to the absorbed dose (energy deposited per unit mass) to the patient. In other words, although the incident particles are photons, it's actually electrons that deposit the absorbed dose and hence need to be measured. These electrons can kill tissue cells by direct or indirect interactions with the molecules in the DNA [6]. Direct interactions are when DNA molecules are directly ionised by the electrons produced by the radiation beam. In indirect interactions the electrons ionise molecules within the tissue (e.g. water) which produce free radicals. These free radicals are highly reactive and can subsequently interact with DNA molecules causing cell death.

1.1.2 Measuring X-ray dose

The dose delivered by a linear accelerator (J / kg or "Gray" (Gy)) is calibrated by a process called absolute dosimetry [7]. This is performed using a gas based ionisation chamber submerged in a water tank. The water is representative of a patient's tissue (which is predominantly water). The radiation causes ionisation (electrons removed from atoms) in the gas cavity of the ionisation chamber; the ionisation charge can then be collected and measured as a small current. This can be related to the absorbed dose at the detector.

Calibration dosimetry is usually performed under a single set of conditions (e.g. the radiation field is a 10 cm x 10 cm square, the depth in water is 10 cm, the distance from the X-ray target to the detector is 100 cm). One method of obtaining dose under alternative condition is 'relative dosimetry'. Relative dosimetry is simply the dose measured under certain conditions relative to the dose measured under the conditions of a reference set of conditions. One example of this is 'output factors', where the field size is changed, but all other conditions remain constant. The dose measured in one field size is normalised to the dose from the reference field size (e.g. a 10 cm x 10 cm square). The output factor (and other relative dosimetry factors) are applied to the absolute dose calibration value to obtain the dose to a patient under the patient specific conditions.

1.1.3 Bragg-Gray cavity theory

Absolute dosimetry of megavoltage photon beams using an ionisation chamber is possible with the use of the Bragg-Gray cavity theory [7-11]. The theory states that the dose to water can be calculated by measuring the dose to a small cavity of gas within the water and multiplying this value by the mass stopping power ratio of water to the gas. Bragg-Gray cavity theory only works if the following conditions are satisfied: the range of the dose depositing electrons must be much greater than the cavity dimensions, charged particle equilibrium must exist, and the detector must not perturb the fluence of the dose depositing electrons.

Under standard measurement conditions for absolute dosimetry [7], the first two conditions mentioned above will be satisfied. However a gas cavity will always have a small effect on the beam fluence. This effect must be taken into account by way of

a correction factor. Also, an ionisation chamber is not pure gas, but rather consists of a central electrode and an outer wall etc. These facts are also taken into account by applying additional correction factors [7]. For relative dosimetry to be performed as a simple measurement ratio, all the Bragg-Gray cavity theory conditions and correction factors mentioned above must be identical in both the reference field size and the test field size.

1.1.4 Monte Carlo modelling of X-ray beams

Monte Carlo modelling is the use of statistical sampling to approximate the outcome of probabilistic events [12]. It is used for radiation transport to simulate the many interactions that can take place between the radiation and matter. In X-ray dosimetry, Monte Carlo modelling can be used as a highly accurate surrogate in situations where physical measurements are not possible [13].

In radiation physics there are many possible interactions which depend on, for example, the particle type, particle energy and the atomic composition of the material it interacts with. Furthermore the results of these interactions are not necessarily discrete, for example the energy imparted to an electron, and the resultant scatter angle of the photon following a Compton interaction are defined by probability distributions, rather than a discrete equation. Given the above, and the multitude of interactions possible within a linear accelerator treatment head, and then within the patient or phantom, it is apparent that a simple solution for defining the dose deposited is not possible. Monte Carlo modelling provides a solution by using random numbers to sample probability distributions of each radiation interaction of a

particle on step-by-step basis. Once an extremely large number particles (sometimes > 1 billion) have been simulated, an overall representation of the radiation beam is "built up". The statistical uncertainty often stated alongside Monte Carlo simulation results usually refers to the overall sampling uncertainty of distributions in the beam model. The statistical uncertainty is proportional to the square root of the number of particles simulated. The more particles that are used, the more closely the Monte Carlo simulation converges on the true mean of an infinitely long simulation of the statistical models used (and hence will closely match the true radiation beam, if hypothetically, modelled perfectly).

1.2 SMALL FIELD DOSIMETRY

1.2.1 Stereotactic radiation therapy

Stereotactic radiation therapy (SRT) is a specialised form of X-ray radiation therapy that in some cases uses very small fields (sometimes < 1 cm^2) to precisely target small tumours [14]. Traditionally this has been performed for brain tumours, but with the evolution of in-treatment-room imaging systems, and patient motion management, stereotactic body radiation therapy (SBRT) is becoming more popular for sites such as the lung [15]. Calculating the dose delivered by the small fields that some patients receives from SRT is much more complicated than standard treatments, and is generally referred to as "small field dosimetry". Small field dosimetry is also important for intensity modulated treatments that use small segments.

1.2.2 Background and problems

A "small field" is generally defined as a field with dimensions smaller than the lateral range of the electrons that contribute to dose [16]. Field sizes below approximately 3 x 3 cm^2 are considered to be small fields in megavoltage photon dosimetry. Below these field sizes the conditions above begin to breakdown [17]. There are three main causes for this breakdown: 1 - Lateral charged particle equilibrium is lost because the size of the field becomes small compared to the range of the dose depositing electrons. 2 – The finite size of the x-ray source means that it becomes relatively large compared to the field size. The result is that small fields have a very large percentage of the field made up by penumbra, making volume averaging within the detector problematic. 3 – The finite size of the detector means that the perturbation of the radiation field by the detector becomes larger as the field size decreases.

Due to the relatively large size of the collecting volume of an ionisation chamber, accurately measuring output factors of sub-centimetre fields is difficult. Diodes provide a good alternative for relative dosimetry because of the very small collecting volume they possess (<0.1 mm^3). However, at very small fields sizes diodes are even limited by perturbation correction factor changes due to the relatively dense collecting medium (Silicon) [18].

The presence of a low density material such as lung or air exacerbates the problem of electronic disequilibrium in small fields as the secondary charged particles can travel even further in these media. Even in larger fields air gaps have been shown to cause a dose reduction in megavoltage dosimetry immediately downstream, which will then

build back up as electronic equilibrium is re-established [19-24]. These studies have concluded that the magnitude of the dose reduction is enhanced by increasing the beam energy, increasing the air gap size, or decreasing the field size.

Incorrect measurement of profiles or output factors will result in incorrect data being entered into the planning system. This could result in mistreatment of patients. Das et al [17] and Taylor et al [25] have excellent summaries of the issues involved in small field dosimetry.

1.2.3 IAEA / AAPM formalism for reference dosimetry of small and nonstandard fields

In 2008 the International Atomic Energy Agency (IAEA) in conjunction with the American Association of Physicists in Medicine (AAPM) released a letter proposing a new formalism for reference dosimetry of small and nonstandard fields [16]. Very briefly, an additional sensitivity of detector factor is applied to the standard dosimetry protocol [7] to account for either: 1 - If a beam is not able to make a standard (10 x 10 cm^2) field size (e.g. CyberKnife). Or 2 - The fact that many intensity modulated beams are delivered differently to a standard reference beam. That is, by way of many beamlets, which when combined might deliver a uniform dose, but separately may not have lateral equilibrium at any stage. Furthermore, an additional sensitivity correction factor may be required for specific non-reference fields. This is certainly the case for very small fields.

1.2.4 Improving the accuracy of small field dosimetry

The response of detectors that are used for small field measurements can vary with small field size [16, 26]. The observed changes in sensitivity can be due to volume averaging [27, 28], or the physical density of the detector active volume being different to that of the phantom material [27, 29, 30]. Other components that make up the detector may also heavily perturb the particle fluence in small fields [28, 31-35]. For example, some diodes contain other high density media which causes an increase in measured signal due to artificial offset of electronic disequilibrium in small fields [33]. Therefore, the exact correction factor required for small field dosimetry depends on each individual detector design. Cranmer-Sarginson *et al* [36] used Monte Carlo simulations to show that for a 5 mm field size, the sensitivity correction factors required were 0.961, 0.939 and 0.906 for a stereotactic diode, an electron diode and a photon diode respectively. This represented a range of sensitivity changes between 4 % and nearly 10 % between the different diodes. In another study Cranmer-Sarginson *et al* [33] demonstrated that differences between the responses were due to the fact that the electron diode contained a thin metal filter plate above the active volume, and the photon diode active volume was completely surrounded by metal shielding.

As mentioned in the previous section (1.2.3), Alfonso *et al* [16] present a methodology where the detector response variation with field size can be corrected for by using a sensitivity correction factor. These correction factors have been obtained for various detectors using both experimental [37-39] and Monte Carlo simulation methods [31, 33, 36, 40-42]. In addition, it has been shown that a detector with an active area of 1 mm^2 or less has negligible volume averaging at a typical linear accelerator field size of 5 mm [27, 33]. Therefore, by making the appropriate detector choice, small field dosimetry is possible at clinically relevant small field sizes. Conversely, it is possible to make a

poor detector choice in standard field dosimetry [7]. Detector selection should therefore be a careful consideration at any field size.

1.3 OVERALL AIM OF THE STUDY

The overall objective of this study is to contribute to the scientific knowledge on small field dosimetry by enabling accurate, consistent and reproducible measurements of output factors in very small fields.

1.4 SPECIFIC OBJECTIVES OF THE STUDY

- To scientifically define a very small field
- To improve the accuracy and consistency of reporting very small field output factor measurements
- To study the effect of detector perturbations of very small fields with a specific focus on air
- To use the understanding of detector perturbations to design a diode which does not require sensitivity correction factors in very small fields

1.5 ACCOUNT OF RESEARCH PROGRESS LINKING THE RESEARCH PAPERS

Regardless of the dosimeter studied, the relative output and corresponding correction factors in the literature appear to have been presented as a function of the nominal field size and not the dosimetric field size. The primary aim of chapter 2 is to investigate whether the consistency of reporting small field output factor measurements is improved by using a field size metric based on the measured

dosimetric field size as opposed to using the nominal field size (see section 2.1 for field size definitions).

Chapter 3 introducs the concept of very small field size. Output factor (OPF) measurements at these field sizes require extremely careful experimental methodology including the measurement of dosimetric field size at the same time as each output factor measurement, as outlined in chapter 2. Two quantifiable scientific definitions of the threshold of very small field size are presented. A practical methodology was established by quantifying at which field size the results from chapter 2 are applicable. A theoretical definition was established by quantifying the field size at which the physics involved in small field dosimetry (see chapter 1) became significantly different.

Chapter 3 shows that lateral electronic disequilibrium causes a significant change in dose as a function of field size at very small fields. Although the effect of air on lateral electronic disequilibrium in standard field sizes with large air gap sizes is well established, the potential problem of very small (less than 1 mm) air gaps on very small fields is not covered in the literature. The principal aim of chapter 4 is to establish the effect of very small air gaps on very small field dosimetry. Air gaps of this magnitude can complicate the dosimetry in many situations. These include their intrinsic existence in certain dosimeters and phantoms; their possible presence as bubbles on a detector placed in water; and that they cannot be resolved on some planning CT scanners.

Due to their small collecting volume diodes are commonly used in small field dosimetry. However the relative sensitivity of a diode increases with decreasing small field size. Conversely, small air gaps are shown in chapter 4 to cause a significant decrease in the sensitivity of a detector as the field size is decreased. Therefore the aim of chapter 5 is to use Monte Carlo simulations to investigate introducing air upstream to diodes such that they measured with a constant sensitivity across all field sizes in small field dosimetry, thus creating a "correction-less" diode.

Chapter 6 extends chapter 5 using Monte Carlo simulations to vary the electron beam incident on to the target from a linear accelerator. This aim of this chapter is to study if a correction-less diode designed in chapter 5 would also function correctly on other similar linear accelerators.

In chapter 7, one of the correction-less diodes designed in chapter 5, as well as a new correction-less diode is physically constructed and tested on real linear accelerators. The concept of designing correction-less diodes in general is also explored in more detail. Note that in chapter 7, these diodes are referred to as "correction-free" diodes. The experimental construction of the "correction-free" diode was successful and was the first diode detector in the world that did not require corrections for very small field output factors.

Very small field dosimetry is quite different to standard field dosimetry due to the differing physics. However if these different effects are well understood then accurate small field dosimetry is possible and can even be used to our advantage.

1.6 REFERENCES

[1] F.M. Khan, *The Physicis of Radiation Therapy - Third Edition*. (Lippincott Williams & Wilkins, Philadelphia, 2003).

[2] J.r. Williams, D.I. Thwaites, *Radiotherapy physics in practice*. (Oxford university press, Oxford, 2000).

[3] A.L. Boyer, T. Schilteiss, "Effects of dosimetric and clinical uncertainty on complication-free local tumor control," Radiotherapy and Oncology **11**, 65-71 (1988).

[4] A. Dutreix, "When and how can we improve radiotherapy?," Radiotherapy and Oncology **2**, 275-292 (1984).

[5] D. Greene, P.C. Williams, *Linear Accelerators for Radiation Therapy*. (Taylor & Francis Group, New York, 1997).

[6] G.G. Steel, *Basic Clinical Radiobiology - Third Edition*. (Hodder Arnold, London, 2002).

[7] D.T.B. P. Andreo, K. Hohlfeld, M. S. Huq, T. Kanai, F. Laitano, V., a.S.V. G. Smyth, "Absorbed dose determination in external beam radiotherapy," Technical Report Series No 3982000).

[8] L.H. Gray, "The Absorption of Penetrating Radiation," Proceedings of the Royal Society A: Mathematical, Physical and Engineering Sciences **122**, 647-668 (1929).

[9] L.H. Gray, "An Ionization Method for the Absolute Measurement of Formula-Ray Energy," Proceedings of the Royal Society A: Mathematical, Physical and Engineering Sciences **156**, 578-596 (1936).

[10] U. Fano, "Note on the Bragg-Gray cavity principle for measuring energy dissipation," Radiation Research **1**, 237-240 (1954).

[11] L.V. Spencer, F.H. Attix, "A theory of cavity ionization," Radiation Research **3**, 239-254 (1955).

[12] D.P. Landau, K. Binder, *A guide to Monte Carlo simulations in statistical physics*. (Cambridge university press, Cambridge, 2000).

[13] D.W. Rogers, "Fifty years of Monte Carlo simulations for medical physics," Phys Med Biol **51**, R287-301 (2006).

[14] M.C. Schell, F.J. Bova, D.A. Larson, W.R. Leavit, W.R. Lutz, E. Podgorsak, A. Wu, "Stereotactic radiosurgery: The report of AAPM Task Group 42," AAPM Report No. 541995).

[15] S.H. Benedict, K.M. Yenice, D. Followill, J.M. Galvin, W. Hinson, B. Kavanagh, P. Keall, M. Lovelock, S. Meeks, L. Papiez, T. Purdie, R. Sadagopan, M.C. Schell, B. Salter, D.J. Schlesinger, A.S. Shiu, T. Solberg, D.Y. Song, V. Stieber, R. Timmerman, W.A. Tomé, D. Verellen, L. Wang, F.-F. Yin, "Stereotactic body radiation therapy: The report of AAPM Task Group 101," Medical Physics **37**, 4078 (2010).

[16] R. Alfonso, P. Andreo, R. Capote, M.S. Huq, W. Kilby, P. Kjäll, T.R. Mackie, H. Palmans, K. Rosser, J. Seuntjens, W. Ullrich, S. Vatnitsky, "A new formalism for reference dosimetry of small and nonstandard fields," Medical Physics **35**, 5179 (2008).

[17] I.J. Das, G.X. Ding, A. Ahnesjö, "Small fields: Nonequilibrium radiation dosimetry," Medical Physics **35**, 206 (2008).

[18] G. Cranmer-Sargison, S. Weston, N.P. Sidhu, D.I. Thwaites, "Experimental small field 6MV output ratio analysis for various diode detector and accelerator combinations," Radiother Oncol **100**, 429-435 (2011).

[19] C.F. Behrens, "Dose build-up behind air cavities for Co-60, 4, 6 and 8 MV. Measurements and Monte Carlo simulations," Phys Med Biol **51**, 5937-5950 (2006).

[20] B. Disher, G. Hajdok, S. Gaede, J.J. Battista, "An in-depth Monte Carlo study of lateral electron disequilibrium for small fields in ultra-low density lung: implications for modern radiation therapy," Phys Med Biol **57**, 1543-1559 (2012).

[21] X. Li, C. Yu, T. Holmes, "A systematic evaluation of air cavity dose perturbation in megavoltage x-ray beams," Medical Physics **27**, 1011-1017 (2000).

[22] A. Rustgi, M. Samuels, S. Rustgi, "Influence of air inhomogeneities in radiosurgical beams," Med Dosim **22**, 95-100 (1997).

[23] T.D. Solberg, F. Holly, A. De Salles, R. Wallace, J. Smathers, "Implications of tissue heterogeneity for radiosurgery in head and neck tumors," Int J Radiat Oncol Biol Phys **32**, 235-239 (1995).

[24] S.J. Wadi-Ramahi, S.A. Naqvi, J.C.H. Chu, "Evaluating the effectiveness of a longitudinal magnetic field in reducing underdosing of the regions around upper respiratory cavities irradiated with photon beams—A Monte Carlo study," Medical Physics **28**, 1711 (2001).

[25] M.L. Taylor, T. Kron, R.D. Franich, "A contemporary review of stereotactic radiotherapy: inherent dosimetric complexities and the potential for detriment," Acta Oncol **50**, 483-508 (2011).

[26] G.X. Ding, F. Ding, "Beam characteristics and stopping-power ratios of small radiosurgery photon beams," Phys Med Biol **57**, 5509-5521 (2012).

[27] A.J. Scott, S. Kumar, A.E. Nahum, J.D. Fenwick, "Characterizing the influence of detector density on dosimeter response in non-equilibrium small photon fields," Phys Med Biol **57**, 4461-4476 (2012).

[28] H. Bouchard, J. Seuntjens, J.-F. Carrier, I. Kawrakow, "Ionization chamber gradient effects in nonstandard beam configurations," Medical Physics **36**, 4654 (2009).

[29] J.D. Fenwick, S. Kumar, A.J. Scott, A.E. Nahum, "Using cavity theory to describe the dependence on detector density of dosimeter response in non-equilibrium small fields," Phys Med Biol **58**, 2901-2923 (2013).

[30] T.S. Underwood, H.C. Winter, M.A. Hill, J.D. Fenwick, "Detector density and small field dosimetry: Integral versus point dose measurement schemes," Medical Physics **40**, 082102 (2013).

[31] P.H. Charles, S.B. Crowe, T. Kairn, R.T. Knight, B. Hill, J. Kenny, C.M. Langton, J.V. Trapp, "Monte Carlo-based diode design for correction-less small field dosimetry," Phys Med Biol **58**, 4501-4512 (2013).

[32] P.H. Charles, S.B. Crowe, T. Kairn, J. Kenny, J. Lehmann, J. Lye, L. Dunn, B. Hill, R.T. Knight, C.M. Langton, J.V. Trapp, "The effect of very small air gaps on small field dosimetry," Phys Med Biol **57**, 6947-6960 (2012).

[33] G. Cranmer-Sargison, S. Weston, J.A. Evans, N.P. Sidhu, D.I. Thwaites, "Monte Carlo modelling of diode detectors for small field MV photon

dosimetry: detector model simplification and the sensitivity of correction factors to source parameterization," Phys Med Biol **57**, 5141-5153 (2012).

[34] F. Crop, N. Reynaert, G. Pittomvils, L. Paelinck, C. De Wagter, L. Vakaet, H. Thierens, "The influence of small field sizes, penumbra, spot size and measurement depth on perturbation factors for microionization chambers," Phys Med Biol **54**, 2951-2969 (2009).

[35] T.S. Underwood, H.C. Winter, M.A. Hill, J.D. Fenwick, "Mass-density compensation can improve the performance of a range of different detectors under non-equilibrium conditions," Phys Med Biol **58**, 8295-8310 (2013).

[36] G. Cranmer-Sargison, S. Weston, J.A. Evans, N.P. Sidhu, D.I. Thwaites, "Implementing a newly proposed Monte Carlo based small field dosimetry formalism for a comprehensive set of diode detectors," Medical Physics **38**, 6592-6602 (2011).

[37] E. Pantelis, A. Moutsatsos, K. Zourari, L. Petrokokkinos, L. Sakelliou, W. Kilby, C. Antypas, P. Papagiannis, P. Karaiskos, E. Georgiou, I. Seimenis, "On the output factor measurements of the CyberKnife iris collimator small fields: Experimental determination of the k(Q(clin),Q(msr)) (f(clin),f(msr)) correction factors for microchamber and diode detectors," Medical Physics **39**, 4875-4885 (2012).

[38] A. Ralston, P. Liu, K. Warrener, D. McKenzie, N. Suchowerska, "Small field diode correction factors derived using an air core fibre optic scintillation dosimeter and EBT2 film," Phys Med Biol **57**, 2587-2602 (2012).

[39] C. Bassinet, C. Huet, S. Derreumaux, G. Brunet, M. Chea, M. Baumann, T. Lacornerie, S. Gaudaire-Josset, F. Trompier, P. Roch, G. Boisserie, I. Clairand, "Small fields output factors measurements and correction factors

determination for several detectors for a CyberKnife and linear accelerators equipped with microMLC and circular cones," Medical Physics **40**, 071725 (2013).

[40] P. Francescon, S. Cora, N. Satariano, "Calculation of k(Q(clin),Q(msr)) (f(clin),f(msr)) for several small detectors and for two linear accelerators using Monte Carlo simulations," Medical Physics **38**, 6513-6527 (2011).

[41] P. Francescon, W. Kilby, N. Satariano, S. Cora, "Monte Carlo simulated correction factors for machine specific reference field dose calibration and output factor measurement using fixed and iris collimators on the CyberKnife system," Phys Med Biol **57**, 3741-3758 (2012).

[42] D. Czarnecki, K. Zink, "Monte Carlo calculated correction factors for diodes and ion chambers in small photon fields," Phys Med Biol **58**, 2431-2444 (2013).

Chapter 2: A methodological approach to reporting corrected small field relative outputs

G Cranmer-Sargison[1,2], P H Charles[3], J V Trapp[3] and D I Thwaites[4]

[1]Department of Medical Physics, Saskatchewan Cancer Agency, Saskatoon, Canada

[2]Academic Unit of Medical Physics, Faculty of Medicine and Health, University of Leeds, UK

[3]School of Chemistry, Physics and Mechanical Engineering, Queensland University of Technology, Brisbane, Australia

[4]Institute of Medical Physics, School of Physics, University of Sydney, Australia

Journal: Radiotherapy and Oncology

Status: Published November 2013

Citations to date: 2

STATEMENT OF JOINT AUTHORSHIP

Title: A methodological approach to reporting corrected small field relative outputs

Authors: Gavin Cranmer-Sargison; Paul Charles; Jamie Trapp; David Thwaites[4]

Paul Charles (candidate)

Involved in the direction of the project and interpretation of results. Performed measurements on 2 (out of 5) machines. Performed Monte Carlo simulations (not published) for result interpretation. Wrote part of the manuscript.

Gavin Cranmer-Sargison

Lead the concept and design of project. Performed all published Monte Carlo simulations. Performed measurements of 3 (out of 5) machines. Wrote the majority of the manuscript.

Jamie Trapp

Provided advice and supervision as required. Helped with interpretation of results.

David Thwaites

Supervised project including contributions to aim and direction. Edited manuscript

ABSTRACT

Purpose: The goal of this work was to set out a methodology for measuring and reporting small field relative output and to assess the application of published correction factors across a population of linear accelerators.

Methods and Materials: Measurements were made at 6 MV on five Varian iX accelerators using two PTW T60017 unshielded diodes. Relative output readings and profile measurements were made for nominal square field sizes of side 0.5 cm to 1.0 cm. The actual field widths were taken to be the FWHM at 50% in A (in-plane) and B (cross-plane). An effective field size, defined as $FS_{eff} = \sqrt{A \cdot B}$, was calculated and is presented as a field size metric. FS_{eff} was used to linearly interpolate between published Monte Carlo calculated $k_{Q_{clin},Q_{msr}}^{f_{clin},f_{msr}}$ values to correct for the diode over-response in small fields.

Results: The relative output data reported as a function of the nominal field size was different across the accelerator population. However, using the effective field size for reporting showed that the actual output ratios were consistent across the accelerator population. Correcting the measured relative output using $k_{Q_{clin},Q_{msr}}^{f_{clin},f_{msr}}$ at both the nominal and effective field sizes produce output factors that were not identical but differ by much less than the reported experimental and/or MC statistical uncertainties

Conclusion: In general, the proposed methodology removes much of the ambiguity in reporting and interpreting small field dosimetric quantities and facilitates a clear

dosimetric comparison across a population of linacs. FS_{eff} is a conceptually simple method for reporting measured small field relative output which can be corrected using linear interpolation between published $k_{Q_{clin},Q_{msr}}^{f_{clin},f_{msr}}$ values.

2.1 INTRODUCTION

The International Electrotechnical Commission (IEC) recommends using the distance intercepted by a given isodose curve (50% level) on a plane perpendicular to the beam axis, at a stated fixed distance from the source (isocenter), to define the dosimetric field size [1]. Often in clinical practice the definition of field size is more loosely taken to mean the light field projection at a fixed distance from the source. In the somewhat dated ICRU Report 24 [2] the light field projection is defined as the geometric field size. For field sizes large enough to ensure no source occlusion and charged particle equilibrium (CPE) the geometric field size may provide an accurate representation of the dosimetric field size, at least to within a given clinical tolerance. However, Das *et al* [3] have reported that for field sizes that do not satisfy the CPE or occlusion criteria the dosimetric field size will be greater than the geometric field size and therefore the traditional close agreement between field size definitions breaks down.

Experimental small field dosimetry can be challenging due to the lack of lateral charged particle equilibrium, spectral changes as a function of field size, detector choice and subsequent perturbations of the charged particle fluence [3]. Alfonso *et al* [4] have presented a well thought out dosimetry formalism for reporting corrected relative output factors for small and non-standard fields. The formalism makes use of a field factor (Ω) which converts absorbed dose to water for the machine-specific reference field (f_{msr}) to that of the clinical field of interest (f_{clin}). This field factor is equal to the ratio of experimental detector readings ($OR_{det}^{f_{clin}}$) multiplied by a detector-

specific correction factor ($k_{Q_{clin},Q_{msr}}^{f_{clin},f_{msr}}$). Although the formalism establishes a framework for correcting small field relative output measurements it could be argued that the reporting, and application, of $k_{Q_{clin},Q_{msr}}^{f_{clin},f_{msr}}$ as a function of field size is still somewhat ambiguous.

Commercial diode detectors have been shown to be a reasonably good choice for small field dosimetry applications [5-11], yet care must be taken when selecting between shielded (photon) and unshielded (electron and stereotactic) diodes. In general, the correction factors required for shielded diodes are approximately twice that required for the unshielded diodes [12, 13] for the same irradiation conditions. An experimental procedure for deriving $k_{Q_{clin},Q_{msr}}^{f_{clin},f_{msr}}$ for various diode detectors has been presented by Pantelis *et al* [10]. The method makes use of an error weighted average of Alanine, TLD, EBT and VIP gel measured relative outputs to derive a water equivalent output factor. The experimental output factor can then be used to correct for the well documented diode over-response in small fields. Ralston *et al* [11] used an air-core fiber optic scintillation dosimeter (FOD) for small field relative output dosimetry and showed the FOD can be used to experimentally determine $k_{Q_{clin},Q_{msr}}^{f_{clin},f_{msr}}$ for other detector types. Cranmer-Sargison *et al* [14] used the FOD and diodes to characterize small fields collimated with a new 160-leaf MLC. The authors recommend that output ratios and field size be measured concurrently and advocate the standard experimental uncertainty on both be quoted when reporting experimental results.

Monte Carlo (MC) simulation has proven to be a powerful tool in overcoming the challenges inherent to small field dosimetry [3, 4, 15-18]. Cranmer-Sargison *et al* [12, 19] and Francescon *et al* [13, 20] have presented MC implementations of the proposed formalism and highlight the importance of systematic experimental validation of the combined accelerator and detector models. Both authors also explored the sensitivity of MC calculated small field output ratios and $k_{Q_{clin},Q_{msr}}^{f_{clin},f_{msr}}$ to the choice of source parameterization and show the correction factors to be a function of field size only. Further work by Scott *et al* [18] has shown that the ratio of dose-to-water to dose-to-detector-in-water varies significantly as a function of field size. For small field sizes this ratio correlates with the mass density of the detector material relative to that of water. The authors also show that all water dose profiles are very similar to profiles simulated with a small isolated silicon volume in water (also see Francescon *et al* [13]).

Regardless of the dosimeter studied, the relative output and corresponding correction factors appear to have been presented as a function of the nominal field size and not the dosimetric field size. The viability of applying small field central axis relative output correction factors to clinically measured data requires standardization in measurement, as well as a field size metric which can be used to appropriately correlate relative output to the measured dosimetric field size. The suitability of applying published $k_{Q_{clin},Q_{msr}}^{f_{clin},f_{msr}}$ correction factors across a population of linacs is also not apparent from the literature nor is it clear how the corrections should be applied to clinical data reported as a function of the measured dosimetric field size. Each aspect is addressed in the work presented here.

2.2 METHOD AND MATERIALS

2.2.1 Defining an effective field size for use in small field dosimetry

For small fields collimated with jaws and/or MLCs there can be a difference between the geometric field size and nominal field size as set on the linac console. The difference can be due to collimator calibration and the positional accuracy of the collimation system itself [5]. Add to this the inherent complication of the dosimetric field size being greater than the geometric field (for example due to leaf end transmission) and the requirements for a systematic framework for reporting and interpreting small field dosimetric values becomes clear. As such, a simple small field metric which can be used to represent the dosimetric field size would be of value. A number of approaches to this are possible, but given the magnitude of the dimensional and scatter component changes (which need to be taken into account an small fields) effective field size is suggested as follows,

$$FS_{eff} = \sqrt{A \cdot B}, \qquad (2.1)$$

where A and B correspond to the in-plane and cross-plane dosimetric field widths defined as the 50% isodose level. Moreover, one can define an equivalent field area such that,

$$FA_{equ} = A \cdot B. \qquad (2.2)$$

Defining FS_{eff} and FA_{equ} provides a simple yet robust methodological framework for comparing small field dosimetric quantities across a population of linacs with different collimation systems (jaws, MLCs and cones, where the FA_{equ} of the latter can be represented by the actual measured area and the FS_{eff} as the square root of this). We first explore the use of FS_{eff} for small nominally square fields and leave the viability of using FA_{equ} for comparison between cone, jaw and MLC collimated small fields for another work.

2.2.2 Experimental measurements

Small field 6 MV relative output measurements were made using two PTW T60017 unshielded diodes on five Varian iX linacs located at three different institutions (See Appendix A for details). Detector specific output ratios ($OR_{det}^{f_{clin}}$) were calculated with respect to a square jaw collimated field of side 3.0 cm for nominal square jaw collimated field sizes of side 1.0, 0.9, 0.8, 0.7, 0.6 and 0.5 cm. Measurements were made at a depth of 5.0 cm with the long axis of the diode detector placed parallel to the beam axis such that the active volume was positioned at isocenter. Positional fine tuning was performed to ensure the active volume of the detector was located at the radiation isocenter and not just centered on the light field. Following this method ensured the detector positional uncertainty was limited only by accuracy of the water tank system quoted by the manufacturer at ± 0.1 mm.

The measurements were repeated three times with the water phantom, detector position and collimation reset between each experimental session. During each

experimental session five central axis output readings and five in-plane and cross-plane profile measurements were made at each field size. The mean output ratio and field widths were calculated across the three experimental sessions as were the standard experimental errors for each. FS_{eff} was calculated using the dosimetric field widths along each axis and $OR_{det}^{f_{clin}}$ values reported as a function of both the nominal and effective field sizes.

2.2.3 Monte Carlo simulations

A previously published BEAMnrc model of a 6 MV Varian iX linear accelerator head [21] was used to create the input phase space data for all subsequent simulations. The baseline electron source parameterization was modelled as a 6.2 MeV mono-energetic Gaussian with a circularly symmetric FWHM = 0.110 cm [12, 19]. Simulated machine output per monitor unit was correctly modelled using the method of Popescu *et al* [22] and azimuthal particle redistribution used to reduce latent phase space uncertainty [23].

DOSRZnrc simulations were run using a previously published T60017 diode detector model [12] such that the statistical dose uncertainty scored to the active volume was approximately ± 0.5%. The EGSnrc transport parameters ECUT, PCUT and ESTEP were set to 0.521 MeV, 0.01 MeV and 0.25 respectively. The EXACT boundary crossing algorithm was used in combination with the PRESTA-II condensed history electron step algorithm (ESAVEIN = 2.0 MeV) and the photon cross-section enhancement variance reduction technique. Phase space data for jaw collimated geometric field sizes of side 0.40, 0.45, 0.50, 0.55, 0.60, 0.65, 0.70, 0.75, 0.80, 0.85,

0.90, 0.95, 1.0 and 3.0 were used as DOSRZnrc input. Simulated output ratios were calculated for each field size as follows,

$$OR_{det_{MC}}^{f_{clin}} = \left(\frac{D_{det_{MC}}^{f_{clin}}}{D_{det_{MC}}^{f_{msr}}} \right) \cdot \left(\frac{D_{monitor_{MC}}^{f_{msr}}}{D_{monitor_{MC}}^{f_{clin}}} \right), \qquad (2.3)$$

where $D_{det_{MC}}^{f_{clin}}$, $D_{det_{MC}}^{f_{msr}}$, $D_{monitor_{MC}}^{f_{clin}}$ and $D_{monitor_{MC}}^{f_{msr}}$ represent the dose per incident particle scored to the active volume of the detector model and linac monitor unit chamber for the f_{clin} and f_{msr} simulations respectively.

DOSXYZnrc simulations were run using the same phase space data used in the DOSRZnrc simulations. The history number was set to give a statistical uncertainty of less than ± 0.5% within a voxel dimension of 0.05 cm x 0.05 cm x 0.25 cm. The in-plane and cross-plane FWHMs at the 50% level were extracted from the data and the dosimetric field widths plotted as a function of the geometric field widths. The sensitivity of FS_{eff} to variations in electron energy and FWHM were investigated using the two data sets. The first set of data was calculated for an electron energy fixed at 6.2 MeV with the Gaussian spatial distribution varied as follows: FWHM = 0.100, 0.110, and 0.120 cm. The second set of data was for electron energies at 5.8, 6.0 and 6.2 MeV with the spatial distribution fixed at a FWHM = 0.110 cm. Once again the dosimetric field widths were extracted from the data and plotted as a function of geometric field widths. For each source parameter combination $OR_{det_{MC}}^{f_{clin}}$ was plotted as a function of both the nominal and effective field size and the results compared to the experimental data.

2.2.4 Interpreting and applying $k_{Q_{clin},Q_{msr}}^{f_{clin},f_{msr}}$

The PTW T60017 diode $k_{Q_{clin},Q_{msr}}^{f_{clin},f_{msr}}$ factors published by Cranmer-Sargison *et al* [12] were used to correct the experimental $OR_{det}^{f_{clin}}$ data in a manner consistent with the Alfonso *et al* formalism. It must be noted that Cranmer-Sargison *et al* present the $k_{Q_{clin},Q_{msr}}^{f_{clin},f_{msr}}$ data at the geometric field sizes and therefore some question remains as to the appropriateness of applying the corrections (or similar corrections) to $OR_{det}^{f_{clin}}$ data reported at FS_{eff}. The experimental $OR_{det}^{f_{clin}}$ data were corrected using the $k_{Q_{clin},Q_{msr}}^{f_{clin},f_{msr}}$ as published at the geometric field sizes and $k_{Q_{clin},Q_{msr}}^{f_{clin},f_{msr}}$ reassigned to the effective field sizes calculated from the DOSXYZnrc simulations. In all cases linear interpolation was used to assign $k_{Q_{clin},Q_{msr}}^{f_{clin},f_{msr}}$ to the corresponding experimental FS_{eff}. It should be noted that an additional correction factor was calculated for the square field of side 0.40 cm and the entire $k_{Q_{clin},Q_{msr}}^{f_{clin},f_{msr}}$ data set [12] renormalized to a reference field size of side 3.0 cm.

2.3 RESULTS

Figure 2.1 shows the measured $OR_{det}^{f_{clin}}$ data plotted as a function of the nominal field size (as set on the linac console) and the effective field size calculated using the measured in-plane and cross-plane dosimetric field widths. When the $OR_{det}^{f_{clin}}$ data is plotted as a function of the nominal field size there appears to be a significant difference in the relative output across the linac population, which could be

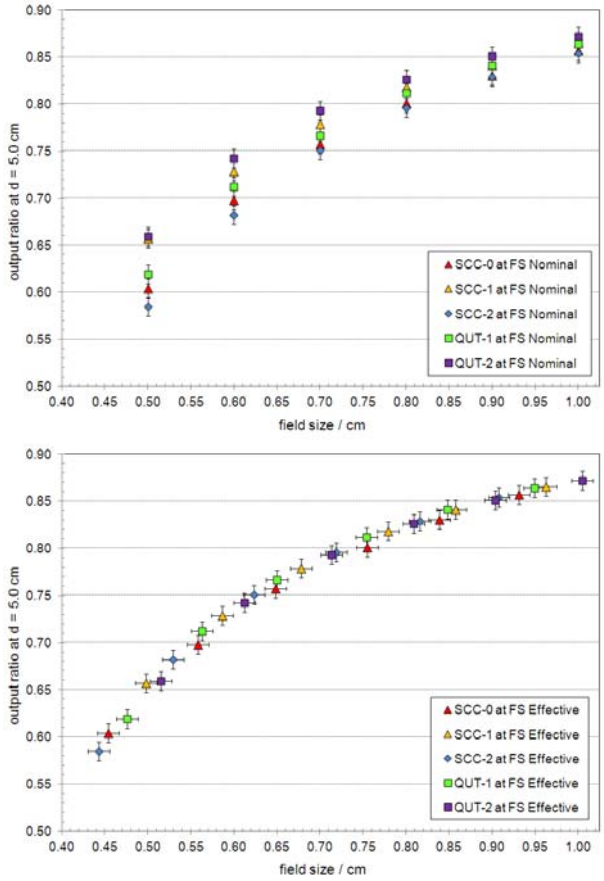

Figure 2.1. Measured $OR_{det}^{f_{clin}}$ data plotted as a function of the nominal (top) and effective (bottom) field sizes. Shown in Appendix B are the effective field sizes and measured output ratios presented in table form. SCC-0,-1,-2 and QUT-1,-2 are labels for the five Varian iX linacs used in this study (See Appendix A for details). It should be noted that the output ratio and measured field widths for linac SCC-0 are from Cranmer-Sargison *et al* [12] and therefore do not include the full characterization in field width uncertainty.

incorrectly interpreted as being a real difference in the electron source width incident on the Bremsstrahlung target. However, when the same $OR_{det}^{f_{clin}}$ data is plotted as a function of FS_{eff} there is no discernible difference in relative output across the population of linacs. The inference being that the linear accelerators included in this study have electron source distributions that are very nearly indistinguishable.

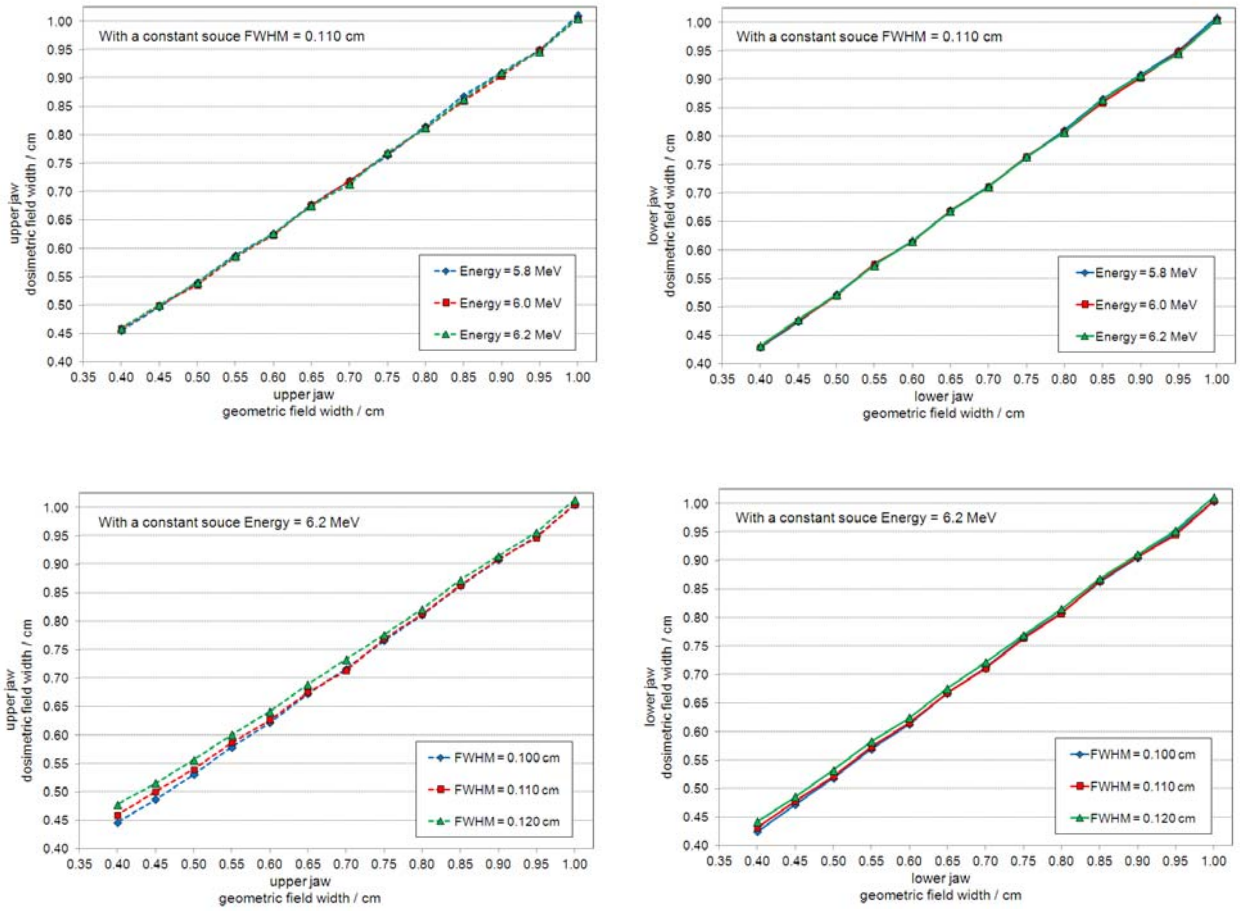

Figure 2.2. DOSXYZnrc simulation data showing the relationship between the dosimetric field widths plotted as a function of the geometric field width for the upper (left) and lower (right) jaws, incident electron energy (top) and FWHM (bottom).

Figure 2.2 shows the DOSXYZnrc simulation data that relates the dosimetric field width to the corresponding geometric field width for the upper and lower jaws. These data reveal a number of interesting characteristics: (1) dosimetric field widths are greater than the geometric field widths for field sizes less than approximately 0.8 cm x 0.8 cm, (2) the effect is greater along the axis collimated by the upper jaw than that collimated by the lower jaw and (3) the effect is independent of source energy but increases as a function of increased source width. The dosimetric field width data can be thought of as measured data from a perfect collimator jaw suffering from no positional error or uncertainty and therefore can be used to elicit the difference

between the geometric and dosimetric field widths for this particular accelerator head.

Shown in Figure 2.3 are the $OR_{det_{MC}}^{f_{clin}}$ data plotted as a function of both the geometric (left) and effective (right) field sizes. Each graph includes the experimental $OR_{det}^{f_{clin}}$ data plotted as a function of the measured effective field sizes (see Figure 2.1). The $OR_{det_{MC}}^{f_{clin}}$ data simulated using a source FWHM = 0.120 cm, and plotted as a function of the geometric field size, agrees best with the experimental data. However, $OR_{det_{MC}}^{f_{clin}}$ simulated using a source FWHM = 0.100 cm is clearly in better agreement if plotted as a function of the effective field size. In both instances the agreement between the experimental and simulated data is reasonable at a source FWHM = 0.110 cm.

The data in Figure 2.4 shows the relative output plotted as a function of the measured effective field size corrected using $k_{Q_{clin},Q_{msr}}^{f_{clin},f_{msr}}$ values at the geometric field size and the same $k_{Q_{clin},Q_{msr}}^{f_{clin},f_{msr}}$ values reassigned to the associated effective field size. Clearly using $k_{Q_{clin},Q_{msr}}^{f_{clin},f_{msr}}$ at the nominal and effective field sizes produce output factors that are not identical but differ by much less than the reported experimental and/or MC statistical uncertainties. The more important criteria for using the proposed methodology is to characterize, correct and report relative output as a function of the effective field size and not the nominal.

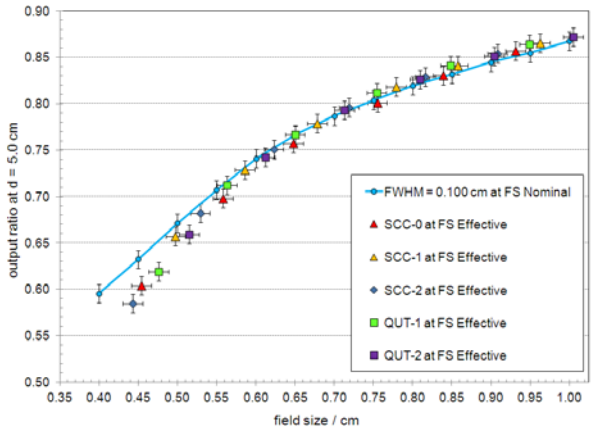
output ratio at d = 5.0 cm
field size / cm
FWHM = 0.100 cm at FS Nominal
SCC-0 at FS Effective
SCC-1 at FS Effective
SCC-2 at FS Effective
QUT-1 at FS Effective
QUT-2 at FS Effective

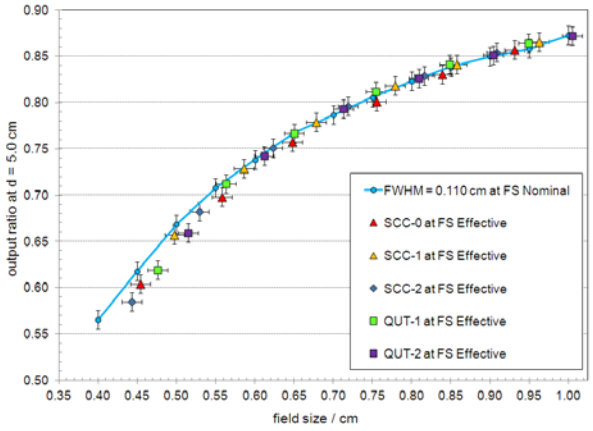
output ratio at d = 5.0 cm
field size / cm
FWHM = 0.110 cm at FS Nominal
SCC-0 at FS Effective
SCC-1 at FS Effective
SCC-2 at FS Effective
QUT-1 at FS Effective
QUT-2 at FS Effective

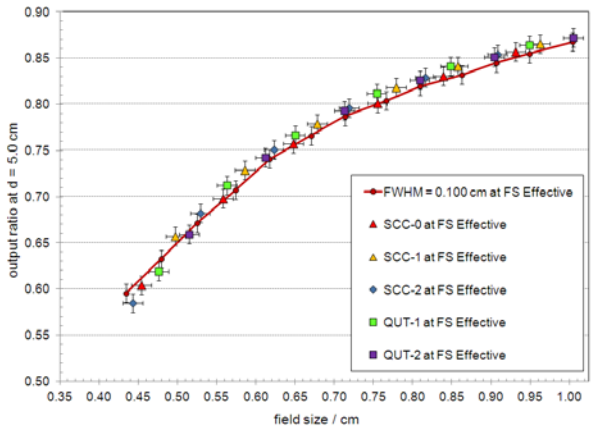
output ratio at d = 5.0 cm
field size / cm
FWHM = 0.100 cm at FS Effective
SCC-0 at FS Effective
SCC-1 at FS Effective
SCC-2 at FS Effective
QUT-1 at FS Effective
QUT-2 at FS Effective

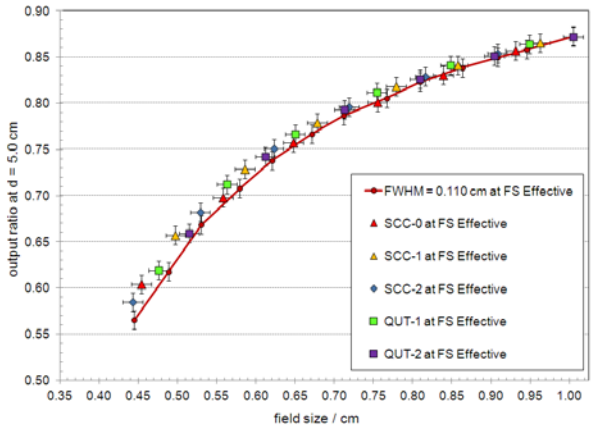
output ratio at d = 5.0 cm
field size / cm
FWHM = 0.110 cm at FS Effective
SCC-0 at FS Effective
SCC-1 at FS Effective
SCC-2 at FS Effective
QUT-1 at FS Effective
QUT-2 at FS Effective

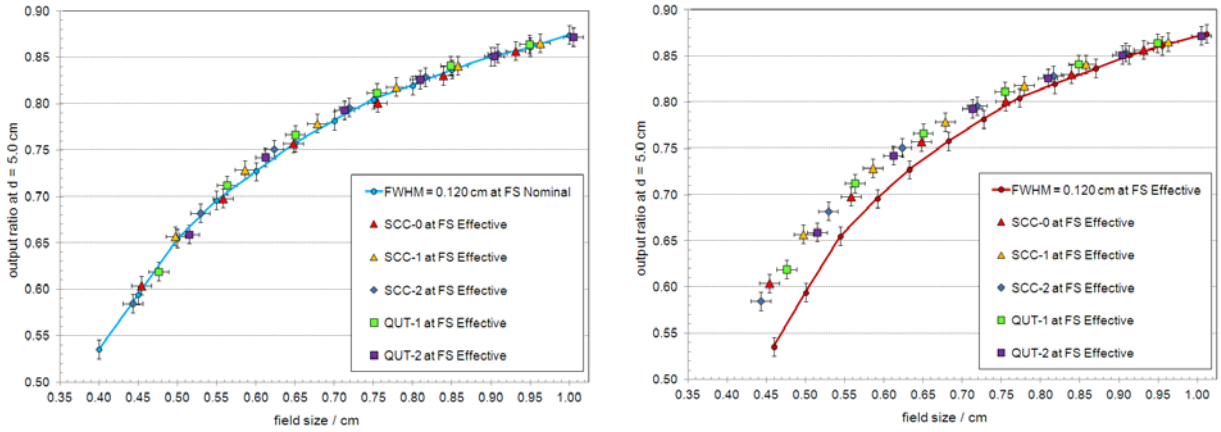

Figure 2.3. DOSRZnrc simulated $OR_{det}^{f_{clin}}$ data (solid line) plotted as a function of the nominal field size (left) and effective field size (right) calculated for the incident electron FWHM shown in Figure 2. In all cases the experimental data is given as a function of the effective field size. The solid line connecting the MC data points is included as a guide only and does not represent a functional fit.

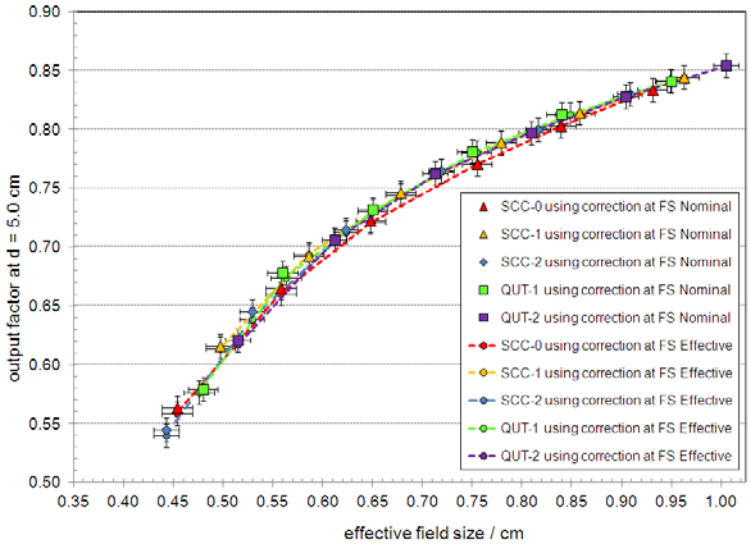

Figure 2.4. Corrected relative output data plotted as a function of the measured effective field size. The dashed lines connect the data points and do not represent a functional fit.

2.4 DISCUSSION

The measured small field relative output data reported as a function of the nominal field size are clearly different across the accelerator population. However, using the effective field size for reporting showed that the actual output ratios were consistent across the accelerator population (see Figure 2.1). This indicates that Varian iX accelerators are generally well matched and that any major discrepancies in the literature may be attributed to reporting relative output as a function of the nominal field size. Understanding the differences between the nominal, geometric and dosimetric field sizes is critical and the implications, as they relate to interpreting small field dosimetric data, should not be discounted. For specialized stereotactic collimators, such as cones or micro-MLCs, the difference between the dosimetric and geometric field widths will be less than that for upstream jaw collimators. This alone highlights the importance of establishing a mechanism which facilitates the presentation of relative output data as a function of the measured equivalent field area.

Reporting measured relative output and dosimetric field widths concurrently is comprehensive but somewhat cumbersome. What has been shown here is that using FS_{eff} as a small field metric relieves much of the ambiguity in reporting and simplifies the measured dosimetric field widths into one representative value. In addition, adopting a standard experimental methodology that includes reporting uncertainties in both the effective field size and measured output ratios is vital and consistent with the importance given to the expression of uncertainties documented in the IAEA dosimetry code of practice [24].

The Monte Carlo simulations clearly show that the dosimetric field size is larger than the geometric field size for small fields (as previously reported by Das *et al* [3] and Aspradakis *et al* [15]). In all cases the dosimetric field width defined by the upper jaws was larger than that defined by the lower jaws. The upper jaws are closer to the source when compared to the lower jaws and therefore require a smaller physical separation to collimate the same geometric field width. The result is greater source occlusion across the upper jaw and therefore an increased effective field size. In short, dosimetric field widths increase as a function of increased source occlusion. For the same reason the dosimetric field widths increase as a function of electron spot size increase. The effective field size should therefore be used when tuning the focal spot size of a linear accelerator Monte Carlo model. As evidenced in Figure 2.3, using the geometric field size may result in an incorrect spot size being determined.

There was a negligible difference in the output factors when $k_{Q_{clin},Q_{msr}}^{f_{clin},f_{msr}}$ was applied using the geometric field size or the effective field size. This is consistent with the work of Scott *et al* [18] which showed that a 1.0 mm field size difference results in a 1.0% difference in $k_{Q_{clin},Q_{msr}}^{f_{clin},f_{msr}}$. However, it is recommended that the effective field size be used when assigning $k_{Q_{clin},Q_{msr}}^{f_{clin},f_{msr}}$, as it provides consistency within the proposed methodology and standardizes the application across a population of linacs.

Presenting small field relative output data as a function of the effective field size, as defined is this work, can be well justified when one considers the phantom and head

scatter factor characteristics of small fields. McKerracher and Thwaites [25] show that for square field sizes of side <4.0 cm measured phantom scatter factors are independent of collimation and linac design and dependent only on measurement depth and the beam area irradiated. It is therefore quite reasonable to argue for the use of FA_{equ} in comparing small field dosimetric quantities across multiple linacs or different collimation systems (jaws, MLCs and cones). Head scatter factors for rectangular field sizes have been shown to be dependent on the collimator exchange effect [26]. However, as Zhu *et al* [27] note, this effect is negligible at field sizes of side <2.0 cm, where source occlusion becomes the dominant effect. Reporting relative output as a function of the FS_{eff}, which one will recall is calculated from the measured dosimetric field widths, clearly takes into account differences in source occlusion for millimetre scale changes in field size. The application of FS_{eff} as a reporting mechanism for rectangular field sizes with sides <2.0 cm would require additional investigation. Naturally there may be limitations in further application of the concepts presented here and in no way should one apply FA_{equ} or FS_{eff} without rigorous experimental validation.

2.5 CONCLUSION

It has been shown that adopting this field size metric and the measurement methodology outlined in this study can provide consistency for small field dosimetry across a population of linear accelerators. However, there could be differences between accelerator designs with greater source occlusion due to a larger focal spot size, a collimation system closer to the source, or simply a smaller field size.

2.6 ACKNOWLEDGEMENTS

Gavin Cranmer-Sargison was funded through a Saskatchewan Cancer Agency research grant. Paul Charles was funded by the Australian Research Council in partnership with the Queensland University of Technology (QUT), the Wesley Research Institute and Premion (Linkage Grant No. LP110100401). Paul Charles would like to Tanya Kairn, Trent Aland and Nigel Middlebrook from Premion for assistance with the measurements.

2.7 APPENDIX 2.A. EQUIPMENT DETAILS

Table 2.1: Equipment details for chapter 2.

Label	Institution	Varian iX	PTW T60017 Electron Diode
SCC-0	Saskatoon Cancer Centre	S/N 2311	S/N 000345
SCC-1		S/N 5141	
SCC-2		S/N 1085	
QUT-1	Premion, Wesley Centre	S/N 3561	S/N 000627
QUT-2	Premion, Chermside Centre	S/N 3850	

2.8 APPENDIX 2.B. MEASURED DATA PRESENTED IN TABLE FORMAT

Table 2.2: Measured data from chapter 2 in table format.

SCC-1 Nominal Field Size (cm)	Dosimetric Field Widths (cm)		Effective Field Size (cm)	Output Ratio f_{msr} = 3 cm x 3 cm
	In-plane	Cross-plane		
1.0	0.951 ± 0.001	0.975 ± 0.006	0.963 ± 0.007	0.866 ± 0.11%
0.9	0.857 ± 0.007	0.858 ± 0.059	0.858 ± 0.059	0.841 ± 0.92%
0.8	0.766 ± 0.013	0.792 ± 0.013	0.779 ± 0.019	0.818 ± 0.02%
0.7	0.659 ± 0.007	0.698 ± 0.005	0.678 ± 0.009	0.779 ± 0.54%
0.6	0.570 ± 0.008	0.603 ± 0.003	0.586 ± 0.008	0.729 ± 0.36%
0.5	0.494 ± 0.007	0.502 ± 0.008	0.498 ± 0.010	0.657 ± 0.18%

SCC-2 Nominal Field Size (cm)	Dosimetric Field Widths (cm)		Effective Field Size (cm)	Output Ratio f_{msr} = 3 cm x 3 cm
	In-plane	Cross-plane		
1.0	0.882 ± 0.001	0.935 ± 0.013	0.908 ± 0.013	0.854 ± 0.13%
0.9	0.793 ± 0.007	0.840 ± 0.008	0.816 ± 0.011	0.829 ± 0.31%
0.8	0.700 ± 0.003	0.737 ± 0.001	0.719 ± 0.003	0.796 ± 0.14%
0.7	0.609 ± 0.005	0.638 ± 0.015	0.623 ± 0.016	0.751 ± 0.61%
0.6	0.511 ± 0.005	0.547 ± 0.012	0.529 ± 0.013	0.682 ± 1.22%
0.5	0.443 ± 0.006	0.452 ± 0.027	0.443 ± 0.028	0.585 ± 1.46%

QUT-1 Nominal Field Size (cm)	Dosimetric Field Widths (cm)		Effective Field Size (cm)	Output Ratio f_{msr} = 3 cm x 3 cm
	In-plane	Cross-plane		
1.0	0.933 ± 0.002	0.963 ± 0.003	0.948 ± 0.004	0.864 ± 0.20%
0.9	0.833 ± 0.002	0.868 ± 0.010	0.850 ± 0.010	0.841 ± 0.38%
0.8	0.745 ± 0.002	0.766 ± 0.015	0.755 ± 0.015	0.812 ± 0.29%
0.7	0.644 ± 0.000	0.649 ± 0.003	0.651 ± 0.003	0.767 ± 0.26%
0.6	0.559 ± 0.007	0.571 ± 0.010	0.565 ± 0.013	0.713 ± 0.42%
0.5	0.471 ± 0.013	0.482 ± 0.012	0.477 ± 0.018	0.619 ± 0.95%

QUT-2 Nominal Field Size (cm)	Dosimetric Field Widths (cm)		Effective Field Size (cm)	Output Ratio f_{msr} = 3 cm x 3 cm
	In-plane	Cross-plane		
1.0	0.963 ± 0.016	1.050 ± 0.012	1.005 ± 0.020	0.872 ± 0.05%
0.9	0.870 ± 0.002	0.940 ± 0.001	0.904 ± 0.002	0.851 ± 0.23%
0.8	0.768 ± 0.027	0.854 ± 0.004	0.810 ± 0.027	0.826 ± 0.49%
0.7	0.683 ± 0.002	0.744 ± 0.016	0.713 ± 0.016	0.793 ± 0.21%
0.6	0.583 ± 0.000	0.643 ± 0.006	0.612 ± 0.006	0.743 ± 0.23%
0.5	0.488 ± 0.012	0.544 ± 0.007	0.515 ± 0.014	0.659 ± 0.36%

2.9 REFERENCES

[1] I. 60976, "Medical electrical equipment - medical electron accelerators - functional performance characteristics, Edition 2.0," 2007).

[2] ICRU, "Determination of absorbed dose in a patient irradiated by beams of x or gamma rays in radiotherapy procedures. Report No. 24," Journal of the ICRU, NP (1976).

[3] I.J. Das, G.X. Ding, A. Ahnesjö, "Small fields: Nonequilibrium radiation dosimetry," Medical Physics **35**, 206 (2008).

[4] R. Alfonso, P. Andreo, R. Capote, M.S. Huq, W. Kilby, P. Kjäll, T.R. Mackie, H. Palmans, K. Rosser, J. Seuntjens, W. Ullrich, S. Vatnitsky, "A new formalism for reference dosimetry of small and nonstandard fields," Medical Physics **35**, 5179 (2008).

[5] G. Cranmer-Sargison, S. Weston, N.P. Sidhu, D.I. Thwaites, "Experimental small field 6MV output ratio analysis for various diode detector and accelerator combinations," Radiother Oncol **100**, 429-435 (2011).

[6] S. Dieterich, G.W. Sherouse, "Experimental comparison of seven commercial dosimetry diodes for measurement of stereotactic radiosurgery cone factors," Medical Physics **38**, 4166 (2011).

[7] C. McKerracher, D.I. Thwaites, "Head scatter factors for small MV photon fields. Part I: a comparison of phantom types and methodologies," Radiother Oncol **85**, 277-285 (2007).

[8] C. McKerracher, D.I. Thwaites, "Head scatter factors for small MV photon fields. Part II: the effects of source size and detector," Radiother Oncol **85**, 286-291 (2007).

[9] C. McKerracher, D.I. Thwaites, "Assessment of new small-field detectors against standard-field detectors for practical stereotactic beam data acquisition " Phys Med Biol **44**, 2143-2160 (1999).

[10] E. Pantelis, A. Moutsatsos, K. Zourari, L. Petrokokkinos, L. Sakelliou, W. Kilby, C. Antypas, P. Papagiannis, P. Karaiskos, E. Georgiou, I. Seimenis, "On the output factor measurements of the CyberKnife iris collimator small fields: Experimental determination of the k(Q(clin),Q(msr)) (f(clin),f(msr)) correction factors for microchamber and diode detectors," Medical Physics **39**, 4875-4885 (2012).

[11] A. Ralston, P. Liu, K. Warrener, D. McKenzie, N. Suchowerska, "Small field diode correction factors derived using an air core fibre optic scintillation dosimeter and EBT2 film," Phys Med Biol **57**, 2587-2602 (2012).

[12] G. Cranmer-Sargison, S. Weston, J.A. Evans, N.P. Sidhu, D.I. Thwaites, "Implementing a newly proposed Monte Carlo based small field dosimetry formalism for a comprehensive set of diode detectors," Medical Physics **38**, 6592-6602 (2011).

[13] P. Francescon, S. Cora, N. Satariano, "Calculation of k(Q(clin),Q(msr)) (f(clin),f(msr)) for several small detectors and for two linear accelerators using Monte Carlo simulations," Medical Physics **38**, 6513-6527 (2011).

[14] G. Cranmer-Sargison, P.Z. Liu, S. Weston, N. Suchowerska, D.I. Thwaites, "Small field dosimetric characterization of a new 160-leaf MLC," Phys Med Biol **58**, 7343-7354 (2013).

[15] IPEM, "Small Field MV Photon Dosimetry," IPEM Report No.2010).

[16] P.H. Charles, S.B. Crowe, T. Kairn, J. Kenny, J. Lehmann, J. Lye, L. Dunn, B. Hill, R.T. Knight, C.M. Langton, J.V. Trapp, "The effect of very small air gaps on small field dosimetry," Phys Med Biol **57**, 6947-6960 (2012).

[17] P.H. Charles, S.B. Crowe, T. Kairn, R.T. Knight, B. Hill, J. Kenny, C.M. Langton, J.V. Trapp, "Monte Carlo-based diode design for correction-less small field dosimetry," Phys Med Biol **58**, 4501-4512 (2013).

[18] A.J.D. Scott, S. Kumar, A.E. Nahum, J.D. Fenwick, "Characterizing the influence of detector density on dosimeter response in non-equilibrium small photon fields," Phys Med Biol **57**, 4461-4476 (2012).

[19] G. Cranmer-Sargison, S. Weston, J.A. Evans, N.P. Sidhu, D.I. Thwaites, "Monte Carlo modelling of diode detectors for small field MV photon dosimetry: detector model simplification and the sensitivity of correction factors to source parameterization," Phys Med Biol **57**, 5141-5153 (2012).

[20] P. Francescon, W. Kilby, N. Satariano, S. Cora, "Monte Carlo simulated correction factors for machine specific reference field dose calibration and output factor measurement using fixed and iris collimators on the CyberKnife system," Phys Med Biol **57**, 3741-3758 (2012).

[21] K. Babcock, G. Cranmer–Sargison, N. Sidhu, "Increasing the speed of DOSXYZnrc Monte Carlo simulations through the introduction of nonvoxelated geometries," Medical Physics **35**, 633 (2008).

[22] I.A. Popescu, C.P. Shaw, S.F. Zavgorodni, W.A. Beckham, "Absolute dose calculations for Monte Carlo simulations of radiotherapy beams," Phys Med Biol **50**, 3375-3392 (2005).

[23] K. Bush, S.F. Zavgorodni, W.A. Beckham, "Azimuthal particle redistribution for the reduction of latent phase-space variance in Monte Carlo simulations," Phys Med Biol **52**, 4345-4360 (2007).

[24] D.T.B. P. Andreo, K. Hohlfeld, M. S. Huq, T. Kanai, F. Laitano, V., a.S.V. G. Smyth, "Absorbed dose determination in external beam radiotherapy," Technical Report Series No 3982000).

[25] C. McKerracher, D.I. Thwaites, "Phantom scatter factors for small MV photon fields," Radiother Oncol **86**, 272-275 (2008).

[26] M. Tatcher, "Head-scatter factors in rectangular photon fields," Medical Physics **20**, 205 (1993).

[27] T.C. Zhu, A. Ahnesjö, K.L. Lam, X.A. Li, C.-M.C. Ma, J.R. Palta, M.B. Sharpe, B. Thomadsen, R.C. Tailor, "Report of AAPM Therapy Physics Committee Task Group 74: In-air output ratio, S[sub c], for megavoltage photon beams," Medical Physics **36**, 5261 (2009).

Chapter 3: A practical and theoretical definition of very small field size for radiotherapy output measurements

P H Charles[1], G Cranmer-Sargison[2,3], D I Thwaites[4], S B Crowe[1], T Kairn[1,5], RT Knight[5], J Kenny[6,7], C M Langton[1], J V Trapp[1]

[1]School of Chemistry, Physics and Mechanical Engineering, Queensland University of Technology, Brisbane, Australia

[2]Department of Medical Physics, Saskatchewan Cancer Agency, Saskatoon, Canada

[3]Academic Unit of Medical Physics, Faculty of Medicine and Health, University of Leeds, UK

[4]Institute of Medical Physics, School of Physics, University of Sydney, Australia

[5]Premion, The Wesley Medical Centre, Brisbane, Australia

[6]The Australian Clinical Dosimetry Service, Australian Radiation Protection and Nuclear Safety Agency, Yallambie, Vic, Australia

[7]Radiation Oncology Queensland, St Andrew's Toowoomba Hospital, Toowoomba, Australia

Journal: Medical Physics

Status: Published April 2014

Accolades:

Medical Physics Editors Choice, April 2014

Most read article in Medical Physics, May 2014

Best student presentation (oral version), Engineering and Physical Scientists in Medicine conference, 2013, Perth.

STATEMENT OF JOINT AUTHORSHIP

Title: A practical and theoretical definition of very small field size for radiotherapy output factor measurements

Authors: Paul Charles; Gavin Cranmer-Sargison; David Thwaites; Scott Crowe; Tanya Kairn; Richard Knight; John Kenny; Christian Langton; Jamie Trapp;

Paul Charles (candidate)
Project concept, direction and design. Performed all Monte Carlo simulations. Analysed an interpreted all results. Wrote the manuscript.

Gavin Cranmer-Sargison
Contributions to the direction of project. Advice and discussion. Editing of manuscript.

David Thwaites
Contributions to the direction of project. Some writing of manuscript. Editing of manuscript.

Scott Crowe
Supplied Monte Carlo model of linac. General advice and supervision as required. Edited manuscript.

Tanya Kairn
Supplied Monte Carlo model of linac. General advice and supervision as required. Edited manuscript.

Richard Knight
General advice and supervision as required.

John Kenny
General advice and supervision as required.

Christian Langton

General advice and supervision as required.

Jamie Trapp

Provided advice and supervision as required. Helped with interpretation of results.

ABSTRACT

Purpose: This work introduces the formal definition of *very small field* size. Output factor (OPF) measurements at these field sizes require extremely careful experimental methodology including the measurement of dosimetric field size at the same time as each OPF measurement. Two quantifiable scientific definitions of the threshold of very small field size are presented.

Methods: A practical definition was established by quantifying the effect that a 1 mm error in field size or detector position had on OPFs, and setting acceptable uncertainties on OPF at 1%. Alternatively, for a theoretical definition of very small field size, the OPFs were separated into additional factors to investigate the specific effects of lateral electronic disequilibrium, photon scatter in the phantom and source occlusion. The dominant effect was established and formed the basis of a theoretical definition of very small fields. Each factor was obtained using Monte Carlo simulations of a Varian iX linear accelerator for various square field sizes of side length from 4 mm to 100 mm, using a nominal photon energy of 6 MV.

Results: According to the practical definition established in this project, field sizes $\leq$ 15 mm were considered to be very small for 6 MV beams for maximal field size uncertainties of 1 mm. If the acceptable uncertainty in the OPF was increased from 1.0 % to 2.0 %, or field size uncertainties are 0.5 mm, field sizes $\leq$ 12 mm were considered to be very small.

Lateral electronic disequilibrium in the phantom was the dominant cause of change in OPF at very small field sizes. Thus the theoretical definition of very small field size coincided to the field size at which lateral electronic disequilibrium clearly caused a greater change in OPF than any other effects. This was found to occur at field sizes $\leq$ 12 mm. Source occlusion also caused a large change in OPF for field sizes $\leq$ 8 mm. Based on the results of this study, field sizes $\leq$ 12 mm were considered to be theoretically very small for 6 MV beams.

Conclusions: Extremely careful experimental methodology including the measurement of dosimetric field size at the same time as output factor measurement for each field size setting and also very precise detector alignment is required at field sizes at least $\leq$ 12 mm and more conservatively $\leq$ 15 mm for 6 MV beams. These recommendations should be applied in addition to all the usual considerations for small field dosimetry, including careful detector selection.

3.1 INTRODUCTION

Small field dosimetry presents many challenges that are not present in standard photon dosimetry. These include source occlusion, lateral electronic disequilibrium, and the choice of detector and evaluation of its response[1]. At present a small field is generally defined as having dimensions smaller than the lateral range of the charged particles that contribute to the dose deposited at a point along the central axis[2]. According to these criteria, field sizes of less than 3 x 3 cm^2 are considered to be small for a 6 MV photon beam. The small field dosimetry task group report from the Institute of Physics and Engineering in Medicine (IPEM)[3] states that it includes field sizes smaller than 40 mm because "...most clinics' confidence in measuring data or in the prediction of their TPSs decreases for collimator setting smaller than around 40 mm. This was a somewhat arbitrary choice". These pragmatic definitions are conservatively robust and are useful to draw attention to when more careful consideration is required for detector selection (active volume in relation to field size and beam profile) and for beginning to consider different and more demanding experimental approaches to measurements as field size gets smaller. However as field size reduces further still, the output factors (the central axis dose in water for a particular field size normalized to the dose from a square field size of side length 100 mm, OPFs) change more rapidly with field size, and the effects of measurement uncertainties become increasingly significant. There is a point when OPF measurements require even more careful methodology, including the measurement of dosimetric field size at the same time as OPF for each field size setting and also very precise detector alignment[4]. Here it is proposed to term these situations 'very small field' (VSF) sizes, to distinguish them as a sub-set of the conventionally accepted term of small fields.

An accurate and highly reproducible experimental setup and methodology is paramount for small field OPF measurements[4-10]. The consistency in reported OPFs for very small fields across a population of linear accelerators has been shown to be greatly increased when the measured dosimetric field size is used, as opposed to simply stating the nominal field size[4]. Reporting in such a manner requires the measurement of cross-axis profiles in a water tank at the same time as each OPF

measurement. These profiles can also assist with the alignment of the detector in small field dosimetry. However, the measurement of profiles with each field size makes OPF measurements very time consuming. It is therefore an important practical consideration for a clinical physicist to understand at which field size such attention to detail is required. This work establishes the field size threshold at which the accuracy of OPFs is not affected by the use of nominal field sizes, and hence introduces a practical working definition of a 'very small' field.

The response of detectors that are used for small field measurements can vary with field size[2, 11]. The observed changes in sensitivity can be due to volume averaging[12, 13], or the physical density of the detector active volume being different to that of the phantom material[12, 14, 15]. Other components that make up the detector may also heavily perturb the particle fluence in small fields[13, 16-20]. Alfonso *et al*[2] present a methodology where the detector response variation with field size can be corrected for by using the factor $k_{Q_{clin},Q_{msr}}^{f_{clin},f_{msr}}$. These correction factors have been obtained for various detectors using both experimental[21-23] and Monte Carlo methods[16, 18, 24-27]. In addition, it has been shown that a detector with an active area of 1 mm^2 or less has negligible volume averaging at a typical linear accelerator field size of 5 mm[12, 18]. Therefore, by making the appropriate detector choice, accurate small field dosimetry is possible at clinically relevant small field sizes. Conversely, it is possible to make a poor detector choice in standard field dosimetry[28]. Detector effects should therefore be an independent consideration at any field size. However, in this study, the impact that common small field detector effects, such as volume averaging and non-water-equivalence, have on the threshold of very small field size is tested.

This work establishes a theoretically-based definition of very small fields by considering the effects of lateral electronic disequilibrium and source occlusion on OPFs. Alternatively a practically-based definition of very small fields is also established based on the influence of measurement conditions on the uncertainties of OPFs. In this study, this is considered specifically for a 6 MV photon beam from a Varian iX linear accelerator, but the findings are likely to be generalizable to other beams of similar quality.

3.2 METHODS

3.2.1 A practical definition of very small field size

Current recommendations suggest that radiation collimation systems and isocentre defining lasers should both be calibrated to permit a maximum positional error of no more than ± 1 mm[29]. It can therefore be assumed that any measured dosimetric field size will be no more than 1 mm different to the nominal field size. Accordingly, the proposed quantifiable practical definition for very small field sizes is as follows: if the OPF changes by ± 1.0 %, given a change in either field size or detector position of up to ± 1 mm, then the field should be considered very small.

This then establishes at which field sizes the accuracy in reporting OPFs, as a function of field size, is significantly affected by the use of the nominal field size, rather than the actual dosimetric field size. That is, the threshold field size is established at which the extremely careful experimental methodology outlined by Cranmer-Sargison *et al*[4] is required to obtain and report accurate OPFs, which is here defined as the threshold for 'very small' fields.

Monte Carlo simulation overview

Monte Carlo modeling was used to enable the properties of small fields to be studied independent of detector influences. All linear accelerator simulations were performed with the BEAMnrc Monte Carlo user code[30], using a model of the Varian 21iX (Varian Medical Systems, Palo Alto, USA) that had been previously been commissioned in other studies for field sizes as small as 5 mm[16, 31, 32]. The incident electron fluence onto the target of this linear accelerator was modeled as centrally symmetric with a Gaussian distribution with a full-width-half-maximum (FWHM) equal to 1.2 mm. All phantom simulations were performed using the EGSnrc C++ user code cavity[33]. Unless otherwise stated, all simulations had an ECUT value of 521 keV and a PCUT value of 10 keV. All simulations were performed at a nominal energy of 6 MV at a depth of 5 cm, and a source-to-measurement distance of 100 cm.

Simulation of output factor

The OPF was simulated at a depth of 5 cm in a 20 x 20 x 20 cm^3 water phantom for square field sizes with side lengths ranging from 4 mm to 20 mm in 1 mm increments, as well as 30 mm, 42 mm, 60 mm, 80 mm and 100 mm. The dose per incident particle was scored to a cylindrical volume of water 0.5 mm in diameter (perpendicular-to-beam direction) and 2 mm deep (beam direction). The OPF was calculated by normalizing the above dose per incident particle from each field size to the dose per incident particle with the 100 mm field size. Monitor chamber backscatter was not considered in this study, as it changes by only 1.5 % between field sizes of 5 mm and 30 mm[24].

The effect of collimator positional error on output factor

The maximum difference due to a collimator error of 1 mm was calculated as a type B uncertainty[34] for a field size of x mm as follows:

$$c(x) = \frac{S_{cp}(x) - S_{cp}(x-1)}{S_{cp}(x)} \qquad (3.1)$$

where $c(x)$ is the error in OPF caused by the collimator position error[29]. S_{cp} is the OPF as a function of field size x. $c(x)$ was plotted as a function of field size in order to observe when the error in simulated OPF increased beyond 1 %.

The effect of detector position on output factor

The effect of detector positioning errors on small field output factors has been studied in detail by Bouchard *et al*[9]. For this study a detector translational error of 1 mm in the direction set by the upper jaws was simulated. The upper jaws result in a greater occlusion of the source than the lower jaws and therefore a detector translational error along the upper jaw axis will result in the greatest change in measured output factor. The change in OPF caused by the 1 mm translational error

was plotted as a function of field size in order to observe when the error in simulated relative output increased beyond 1 %.

The effect of detector size and density on the practical definition

In order to assess if volume averaging (that may be present in measurements with some small field detectors) affected the practical threshold of very small field size, sections *Simulation of output factor* and *The effect of collimator positional error on output factor* were repeated with the width of the small volume of water increased to 1 mm, 2 mm and 3 mm respectively.

Section *The effect of collimator positional error on output factor* was also repeated using uncorrected OPFs from three detectors: PTW 60016 shielded diode, PTW 60017 unshielded diode, and PTW 31014 PinPoint ion chamber (PTW, Freiburg, Germany). The uncorrected OPF that would be measured by the three detectors was calculated as follows:

$$S_{cp}^{det} = \frac{S_{cp}}{k_{Q_{clin},Q_{msr}}^{f_{clin},f_{msr}}} \qquad (3.2)$$

$k_{Q_{clin},Q_{msr}}^{f_{clin},f_{msr}}$ for the two diodes was obtained from Charles *et al*[16], a study which used exactly the same Monte Carlo model of the linear accelerator as in this study. $k_{Q_{clin},Q_{msr}}^{f_{clin},f_{msr}}$ for the PinPoint chamber was taken from Francescon *et al*[25]. It must be noted that the values from Franscescon *et al* were calculated using simulations of an Elekta Synergy and a Siemens Primus linear accelerator. Therefore these values may not necessarily translate to a Varian iX linear accelerator. However in this section, only the normalized change in OPF is quantified (see equation 1) and therefore any small systematic uncertainty in $k_{Q_{clin},Q_{msr}}^{f_{clin},f_{msr}}$ will have minimal effect on the aim of this section.

The diodes have an active area with a diameter of 1.1 mm in the perpendicular-to-beam direction, while the diameter of the PinPoint chamber in this direction is 2 mm, therefore volume averaging may have an influence on the results. More importantly however, the non-water equivalence of these detectors was also tested.

3.2.2 A theoretical definition of very small field size

To establish a theoretical definition of very small field sizes, the change in each scatter factor component was examined in detail. The physical interaction that dominates the cause of the rapid reduction in relative dose, as a function of decreasing field size, was quantified and leads to the establishment of a working theoretical definition of a very small field.

The OPF (which is the total scatter factor) can be separated into collimator scatter factor and phantom scatter factor[35].

$$S_{cp} = S_c S_p \qquad (3.3)$$

S_c is the collimator scatter factor and S_p is the phantom scatter factor. In this work the collimator scatter factor has been further separated to account for primary source occlusion effects and the traditional effects such as the flattening filter and collimator scatter[36].

$$S_c = S_{cs} S_{occ} \qquad (3.4)$$

S_{occ} is the change in output factor due to primary source occlusion and S_{cs} is the change in collimator scatter factor due to the remaining head scatter. Note that S_{occ} as defined in this study is different to that used by Scott *et al*[36], who use an additive approach, rather than the multiplicative approach seen in equation 3.4.

The phantom scatter has also been separated into components that relate to photon scatter and lateral electronic disequilibrium[14].

$$S_p = S_{phot} S_{ee} \qquad (3.5)$$

S_{phot} is the change in phantom scatter due to photon scatter within the phantom. S_{ee} is the change in phantom scatter due to the loss of lateral electronic equilibrium at the point of measurement.

Throughout this work S_{cs}, S_{occ}, S_{phot} and S_{ee} were each plotted as a function of field size in order to quantify how each scatter component affects the change in relative dose at the point of measurement along the central axis. The field size at which the most dominant factor begins to cause a 1 % change in relative dose per 1 mm in field size change was then used as the theoretical definition of a very small field.

Simulation of collimator factor and phantom scatter

The collimator scatter factor, S_c, was calculated in a similar manner to Fenwick *et al*[14]. Specifically, the dose to the small cylindrical volume of water described above was simulated surrounded by air in place of the water phantom. This was performed for all field sizes and the results were normalized to the 100 mm field size dose. The phantom scatter factor, S_p, was then calculated using equation 3.3.

Simulation of source occlusion and collimator scatter components

The simulations used for the collimator scatter factor, S_c, were repeated using BEAMnrc phase-space files that were created using a pencil beam electron source incident on the linear accelerator target. Specifically the electron spot size was set to 0.0001 mm FWHM (whereas the actual electron spot size was equal to 1.2 mm FWHM). This eliminated the effects of source occlusion caused by the finite size of the electron source. The photon spot size emanating from the target would still be finite due to electron scatter in the target, however it was assumed to be small enough not to be occluded by the smallest field size used in this study (4 mm). Therefore this was considered a direct calculation of S_{cs}. S_{occ} was then calculated using equation 3.4.

Simulation of photon scatter and lateral electronic disequilibrium

The photon scatter factor, S_{phot}, was calculated using the procedure outlined by Fenwick *et al*[14]. That is, the total scatter factor simulations were repeated with the electron cut off energy increased to 30 MeV (much greater than the energy of all electrons simulated) in the phantom. This excluded electron transport and thus any changes in the total scatter factor can then be attributed to photon scatter alone (assuming that there is transient charged particle equilibrium surrounding the dose scoring volume). For simplicity this will be referred to as the total scatter factor that results from photons only, "$S_{cp(phot)}$". The effect of photon scatter in the phantom was then calculated by factoring out the collimator scatter factor:

$$S_{phot} = \frac{S_{cp(phot)}}{S_c} \qquad (3.6)$$

The phantom scatter component caused by lateral electronic disequilibrium, S_{ee}, was assessed using equations 3.3, 3.5 and 3.6:

$$S_{ee} = \frac{S_{cp}}{S_{cp(phot)}} \qquad (3.7)$$

Quantifying the change in dose component with field size

For comparison, all calculated factors were plotted against the simulated field size. The change in factor as a function of field size was also calculated as follows:

$$\frac{\Delta S_*}{\Delta x}\left(x - \frac{1}{2}\right) = \frac{2[S_*(x) - S_*(x-1)]}{[S_*(x) + S_*(x-1)]} \qquad (3.8)$$

Where x is the size of the field and * is used as a general indicator of any factor. In this study Δx was constant and equal to 1 mm and therefore will be left out of all subsequent notations. ΔS_c, ΔS_{phot} and ΔS_{ee} were plotted as a function of field size. With the exception of the first and last data points, a moving average filter (using 1 data point each side) was applied to smooth out any residual low level statistical noise in the MC output simulations. The field size at which the most dominant factor

began to have the highest ΔS_* value was used as the threshold for the theoretical definition of a very small field size. As will be shown, this was the field size where ΔS_{ee} became significantly larger than the other factors.

3.3 RESULTS

3.3.1 Practical definition of very small field size

The maximum error induced by collimator positioning errors and detector positioning errors as a function of field size is displayed in figure 3.1. A field size error of 1 mm had a much larger affect on the OPF than did an error of 1 mm in detector position (in the plane of the upper-jaw). A field size error of 1 mm caused an OPF change of more than 1 % at field sizes of ≤ 15 mm. One could therefore take this value as a practical very small field definition for use in clinical practice for a 6 MV beam on a Varian iX linear accelerator.

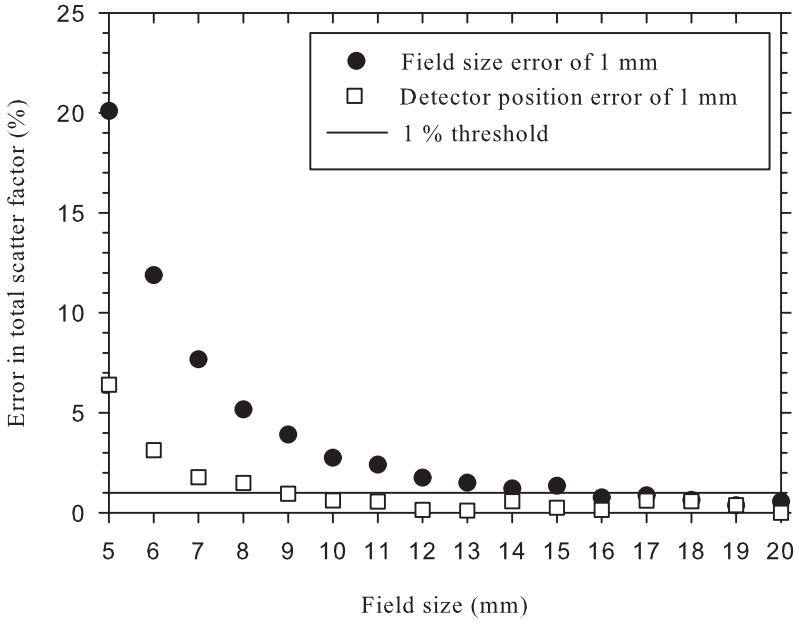

Figure 3.1. The error in OPF caused by a field size error of 1 mm and a detector positioning error of 1 mm. The total statistical uncertainty from the Monte Carlo simulations was 0.3 % (approximately equal to the marker size).

Figure 3.2 shows how the maximum error in OPF cause by a collimator positioning error is affected by detector volume averaging. It is clear that the threshold of very small field size is independent of detector size (up to 3 mm). Figure 3.3 displays how the maximum error in OPF caused by a collimator positioning error is affected by the use of real, non-water-equivalent detectors. It is apparent that OPFs measured with detectors of higher density than water are less affected by a collimator position error, while the air based ion chamber showed an increase in dependence on field size error. The practical threshold of 15 mm was unaffected by the use of realistic detectors.

3.3.2 Theoretical definition of very small field size

S_{cp}, S_c and S_p are displayed in figure 3.4. S_p appears to decrease at a greater rate with decreasing field size than S_c. In figure 3.5, S_c is separated into S_{cs} and S_{occ}. Figure 3.6 shows S_p separated into S_{phot} and S_{ee}. The rapid change in S_c for field sizes of side less than 8 mm is also shown for S_{occ}. It can be seen in figure 3.5 that there is no sudden decrease in S_{cs}, validating the assumption that the photon source used to obtain S_{cs} was not occluded by the field sizes used in this study. Note that S_{occ} cannot be greater than 1 by definition, but may appear so due to statistical uncertainty. The large decrease in S_p at small field sizes is clearly due to changes in S_{ee} (see figure 3.6). Figure 3.7 displays ΔS_c, ΔS_{phot} and ΔS_{ee} as a function of field size. One can see that ΔS_{ee} is significantly larger than ΔS_c and ΔS_{phot} for field sizes of 12 mm and less.

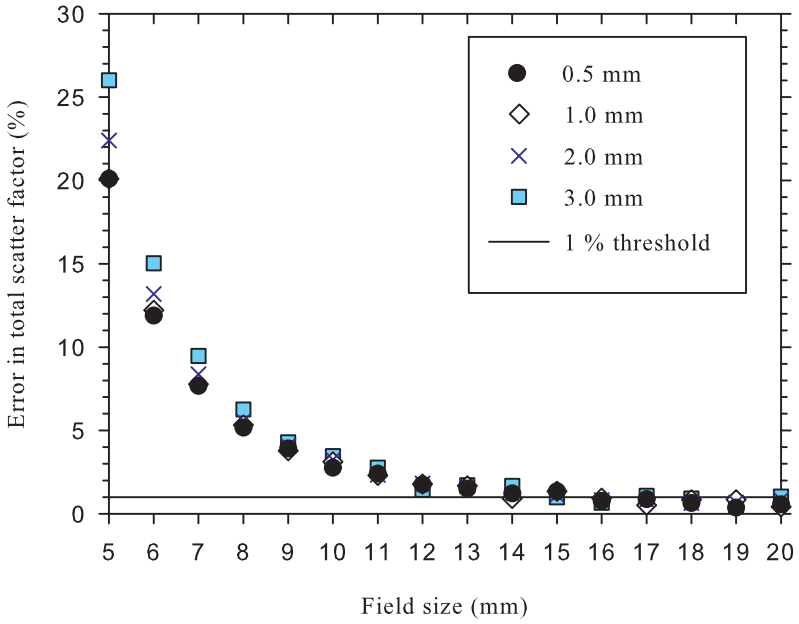

Figure 3.2. The error in OPF caused by a field size error of 1 mm, simulated using scoring volumes of various widths (non-beam direction) from 0.5 mm to 3 mm. The total statistical uncertainty from the Monte Carlo simulations was equal to 0.3 % (approximately equal to the marker size).

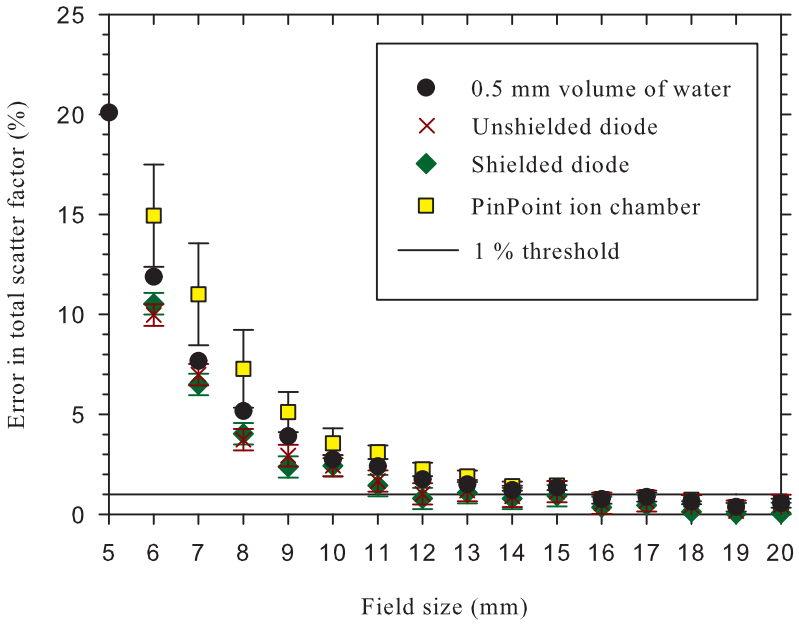

Figure 3.3. The error in uncorrected OPF using three detectors caused by a field size error of 1 mm. Also shown is the small water volume, which had a Monte Carlo statistical uncertainty equal to 0.3 % (approximately equal to the marker size). The uncertainty for each detector is shown as error bars (calculated from the papers which contained the respective $k_{Q_{clin},Q_{msr}}^{f_{clin},f_{msr}}$ values[16, 25]).

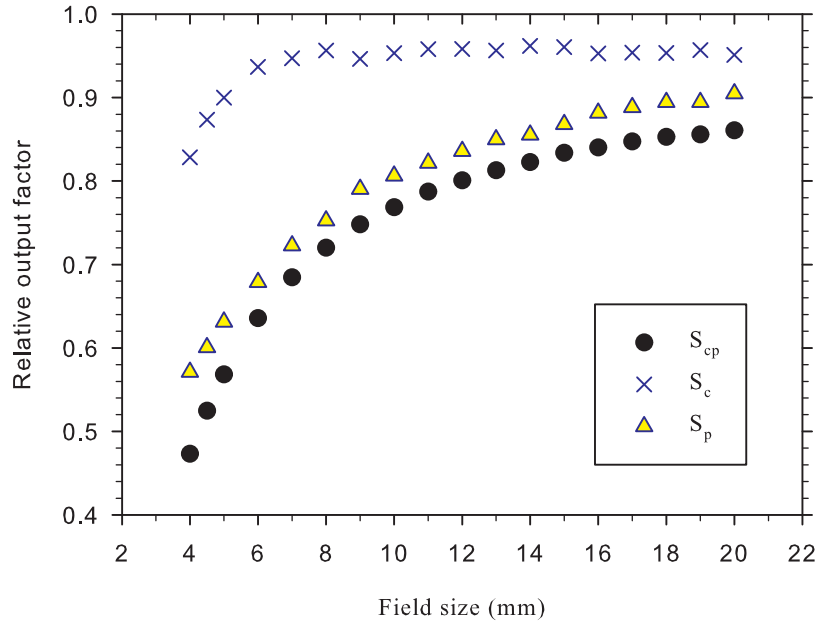

Figure 3.4. Scp, Sc, and Sp as a function of field size. All factors are normalized to a field size of 100 mm. The Monte Carlo statistical uncertainty was 0.3 % (smaller than the marker size).

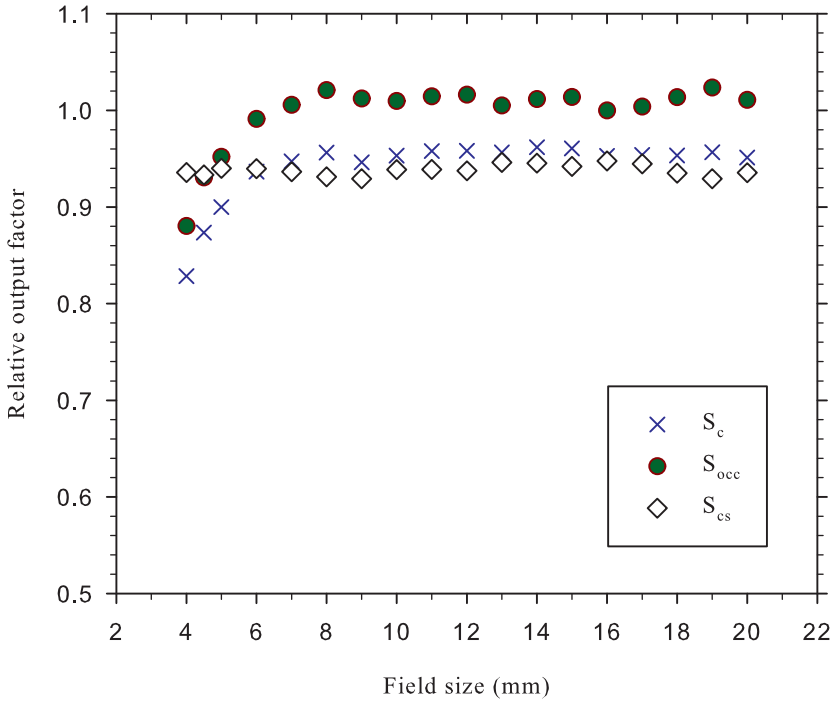

Figure 3.5. Sc, Socc, and Scs as a function of field size. All factors are normalized to a field size of 100 mm. The Monte Carlo statistical uncertainty is 0.5 % (approximately equal to the marker size).

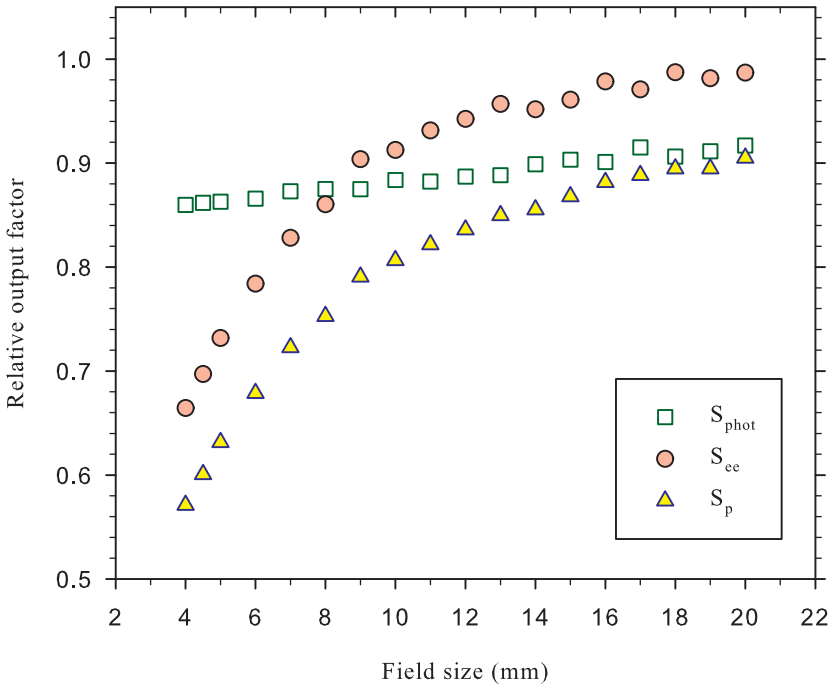

(a)

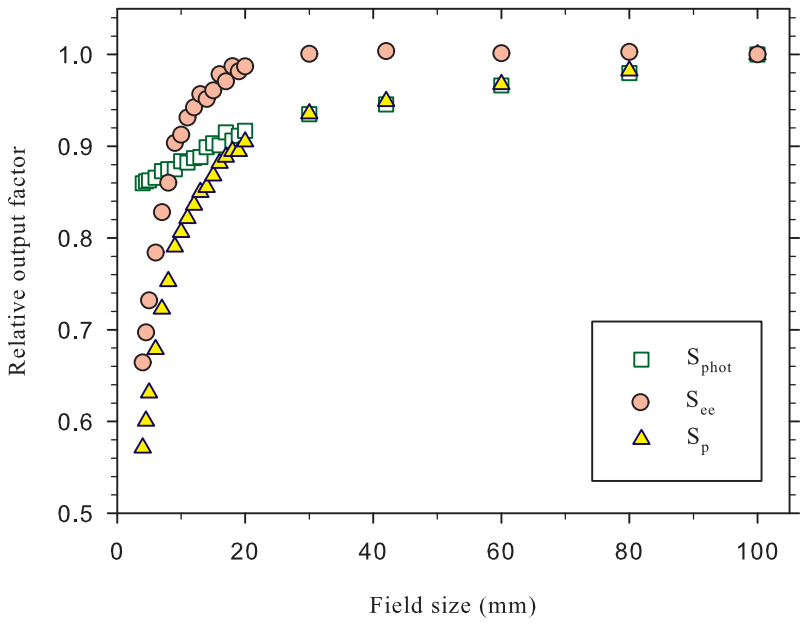

(b)

Figure 3.6. Sp, Sphot and See as a function of field size. All factors are normalized to a field size of 100 mm. The Monte statistical uncertainty was 0.5 % (approximately equal to the marker size). The factors for field sizes from 4 – 20 mm are shown in detail in (a). All factors up to 100 mm are shown in (b).

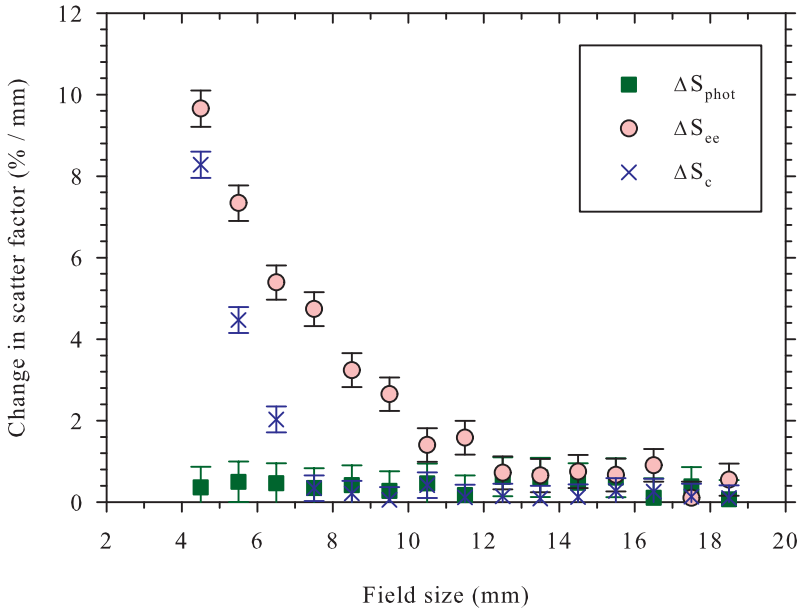

Figure 3.7. The change in scatter factor with field size: ΔS_c, ΔS_{phot}, ΔS_{ee}. The error bars indicate the raw Monte Carlo statistical uncertainty (pre-smoothing).

3.4 DISCUSSION

The change in phantom scatter was more pronounced than the change in collimator scatter factor at small field sizes (see figure 3.4). For field sizes > 30 mm the change in phantom scatter was entirely attributed to the change in photon scatter within the phantom (see figure 3.6(b)); that is S_{ee} was equal to 1.000 at field sizes > 30 mm. At field sizes smaller than 30 mm, lateral electronic disequilibrium caused a reduction in phantom scatter. This lent credence to the current notion that field sizes of less than around 30 mm should be considered small[2]. However, the rate of change in lateral electronic disequilibrium was small above field sizes of 12 mm (see figure 3.7). For example, S_{ee} was equal to 0.987 and 0.971 at field sizes of 20 mm and 17 mm respectively. At field sizes below 12 mm, lateral electronic disequilibrium increased sharply with decreasing field size. Based on these results, and the definitions used in this work to define a very small field, it can be concluded that a square field size of side 12 mm should be considered theoretically very small for a 6 MV beam.

The practical threshold of very small field (15 mm) was unaffected by the use of realistic detectors (see figures 3.2 and 3.3). The effect of volume averaging in isolation for detectors up to 3 mm in size was only noticeable at field sizes of ≤ 8 mm. This was also shown by Scott *et al*[12]. The inherent over-response of the diodes, which increases with decreasing field size, meant that OPFs measured with detectors containing high density materials were less susceptible to field size uncertainties. Conversely, the air-based ion chamber measurements were more susceptible. Importantly, neither case deviated substantially from the results of the small volume of water (see figure 3.1) at field sizes larger than 12 mm. This is coincident with the theoretical threshold of a very small field size and therefore suggests that the density of the detector becomes increasingly important when lateral electronic disequilibrium breaks down significantly, or put more succinctly – at very small field sizes. This effect is consistent with the findings of other studies[12, 14, 15].

Below field sizes of 8 mm the effects of source occlusion were a prominent component of the decrease in relative dose (see figures 3.5 and 3.7). However, at a field size of 12 mm this effect was negligible. In this study the linear accelerator jaws on a Varian iX were used to collimate the fields, however common collimation systems that are used for small field patient treatments (for example cones or some designs of multi-leaf collimators) are typically placed lower in the treatment head, which would result in less source occlusion.

The electron spot size also affects the amount of source occlusion. In this study a circular spot size of 1.2 mm FWHM was used for the Varian iX linear accelerator. Francescon *et al* have used similar Monte Carlo methods to establish the spot size of a Siemens Primus and an Elekta Precise linear accelerator to be elliptical and 0.5 mm x 0.8 mm, and 0.9 mm x 2.0 mm FWHM respectively[25]. McKerracher and Thwaites showed that phantom scatter is independent of machine design for field sizes of side as small as 5 mm[7]. Therefore, one can infer that the phantom scatter results shown in this work will be applicable to other machines; however the effect of source occlusion would need to be verified, particularly if the source was larger than that used in this study.

According to the practical definition of very small field size, and the results shown in this study, a field size ≤ 15 mm should be considered very small for 6 MV beams. This is larger than the theoretical definition of 12 mm. The error in OPF caused by a 1 mm field size (collimation) error at a field size of 12 mm was 1.7 %, and increased sharply with decreasing field size below 12 mm (see figure 3.1). If a tolerance of 2 % was used for the acceptable change in OPF, field sizes ≤ 12 mm would be considered very small. Alternatively, if the maximum collimation error was 0.5 mm instead of 1.0 mm, then again 12 mm would be the practical threshold of a very small field.

Overall, the work suggests that for field sizes larger than 15 mm OPFs can be measured in a 'standard' experimental manner. That is to say, the requirement for profiles to be measured at the same time for each field size setting is not required and the results will generally be within a 1% uncertainty tolerance, whereas for field sizes smaller than 15 mm, the more detailed experimental approach to OPF measurement is required. The theoretical definition of very small field indicates that a value of 12 mm denotes a transition, but the more conservative approach is as above, to take profiles at the same time as output factors for field sizes of ≤ 15 mm. In this study, this has been considered specifically for a 6 MV photon beam from a Varian iX linear accelerator, but the findings are likely to be generalizable to other beams of similar quality.

Detector selection is still an important part of small field dosimetry, independent of the results of this study. For example most commercial diodes will have some over-response at a field size of 12 mm and need corrections to the raw output ratios[18, 24], whilst detectors with dimensions which are large in comparison to the field size (dose profile) would clearly have significant volume averaging. One must therefore not use the results of this study as an indication that standard dosimetry devices such as ion chambers can be used at these field sizes. An appropriate detector choice should made by each user based on the smallest field size to be measured. After correct detector selection is made, the results from this study can be used as a threshold for when the extremely careful experimental methodology needed for very small field dosimetry is required.

3.5 CONCLUSIONS

This work introduces the concept of a very small field and establishes two scientific definitions of the threshold of very small field size. Field sizes $\leq$ 12 mm are found to be theoretically very small for 6 MV beams, based on the relatively large increase in lateral electronic disequilibrium. According to the practical definition, field sizes $\leq$ 15 mm can be considered very small for 6 MV beams at a 1% output factor uncertainty level. If it is acceptable to increase the latter to 2%, then the practical definition of very small field size would be 12 mm, in line with the theoretical definition. This work gave a clear indication that careful experimental methodology, with profiles measured at the same time as output factors for each field size setting is required for field sizes $\leq$ 12 mm and more conservatively for field sizes $\leq$ 15mm. These results do not consider detector selection, which is an independent consideration, thus these recommendations should be applied in addition to all the usual considerations for small field dosimetry, including careful detector selection.

3.6 ACKNOWLEDGEMENTS

This work was funded by the Australian Research Council in partnership with the Queensland University of Technology (QUT), the Wesley Research Institute and Premion (Linkage Grant No. LP110100401). Computational resources and services used in this work were provided by the High Performance Computing and Research Support Unit, (QUT), Brisbane, Australia.

3.7 REFERENCES

1 I.J. Das, G.X. Ding, A. Ahnesjö, "Small fields: Nonequilibrium radiation dosimetry," Medical Physics **35**, 206 (2008).

2 R. Alfonso, P. Andreo, R. Capote, M.S. Huq, W. Kilby, P. Kjäll, T.R. Mackie, H. Palmans, K. Rosser, J. Seuntjens, W. Ullrich, S. Vatnitsky, "A

new formalism for reference dosimetry of small and nonstandard fields," Medical Physics **35**, 5179 (2008).

[3] IPEM, "Small Field MV Photon Dosimetry," IPEM Report No.2010).

[4] G. Cranmer-Sargison, P.H. Charles, J.V. Trapp, D.I. Thwaites, "A methodological approach to reporting corrected small field relative outputs," Radiother Oncol **109**, 350-355 (2013).

[5] C. McKerracher, D.I. Thwaites, "Head scatter factors for small MV photon fields. Part I: a comparison of phantom types and methodologies," Radiother Oncol **85**, 277-285 (2007).

[6] C. McKerracher, D.I. Thwaites, "Head scatter factors for small MV photon fields. Part II: the effects of source size and detector," Radiother Oncol **85**, 286-291 (2007).

[7] C. McKerracher, D.I. Thwaites, "Phantom scatter factors for small MV photon fields," Radiother Oncol **86**, 272-275 (2008).

[8] G. Cranmer-Sargison, S. Weston, N.P. Sidhu, D.I. Thwaites, "Experimental small field 6MV output ratio analysis for various diode detector and accelerator combinations," Radiother Oncol **100**, 429-435 (2011).

[9] H. Bouchard, J. Seuntjens, I. Kawrakow, "A Monte Carlo method to evaluate the impact of positioning errors on detector response and quality correction factors in nonstandard beams," Phys Med Biol **56**, 2617-2634 (2011).

[10] G. Cranmer-Sargison, P.Z. Liu, S. Weston, N. Suchowerska, D.I. Thwaites, "Small field dosimetric characterization of a new 160-leaf MLC," Phys Med Biol **58**, 7343-7354 (2013).

[11] G.X. Ding, F. Ding, "Beam characteristics and stopping-power ratios of small radiosurgery photon beams," Phys Med Biol **57**, 5509-5521 (2012).

[12] A.J. Scott, S. Kumar, A.E. Nahum, J.D. Fenwick, "Characterizing the influence of detector density on dosimeter response in non-equilibrium small photon fields," Phys Med Biol **57**, 4461-4476 (2012).

[13] H. Bouchard, J. Seuntjens, J.-F. Carrier, I. Kawrakow, "Ionization chamber gradient effects in nonstandard beam configurations," Medical Physics **36**, 4654 (2009).

[14] J.D. Fenwick, S. Kumar, A.J. Scott, A.E. Nahum, "Using cavity theory to describe the dependence on detector density of dosimeter response in non-equilibrium small fields," Phys Med Biol **58**, 2901-2923 (2013).

[15] T.S. Underwood, H.C. Winter, M.A. Hill, J.D. Fenwick, "Detector density and small field dosimetry: Integral versus point dose measurement schemes," Medical Physics **40**, 082102 (2013).

[16] P.H. Charles, S.B. Crowe, T. Kairn, R.T. Knight, B. Hill, J. Kenny, C.M. Langton, J.V. Trapp, "Monte Carlo-based diode design for correction-less small field dosimetry," Phys Med Biol **58**, 4501-4512 (2013).

[17] P.H. Charles, S.B. Crowe, T. Kairn, J. Kenny, J. Lehmann, J. Lye, L. Dunn, B. Hill, R.T. Knight, C.M. Langton, J.V. Trapp, "The effect of very small air gaps on small field dosimetry," Phys Med Biol **57**, 6947-6960 (2012).

[18] G. Cranmer-Sargison, S. Weston, J.A. Evans, N.P. Sidhu, D.I. Thwaites, "Monte Carlo modelling of diode detectors for small field MV photon dosimetry: detector model simplification and the sensitivity of correction factors to source parameterization," Phys Med Biol **57**, 5141-5153 (2012).

[19] F. Crop, N. Reynaert, G. Pittomvils, L. Paelinck, C. De Wagter, L. Vakaet, H. Thierens, "The influence of small field sizes, penumbra, spot size and measurement depth on perturbation factors for microionization chambers," Phys Med Biol **54**, 2951-2969 (2009).

[20] T.S. Underwood, H.C. Winter, M.A. Hill, J.D. Fenwick, "Mass-density compensation can improve the performance of a range of different detectors under non-equilibrium conditions," Phys Med Biol **58**, 8295-8310 (2013).

[21] E. Pantelis, A. Moutsatsos, K. Zourari, L. Petrokokkinos, L. Sakelliou, W. Kilby, C. Antypas, P. Papagiannis, P. Karaiskos, E. Georgiou, I. Seimenis, "On the output factor measurements of the CyberKnife iris collimator small fields: Experimental determination of the k(Q(clin),Q(msr)) (f(clin),f(msr)) correction factors for microchamber and diode detectors," Medical Physics **39**, 4875-4885 (2012).

[22] A. Ralston, P. Liu, K. Warrener, D. McKenzie, N. Suchowerska, "Small field diode correction factors derived using an air core fibre optic scintillation dosimeter and EBT2 film," Phys Med Biol **57**, 2587-2602 (2012).

[23] C. Bassinet, C. Huet, S. Derreumaux, G. Brunet, M. Chea, M. Baumann, T. Lacornerie, S. Gaudaire-Josset, F. Trompier, P. Roch, G. Boisserie, I. Clairand, "Small fields output factors measurements and correction factors determination for several detectors for a CyberKnife and linear accelerators

equipped with microMLC and circular cones," Medical Physics **40**, 071725 (2013).

[24] G. Cranmer-Sargison, S. Weston, J.A. Evans, N.P. Sidhu, D.I. Thwaites, "Implementing a newly proposed Monte Carlo based small field dosimetry formalism for a comprehensive set of diode detectors," Medical Physics **38**, 6592-6602 (2011).

[25] P. Francescon, S. Cora, N. Satariano, "Calculation of k(Q(clin),Q(msr)) (f(clin),f(msr)) for several small detectors and for two linear accelerators using Monte Carlo simulations," Medical Physics **38**, 6513-6527 (2011).

[26] P. Francescon, W. Kilby, N. Satariano, S. Cora, "Monte Carlo simulated correction factors for machine specific reference field dose calibration and output factor measurement using fixed and iris collimators on the CyberKnife system," Phys Med Biol **57**, 3741-3758 (2012).

[27] D. Czarnecki, K. Zink, "Monte Carlo calculated correction factors for diodes and ion chambers in small photon fields," Phys Med Biol **58**, 2431-2444 (2013).

[28] D.T.B. P. Andreo, K. Hohlfeld, M. S. Huq, T. Kanai, F. Laitano, V., a.S.V. G. Smyth, "Absorbed dose determination in external beam radiotherapy," Technical Report Series No 3982000).

[29] E.E. Klein, J. Hanley, J. Bayouth, F.-F. Yin, W. Simon, S. Dresser, C. Serago, F. Aguirre, L. Ma, B. Arjomandy, C. Liu, C. Sandin, T. Holmes, "Task Group 142 report: Quality assurance of medical accelerators," Medical Physics **36**, 4197 (2009).

[30] D.W.O. Rogers, B.A. Faddegon, G.X. Ding, C.M. Ma, J. We, "BEAM: A Monte Carlo code to simulate radiotherapy treatment units," Medical Physics **22**, 503 - 524 (1995).

[31] T. Kairn, T. Aland, R.D. Franich, P.N. Johnston, M.B. Kakakhel, J. Kenny, R.T. Knight, C.M. Langton, D. Schlect, M.L. Taylor, J.V. Trapp, "Adapting a generic BEAMnrc model of the BrainLAB m3 micro-multileaf collimator to simulate a local collimation device," Phys Med Biol **55**, N451-463 (2010).

[32] T. Kairn, J. Kenny, S.B. Crowe, A.L. Fielding, R.D. Franich, P.N. Johnston, R.T. Knight, C.M. Langton, D. Schlect, J.V. Trapp, "Technical Note: Modeling a complex micro-multileaf collimator using the standard BEAMnrc distribution," Medical Physics **37**, 1761 (2010).

[33] I. Kawrakow, E. Mainegra-Hing, F. Tessier, B.R.B. Walters, "The EGSnrc C++ class library, ," NRC Report PIRS-898 (rev A)2009).

[34] ISO, 1995.

[35] F.M. Khan, *The Physicis of Radiation Therapy - Third Edition*. (Lippincott Williams & Wilkins, Philadelphia, 2003).

[36] A.J.D. Scott, A.E. Nahum, J.D. Fenwick, "Monte Carlo modeling of small photon fields: Quantifying the impact of focal spot size on source occlusion and output factors, and exploring miniphantom design for small-field measurements," Medical Physics **36**, 3132 (2009).

Chapter 4: The effect of very small air gaps on small field dosimetry

P H Charles[1], S B Crowe[1], T Kairn[2], J Kenny[3], J Lehmann[3], J Lye[3], L Dunn[3], B Hill[2], R T Knight[2], C M Langton[1] and J V Trapp[1]

[1] School of Chemistry, Physics and Mechanical Engineering, Queensland University of Technology, Brisbane, Australia

[2] Premion, The Wesley Medical Centre, Auchenflower, QLD, Australia

[3] The Australian Clinical Dosimetry Service, Australian Radiation Protection and Nuclear Safety Agency, Yallambie, Vic, Australia

Journal: Physics in Medicine and Biology

Status: Published October 2012

Citations to date: 7

STATEMENT OF JOINT AUTHORSHIP

Title: The effect of very small air gaps on small field dosimetry

Authors: Paul Charles; Scott Crowe; Tanya Kairn; John Kenny; Joerg Lehmann; Jessica Lye; Leon Dunn; Brendan Hill; Richard Knight; Christian Langton; Jamie Trapp;

Paul Charles (candidate)
Project concept, direction and design. Performed all Monte Carlo simulations. Analysed an interpreted all results. Wrote the manuscript.

Scott Crowe
OLSD measurements. Assisted reading out OSLDs. Supplied Monte Carlo model of linac. General advice and supervision as required. Edited manuscript.

Tanya Kairn
OLSD measurements. Assisted reading out OSLDs. Supplied Monte Carlo model of linac. General advice and supervision as required. Edited manuscript

John Kenny
Co-ordination of OSLD measurements. Supervision of OSLD read-out in Melbourne. Editing of manuscript.

Joerg Lehmann
Assisted analysis and interpretation of OSLD results. Edited of manuscript.

Jessica Lye
Readout OSLD results. Analysed OSLD results.

Leon Dunn
Readout OSLD results. Analysed OSLD results.

Brendan Hill

General advice and supervision as required. Edited manuscript

Richard Knight

General advice and supervision as required.

Christian Langton

General advice and supervision as required.

Jamie Trapp

General advice and supervision as required. Edited manuscript.

ABSTRACT

The purpose of this study was to investigate the effect of very small air gaps (less than 1 mm) on the dosimetry of small photon fields used for stereotactic treatments. Measurements were performed with optically stimulated luminescent dosimeters (OSLDs) for 6 MV photons on a Varian 21iX linear accelerator with a Brainlab μMLC attachment for square field sizes down to 6 mm × 6 mm. Monte Carlo simulations were performed using EGSnrc C++ user code cavity. It was found that the Monte Carlo model used in this study accurately simulated the OSLD measurements on the linear accelerator. For the 6 mm field size, the 0.5 mm air gap upstream to the active area of the OSLD caused a 5.3 % dose reduction relative to a Monte Carlo simulation with no air gap. A hypothetical 0.2 mm air gap caused a dose reduction > 2 %, emphasizing the fact that even the tiniest air gaps can cause a large reduction in measured dose. The negligible effect on an 18 mm field size illustrated that the electronic disequilibrium caused by such small air gaps only affects the dosimetry of the very small fields. When performing small field dosimetry, care must be taken to avoid any air gaps, as can be often present when inserting detectors into solid phantoms. It is recommended that very small field dosimetry is performed in liquid water. When using small photon fields, sub-millimetre air gaps can also affect patient dosimetry if they cannot be spatially resolved on a CT scan. However the effect on the patient is debatable as the dose reduction caused by a 1 mm air gap, starting out at 19% in the first 0.1 mm behind the air gap, decreases to < 5 % after just 2 mm, and electronic equilibrium is fully re-established after just 5 mm.

4.1 INTRODUCTION

In megavoltage photon beam dosimetry a "small field" is defined as a field with dimensions smaller than the lateral range of the charged particles that contribute to dose [1]. That is, unlike "standard fields", particles that depart the centre of a radiation field are not replaced by particles from the outer area of the field. This results in several complicated issues as summarized by Das *et al* [2] and Taylor *et al* [3]. Depending on the size of the low density cavity or gap, even standard fields experience a loss in charged particle equilibrium [4-6]. The presence of a low density material such as lung or air exacerbates the problem as the secondary charged particles can travel even further in these media.

Air gaps have been shown to cause a dose reduction in megavoltage dosimetry immediately downstream, which will then build back up as electronic equilibrium is re-established [4-9]. These studies have concluded that the magnitude of the dose reduction is enhanced by increasing the beam energy, increasing the air gap size, or decreasing the field size.

Solberg *et al* [8] calculated the dose reduction that resulted from air gaps as small as 3 mm. They measured this effect using 10 MV stereotactic fields as small as 5 mm in diameter. The 3 mm air gap caused a dose reduction of 21 % for a 10 mm field size which increased to approximately 35 % for a 5 mm field size. The authors also noted that the loss in electronic equilibrium that caused this dose reduction also caused a widening of the beam profiles immediately beyond the air gap. For example, the full width tenth maximum for the 10 mm field size increased from 15.5 mm with no air gap to 19.0 mm with a 3 mm air gap. Rustgi *et al* [7] performed a similar study with 6 MV photons. In this case a 3 mm air gap caused an 11 % dose reduction for a 12.5 mm circular field. The dose reduction for a 25 mm diameter field was 3 %. For a 6 MV photon beam, such thin air gaps only affect the very small field sizes that are used in stereotactic treatments. The dose build-up beyond the air gap was only 4-6 mm before electronic equilibrium was re-established. For the 6 MV, 12.5 mm field, the penumbral width (90 % - 10 %) of a profile immediately below the location of

the air gap increased from 4.4 mm with no air gap to 6.8 mm when a 3 mm air gap was introduced.

Although the effect on electronic disequilibrium of field size and air gap size is well established, the potential problem of very small (less than 1 mm) air gaps is not covered in the literature. The principal aim of this work is to establish the effect of very small air gaps on small field dosimetry. Air gaps of this magnitude can complicate the dosimetry in many situations. These include their intrinsic existence in certain dosimeters such as optically stimulated luminescence dosimeters (OSLD) casings, and the potential presence of small air gaps in solid phantom dosimetry. Also, such small air gaps cannot be resolved by typical CT scanners used for patient treatment planning and therefore add dosimetric uncertainty to the patient's radiation treatment plan, over and above the accuracy of the dose calculation algorithm.

Output factors of 6 MV small photon fields, down to a size of 6 mm square were measured with Landauer® nanoDots™ (Landauer, Inc., Glenwood, IL). These detectors have intrinsic air gaps of approximately 0.5 mm around the active volume. Extensive Monte Carlo simulations of the OSLDs were performed to analyse the effect of the air gap in detail.

4.2 METHODOLOGY

4.2.1 OSLD measurements

Output factors were measured using Landauer nanoDot OSLDs (Landauer, Inc., Glenwood, IL) for square fields with the following side lengths: 6 mm, 12 mm, 18 mm, 24 mm, 30 mm, 42 mm, 60 mm, 80 mm and 98 mm. The results were normalized to the 98 mm square field. These detectors have intrinsic air gaps of approximately 0.5 mm around the active volume. OSLDs are generally used in radiation therapy for in vivo dosimetry [10-12]. There is much information in the literature on OSL dosimetry theory (see for example [12]).

The measurements were performed with 6 MV photons on a Varian 21iX linear accelerator (Varian Medical Systems, Palo Alto, CA) using the Brainlab M3 μMLC attachment (Brainlab, AG, Germany) for collimation. 6 mm and 98 mm were the smallest (centred on the central axis) and largest square field sizes possible respectively. The output factors were measured with the upper surface of the OSLD active volume at the depth of 15 mm in Plastic Water DT (CIRS, Norfolk, VA) at a source to surface distance of 100 cm. A custom holder for the OSLDs was also manufactured out of Plastic Water. The water equivalency of Plastic Water is well established (see for example [13]). Each measurement was repeated 5 times (with 5 separate OSLDs) to obtain an average. The error of the measurements was calculated as the standard deviation of the 5 readings. The OSLDs were part of the InLightTM OSL system (Landauer, Inc., Glenwood, IL) and were read out with the MicroStar reader.

4.2.2 Monte Carlo simulations

Extensive Monte Carlo simulations of the OSLDs were performed to analyse the effect of the air gap in detail.

Output factors with OSLDs.

Monte Carlo simulations of the OSLD experimental setup were performed and compared with OSLD measured output factors. Simulations in the same phantom but with all volumes assigned water were also performed to quantify the effect of the detector on output factors. The EGSnrc C++ user code cavity [14] was used to simulate the OSLD geometry. The input source was a previously modelled BEAMnrc [15] phase-space file of the linear accelerator which had been extensively commissioned [16, 17]. The only change to the model for this work was to slightly tune the spot size of the electrons incident onto the target. This ensured that the Monte Carlo simulations matched the machine measurements for output factors down to 6 mm as measured with a PTW T30016 photon diode (PTW, Freiburg, Germany). This is a procedure required to ensure the accuracy of small field simulations [18, 19]. In the phantom material, the electron and photon cut off energies were chosen to be 521 keV and 10

keV respectively. Inside the volume of the simulated OSLD they were reduced to 512 keV and 1 keV respectively for increased accuracy within the detector volume only.

The Monte Carlo simulations of the OSLDs were performed in two ways: firstly with only the Al_2O_3 active volume (5 mm diameter, 0.2 mm thick) in water; secondly with the chip encased in the 0.05 mm polyester binding foils, and the air that is within the OSLD holder (see Figure 4.1). The later geometry is identical to that simulated by Kerns et al [20]. In the beam direction, the size of the air gap was 0.49 mm both above and below the active volume. The plastic casing of the OSLD was not modelled (i.e. it was assumed to be water) as it was reported to be 0.036 cm thick and approximately water equivalent [10]. The small area of plastic directly to the sides (forming the "cup") of the OSLD active area was also expected to have negligible effect. Comparing the results of the two geometries described above enabled the effect of the surrounding air encasing (or air gap) to be isolated.

The Monte Carlo simulations of the OSLD setup were compared to the machine measurements with the OSLDs to verify the accuracy of the Monte Carlo model. They were also compared to Monte Carlo simulations of a phantom entirely assigned water (no detector) to quantify the accuracy of OSLDs for measuring small fields.

The effect of different components of the air gap.

The effect that the air gap had on dose was further isolated to different regions of the air encapsulation. Simulations were performed with three different versions of the geometry in Figure 4.1: using air in only one region of interest: to the sides of the active volume, upstream of the active area, and downstream of the active volume. For each of these simulations, the remainder of the geometry (except the active volume) was assigned water.

Removal of volume averaging.

Due to the large diameter of the OSLD active volume (5 mm) with respect to the smallest field simulated (6 mm x 6 mm), volume averaging may cloud any results found. Therefore, the Monte Carlo simulations were repeated with a hypothetical reduced diameter of 1 mm. The results were compared to the 5 mm active volume results to determine if volume averaging significantly affected the results of this study. Note that both active volumes had the same thickness (0.2 mm).

The effect of air gap size.

The size of the air gap above the OSLD active area was varied in 0.2 mm steps from 0.0 mm to 2.0 mm in order to quantify the magnitude of dose reduction for various small air gap sizes. This was performed for the field sizes mentioned above from 6 mm to 30 mm as

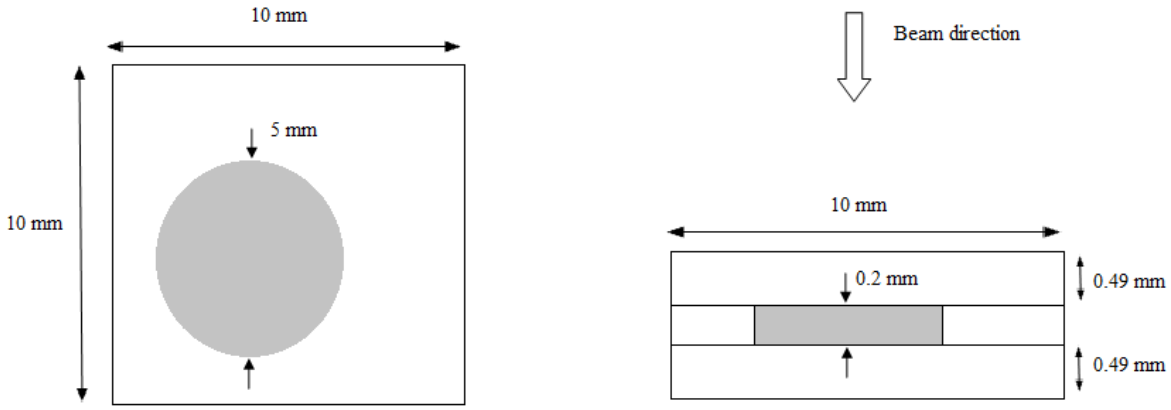

Figure 4.1. The Monte Carlo simulation geometry of the OSLD. The Al_2O_3 active area (grey) is encapsulated by an air gap (white) descriptive of the OSLD holder. The section view on the right hand side also has lines which define the three components of the surrounding air gap (upstream, sides and downstream). Note that the 0.05 mm polyester binding foils have been left out for clarity. Also note that the OSLD active volume is offset 1 mm in each dimension in the perpendicular to beam plane.

well as the 98 mm field. The air gap to the sides and downstream of the active volume were removed for these simulations in order to isolate the effect of the upstream air gap.

Angular and energy distributions of secondary electrons just beyond air gap.

To examine the observed electronic disequilibrium caused by such a small air gap in detail, the angular distribution and energy distribution of the secondary electrons at the air – active volume interface were plotted. For this the OSLD was modelled in BEAMnrc with the upstream to the active volume air gap only. A phase-space file was collected in the plane immediately below the air gap (i.e. immediately above the active area) and analysed using BEAMDP [21]. The angular and energy distributions at the same plane when no air gap was present were also simulated. This was performed for all field sizes mentioned above.

Re-establishment of electronic equilibrium beyond air gap.

The distance required to re-establish electronic equilibrium beyond the air gap for the 6 mm field size was established using the user code DOSXYZnrc [22]. For these simulations, a 1 mm air gap above the active area was modelled, and the rest of the geometry was set to water (including the active volume). The percentage depth dose beyond the air gap was modelled in 0.1 mm steps (the voxels were 1 mm × 1 mm in the perpendicular to beam directions). These results were compared to the results from a simulation with no air gap (all water) in order to see the extent of electronic disequilibrium with distance beyond the air gap.

4.3 RESULTS

4.3.1 Small field output factors measured with OSLDs

The Monte Carlo simulated output factors matched the output factors measured on the linear accelerator within 2 standard deviations of uncertainty for all field sizes. Given the relatively large size of the active area (5 mm) compared to the smallest field size (6 mm), the potential for disagreement was high. Figure 4.2 shows the comparison between the Monte Carlo simulated output factors and the measured output factors.

4.3.2 The effect of the air gap on OSLD results

A comparison between the simulation results with and without the air gap is shown in Figure 4.3. Also shown in Figure 4.3 are the Monte Carlo calculated output factors in water only (i.e. no detector present).

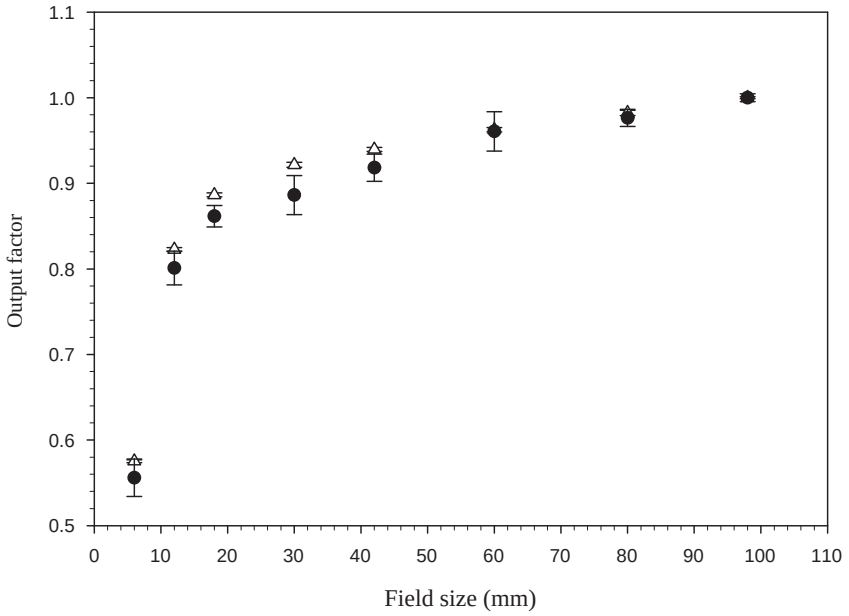

Figure 4.2. Comparison of OSLD measurements from a linear accelerator (black circles) to the complete Monte Carlo model of OSLD (white triangles) for small field output factors. The factors are normalized to the 98 mm square field. The error bars shown indicate one standard deviation of statistical error.

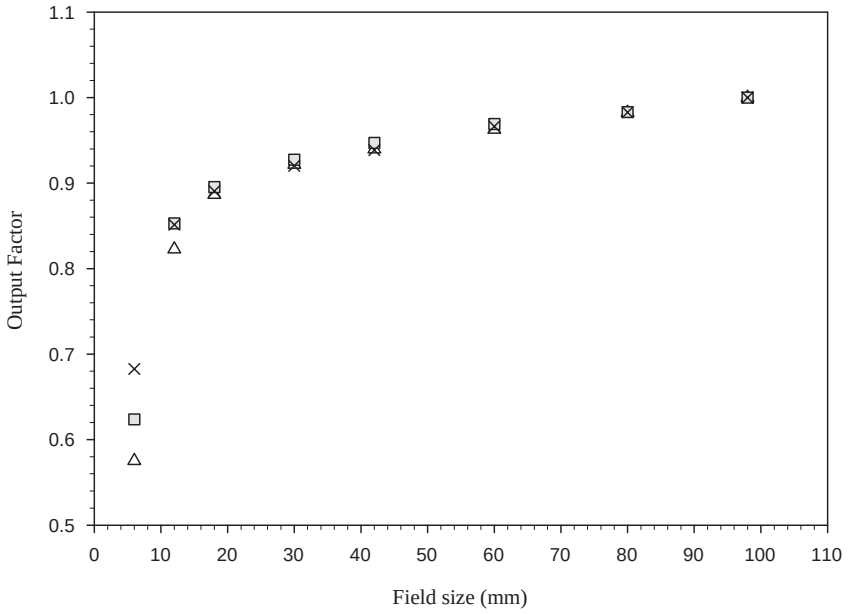

Figure 4.3. Monte Carlo simulated output factors of OSLDs both with the surrounding air gap (white triangles) and without the surrounding air gap (grey squares). Also shown are the output factors in a detector-less simulation (crosses).

Table 4.1 summarizes the effect that the 0.5 mm air gap has on the dose to the active volume as function of field size. The air gap has negligible effect on "normal" field sizes (> 30 mm), a very slight effect on the 18 mm field size increasing to a large effect on the 6 mm field size (-7.8 %). Therefore air gaps will play an important role in stereotactic dosimetry – heavily dependent on the size of the small field. The Al_2O_3 active volume by itself has negligible perturbation of the photon beam down to a field size of 30 mm. At the field size of 6 mm where the OSLD 'active volume only' simulation was 8.6 % lower than the water only simulation. The discrepancy at this field size is dominated by volume averaging as the detector (5 mm) is nearly as large as the field, where as the water only simulations were scored with a diameter of just 0.25 mm.

Table 4.1. The dose reduction to the OSLD active volume caused by the air encapsulation as a function of field size. The error column refers to statistical simulation uncertainty.

Field Size (mm)	Dose reduction (%)	Error (%)
6	-7.8	0.3
12	-3.6	0.3
18	-1.0	0.3
30	-0.7	0.4
42	-0.8	0.4
60	-0.7	0.4
80	-0.1	0.4
98	-0.1	0.3

4.3.3 The effect of different components of the air gap

Shown in Table 4.2 is the dose reduction caused by different components of the air gap (see Figure 1 for a schematic of the different components) for the 6 mm field

size. The air gap above (upstream to) the active area has the largest effect, as expected.

4.3.4 Removal of volume averaging

The comparison between the dose reduction to the active volume for the actual size of 5 mm, compared to a theoretical size of 1 mm is displayed in Table 4.2 for the 6 mm field size. There is an increased dose reduction due to air gap on sides of the active area from -0.1 % to -2.6 %. There are only small (1.2 %) changes to the dose reduction caused by the upstream and downstream air gaps.

Table 4.2. The dose reduction to the OSLD active volume caused by different components of the surrounding air gap. Displayed are the results for the real OSLD with a 5 mm diameter Al_2O_3 active volume, and a hypothetical OSLD with a 1 mm diameter Al_2O_3 active volume. The thickness of the active volume was 0.2 mm for both simulations, which corresponds to that of the real OSLD. Note that each result has a statistical uncertainty of 0.3 %.

Position of air gap	Dose reduction (%)	
	5 mm active area	1 mm active area
All (full air gap)	-7.8	-11.1
Upstream only	-5.3	-6.5
Sides only	-0.1	-2.6
Downstream only	-1.4	-2.6

4.3.5 The effect of air gap size

The effect of the air gap thickness in the beam direction is shown in Figure 4.4. It can be seen that the air gap has no effect on the 30 mm and 100 mm field sizes. There is a noticeable effect for the 12 mm field size and a large effect for the 6 mm field size. The dose reduction due to the air gap is linear with a regression of $R^2 = 0.995$ for the 12 mm field size and $R^2 = 0.998$ for the 6 mm field size. The dose reduction can be quantified as -3.9 % / mm and -11.5 % / mm for the 12 mm and 6 mm field sizes respectively.

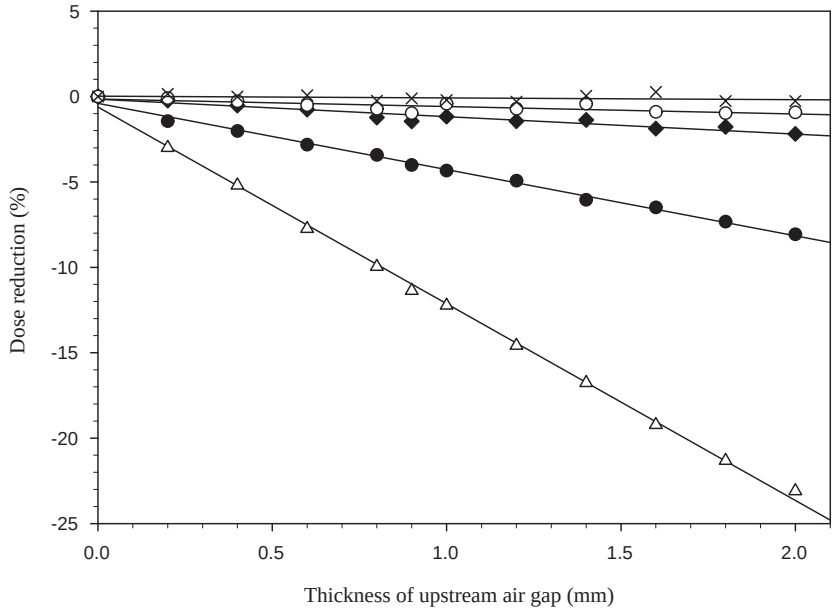

Figure 4.4. Dose reduction caused by varying thickness of upstream air gap size. Dose reduction refers to dose loss relative to a simulation with no air gaps. The results for the following field sizes are shown: 6 mm (white triangles), 12 mm (black circles), 18 mm (black diamonds), 30 mm (white circles) and 98 mm (crosses). A linear regression line of best fit is also shown for each data set.

4.3.6 Angular and energy distributions of secondary electrons just beyond air gap

The angular distributions at the proximal interface of the active area for 5 different field sizes: 6 mm, 12 mm, 18 mm, 30 mm, and 100 mm are plotted in Figure 4.5. Results for each field size are plotted for both simulations with and without the surrounding air gap in the OSLD. It can be seen from Figure 4.5 that all field sizes have effectively the same angular distribution when there is no air gap. The air gap has no affect on the angular distribution of the 30 mm and 100 mm field sizes but quite drastically reduces the number of electrons with a high angle of incidence in the 6 mm beam. This effect is magnified in terms of dose reduction by the fact that electrons with high angle of incidence have a lower energy (and therefore more easily stopped). This was confirmed by simulating the electron energy distribution both with and without the air gap for the 6 mm field size. These results are shown in Figure 4.6.

Simulations of the dose and angular distribution in different regions of the OSLD active area revealed that both of these were uniform across the active area for a 30 mm field size and that the presence of the air gap had no effect on either. The angular distribution results are shown in Figure 4.7. However, for the 6 mm field size there were a much greater number of electrons with low angle of incidence in the centre compared to the outer region of the active area. Also, the air gap effectively removed electrons with high angle of incidence from both regions (see Figure 4.8).

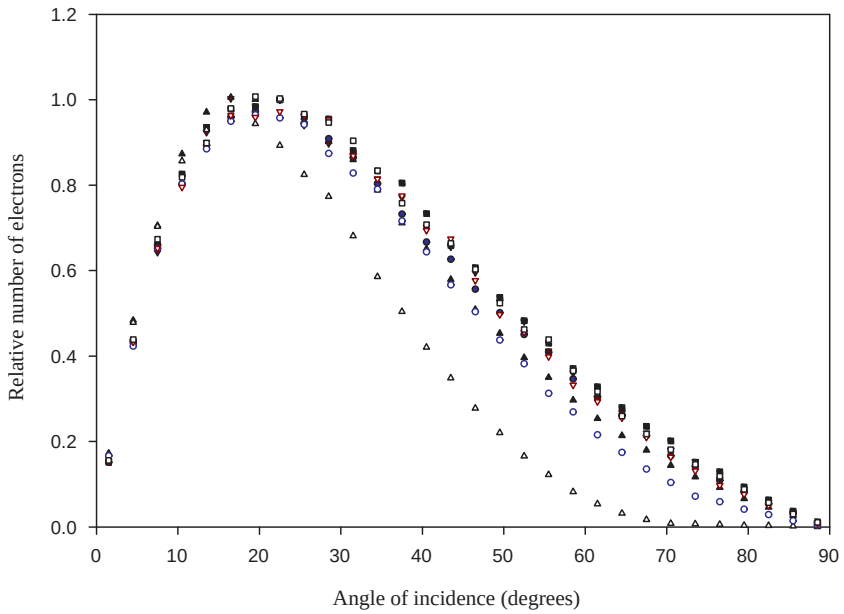

Figure 4.5. The angular distribution of secondary electrons incident onto the proximal surface of the OSLD active volume. Distributions with and without the air gap are plotted. Each graph pair has been normalised to the 'no air gap' simulation at 22.5 degrees (as this was generally the maximum). The following field sizes are shown: 6 mm (triangles), 12 mm (circles), 18 mm (upside down triangles), and 30 mm (squares). The results without the air gap have filled markers, and those with the air gap have hollow (or white) markers.

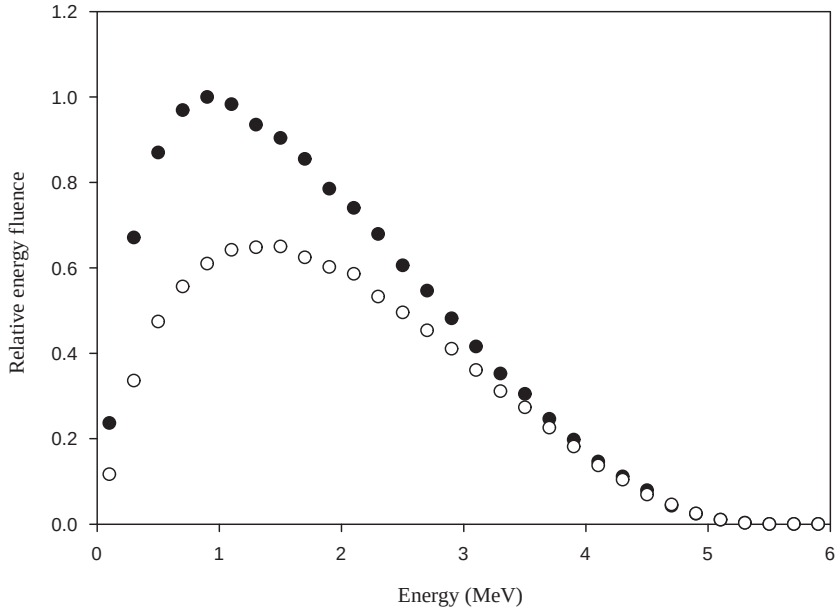

Figure 4.6. The energy distribution (spectrum) of secondary electrons incident onto the OSLD active area. Distributions with the air gap (white circles) and without the air gap (black circles) for the 6 mm field size are plotted.

4.3.7 Re-establishment of electronic equilibrium beyond air gap

Figure 4.9 shows the dose reduction in water downstream of a 1 mm air gap. The figure displays the re-build up of electronic equilibrium in 0.1 mm steps for the 6 mm field size. The dose reduction caused by the air gap is 19 % in the first 0.1 mm of water. The dose difference between the

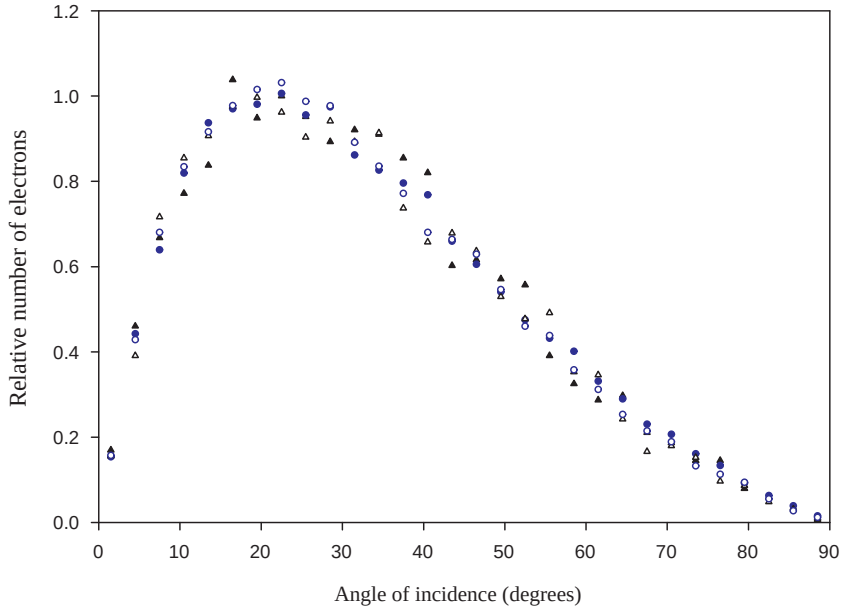

Figure 4.7. The angular distribution of secondary electrons incident on to different annular regions of the proximal surface of the OSLD active volume for a 30 mm field size. Distributions with the air gap (hollow or white markers) and without the air gap (filled markers) are plotted. For clarity only the inner most 5 mm (triangles) and outer most 5 mm (circles) regions are shown.

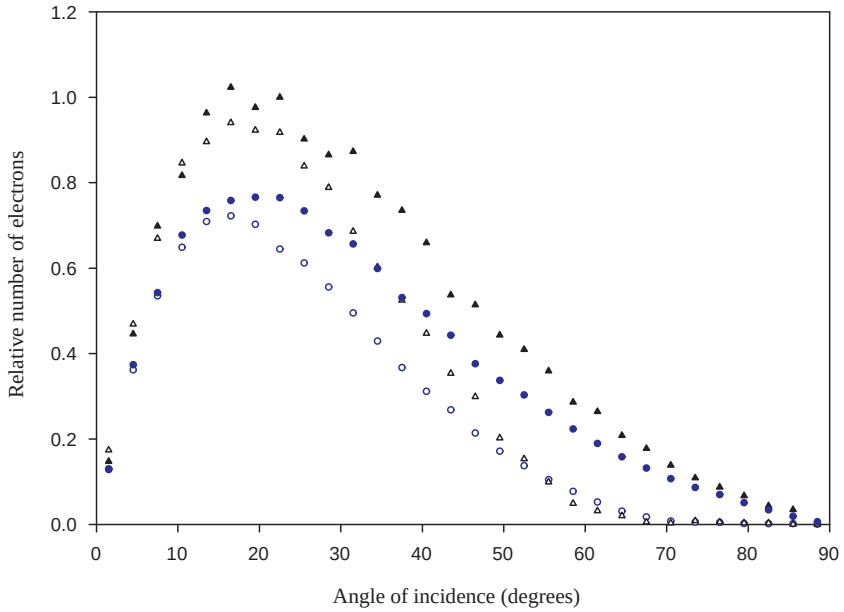

Figure 4.8. The angular distribution of secondary electrons incident on to different annular regions of the proximal surface of the OSLD active volume for a 6 mm field size. Distributions with the air gap (hollow or white markers) and without the air gap (filled markers) are plotted. For clarity only the inner most 0.5 mm (triangles) and outer most 0.5 mm (circles) regions are shown.

air gap and no air gap simulations is reduced to 5 % after just 2 mm and to 2 % after 3 mm. There is full re-establishment of electronic equilibrium after 5 mm.

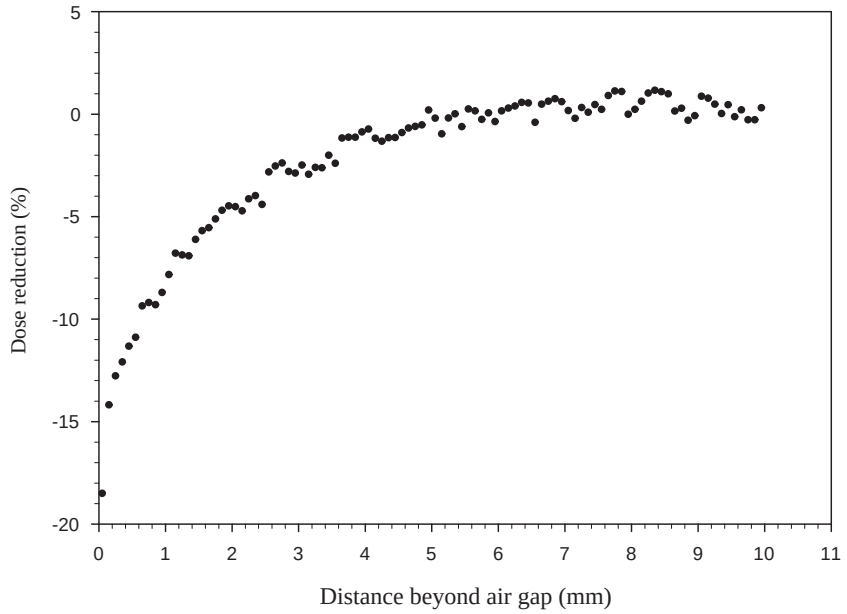

Figure 4.9. Dose reduction as a function of distance beyond a 1 mm air gap in a water phantom (no detector), for the 6 mm square field size. Dose reduction refers to dose loss relative to a simulation with no air gap.

4.4 DISCUSSION

The simplified Monte Carlo model of the OSLD proposed by Kerns et al [20] was proven to be an accurate representation for simulating output factors down to 6 mm. It was only necessary to model the Al_2O_3 active area and the surrounding air gap, and not any of casing material for this purpose. As expected, it was the proximal air gap that had the most pronounced effect on the dose to small fields, due to the loss of lateral electronic equilibrium. Lateral electronic disequilibrium is a well known phenomenon. Because most photon fields used in the clinic contain lateral scatter equilibrium, a small air gap in a phantom or patient will have no effect. There will be much fewer secondary electrons created in the air gap above the detector, but equally other electrons created above the air gap will not be attenuated by the air gap

and continue through to the detector. These two effects will cancel out and therefore the air gap has no effect. The secondary electrons created by the primary photon beams have a large angular spread (see Figure 4.5). Therefore for very small beams, a proportion of the electrons that traverse the air gap will miss the detector, thus reducing the dose to the detector. Figure 4.10 shows a schematic of this. In the example in Figure 4.10, 3 of the electrons reach the detector whilst 4 will miss due to the air gap. The reason that this does not affect larger beams is the very definition of lateral scatter equilibrium. As depicted in Figure 4.11, the electrons that miss the detector due to the air gap will be replaced by electrons that will now reach the detector that otherwise would not have if there was no air gap. In the example given in Figure 4.11, 7 electrons will reach the detector (the same amount as if the air gap was not present), however 4 of those have not come from directly above the centre of the detector.

The Al_2O_3 active volume had minimal effect on the output factor, suggesting that if an OSLD was designed with a smaller diameter and no surrounding air gap then it's accuracy in small field dosimetry should be improved. The smaller diameter would reduce the effect of volume averaging. Removing the air gap would eliminate the issues detailed in this study, but may not be mechanically feasible as the active volume needs to be removed from the case by the reader in order to be read out.

A linear relationship was found between the dose reduction due to the air gap and the size of the air gap. For example there was an 11.5 % / mm (r^2 = 0.998) dose reduction for the 6 mm field size. This

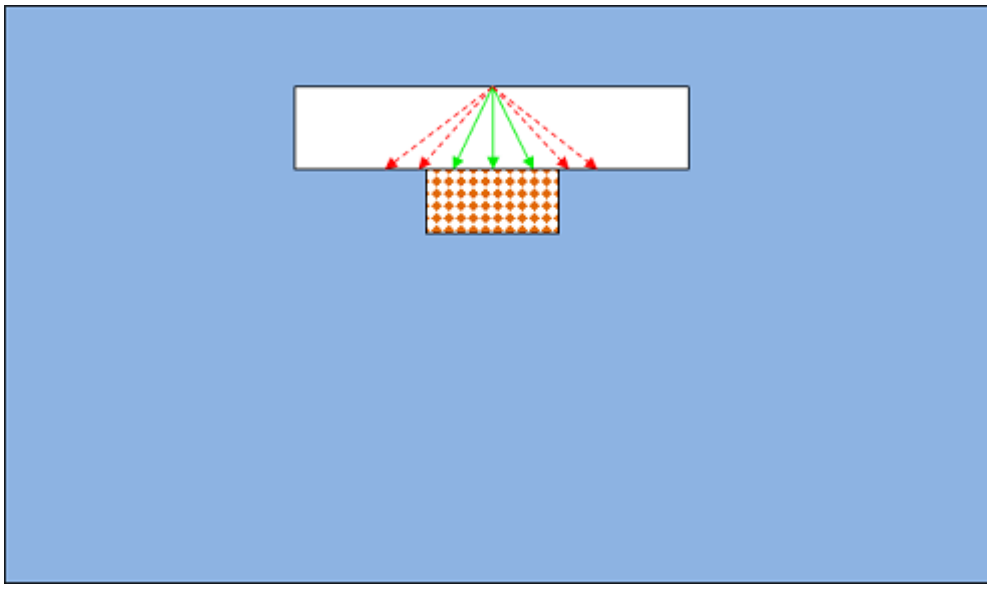

Figure 4.10. A depiction of secondary electrons crossing an air gap (white box) and reaching a detector (checkered box), for a very small field. The green (solid) arrows represent electrons that reach the detector; the red (dashed) arrows represent those that miss due to the air gap.

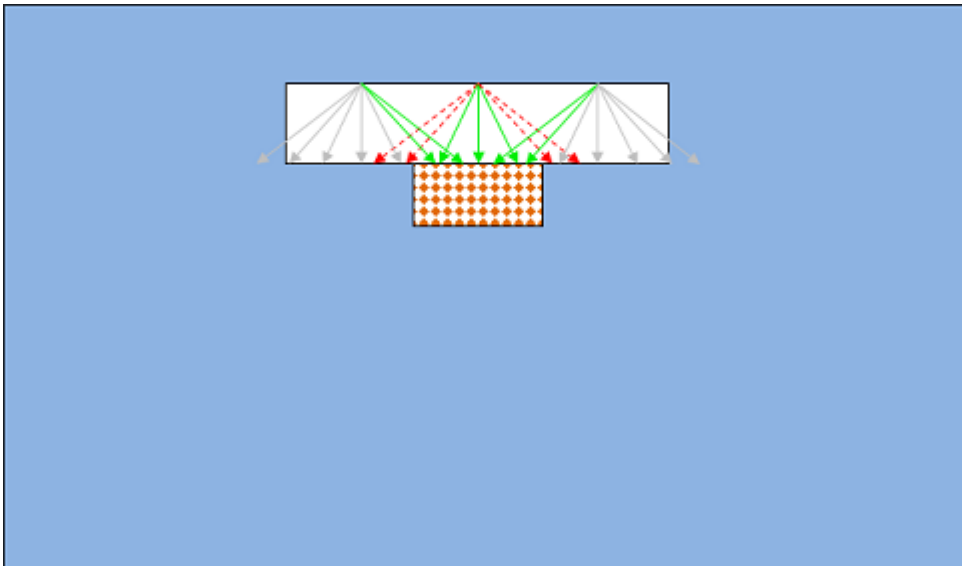

Figure 4.11. A depiction of secondary electrons crossing an air gap (white box) and reaching a detector (checkered box), for a field with lateral scatter equilibrium. The green (solid) arrows represent electrons that reach the detector; the red (dashed) arrows represent those that miss due to the air gap. The light grey lines represent electrons that would not reach the detector regardless of the air gap.

can be used as a guide for estimating the dose reduction caused by a known air gap size without the need to measure various sizes. It must be stressed that the linear relation was only tested between 0 - 2 mm (i.e. it exists for very small air gaps). It is very dependent on field size. Also, the size of the detector volume beyond the air gap

is very important. For example the above 11.5 % / mm relationship pertained to 0.2 mm of Al_2O_3, however as demonstrated in Figure 4.9, when the detector immediately beyond a 1 mm air gap is 0.1 mm of water, then the dose reduction is 18.5 %. The heavy dependence on detector thickness and material is due to the rapid re-establishment of electronic equilibrium as shown in Figure 4.9.

It has been proven in this study that for sub-centimetre field sizes, even air gaps < 1 mm in size can cause electronic disequilibrium. For example there is an 11.5 % dose reduction in a 6 mm square field size when there is a 1 mm air gap immediately upstream to the point of interest. The dose reduction is still > 5 % when the air gap is only 0.5 mm. This can lead to large uncertainty in dosimetry measurements if a small air gap exists immediately above a detector. The air gap in OSLDs is a known phenomenon so can potentially be accounted for by Monte Carlo simulations if the air gap size is reproducible; but when the air gap is not expected it can alter results considerably. This may occur in solid phantom dosimetry if a detector cavity is not perfectly flush with the solid material immediately above it, or if imperfect casting of the plastic has lead to air bubbles.

The dose reduction depends on the density of the detector so it is expected that any air gaps above air based ion chambers would lead to larger dose reductions than shown in this study. As a simple solution, it is recommended that all stereotactic dosimetry be performed in liquid water where possible, ensuring any waterproofing material used is perfectly flush with the active volume of the detector. It may also be difficult to detect sub-millimetre air gaps on CT scans if for example a coarse resolution (> 2 mm) was used to scan the patient. If the air gaps are not in the CT scan, not even the most complicated dose calculation algorithm will fully account for the dose reduction in a patient plan. This could lead to large under dosing to the patient tissue immediately beyond an air gap.

4.5 CONCLUSIONS

It has been shown in this study that very small air gaps have a significant effect on small field dosimetry. Care should be taken to eliminate all air gaps where possible.

This applies to waterproofing any detector for use in water phantoms using a sleeve as well as to inserting detectors into solid phantoms. Where there is an intrinsic air gap, as is the case with the Landauer nanodot OSLDs, then this must be accounted for if they are to be used in small field measurements. The Monte Carlo model of the Al_2O_3 active volume proposed by Kerns et al [20] was used for simulating OSLDs down to a field size of 6 mm. Although the simulated output factors were within 2 standard deviations of the measured factors, which is acceptable for this study, further work may be needed for high precision small field output factor simulations. This may include modelling the plastic casing and active volume "cup".

4.6 ACKNOWLEDGEMENTS

This work was funded by the Australian Research Council in partnership with the Queensland University of Technology, the Wesley Research Institute and Premion (Linkage Grant No. LP110100401). The Australian Clinical Dosimetry Service is a joint initiative between the Department of Health and Ageing and the Australian Radiation Protection and Nuclear Safety Agency. Computational resources and services used in this work were provided by the High Performance Computing and Research Support Unit, Queensland University of Technology (QUT), Brisbane, Australia.

4.7 REFERENCES

1 R. Alfonso, P. Andreo, R. Capote, M.S. Huq, W. Kilby, P. Kjäll, T.R. Mackie, H. Palmans, K. Rosser, J. Seuntjens, W. Ullrich, S. Vatnitsky, "A new formalism for reference dosimetry of small and nonstandard fields," Medical Physics **35**, 5179 (2008).

2 I.J. Das, G.X. Ding, A. Ahnesjö, "Small fields: Nonequilibrium radiation dosimetry," Medical Physics **35**, 206 (2008).

3 M.L. Taylor, T. Kron, R.D. Franich, "A contemporary review of stereotactic radiotherapy: inherent dosimetric complexities and the potential for detriment," Acta Oncol **50**, 483-508 (2011).

[4] C.F. Behrens, "Dose build-up behind air cavities for Co-60, 4, 6 and 8 MV. Measurements and Monte Carlo simulations," Phys Med Biol **51**, 5937-5950 (2006).

[5] B. Disher, G. Hajdok, S. Gaede, J.J. Battista, "An in-depth Monte Carlo study of lateral electron disequilibrium for small fields in ultra-low density lung: implications for modern radiation therapy," Phys Med Biol **57**, 1543-1559 (2012).

[6] X. Li, C. Yu, T. Holmes, "A systematic evaluation of air cavity dose perturbation in megavoltage x-ray beams," Medical Physics **27**, 1011-1017 (2000).

[7] A. Rustgi, M. Samuels, S. Rustgi, "Influence of air inhomogeneities in radiosurgical beams," Med Dosim **22**, 95-100 (1997).

[8] T.D. Solberg, F. Holly, A. De Salles, R. Wallace, J. Smathers, "Implications of tissue heterogeneity for radiosurgery in head and neck tumors," Int J Radiat Oncol Biol Phys **32**, 235-239 (1995).

[9] S.J. Wadi-Ramahi, S.A. Naqvi, J.C.H. Chu, "Evaluating the effectiveness of a longitudinal magnetic field in reducing underdosing of the regions around upper respiratory cavities irradiated with photon beams—A Monte Carlo study," Medical Physics **28**, 1711 (2001).

[10] P.A. Jursinic, "Characterization of optically stimulated luminescent dosimeters, OSLDs, for clinical dosimetric measurements," Medical Physics **34**, 4594 (2007).

[11] I. Mrcela, T. Bokulic, J. Izewska, M. Budanec, A. Frobe, Z. Kusic, "Optically stimulated luminescence in vivo dosimetry for radiotherapy: physical characterization and clinical measurements in (60)Co beams," Phys Med Biol **56**, 6065-6082 (2011).

[12] E.G. Yukihara, S.W. McKeever, "Optically stimulated luminescence (OSL) dosimetry in medicine," Phys Med Biol **53**, R351-379 (2008).

[13] K.Y. Seet, P.M. Hanlon, P.H. Charles, "Determination of RW3-to-water mass-energy absorption coefficient ratio for absolute dosimetry," Australas Phys Eng Sci Med **34**, 553-558 (2011).

[14] I. Kawrakow, E. Mainegra-Hing, F. Tessier, B.R.B. Walters, "The EGSnrc C++ class library, ," NRC Report PIRS-898 (rev A)2009).

[15] D.W.O. Rogers, B. Walters, I. Kawrakow, 2011.

[16] T. Kairn, T. Aland, R.D. Franich, P.N. Johnston, M.B. Kakakhel, J. Kenny, R.T. Knight, C.M. Langton, D. Schlect, M.L. Taylor, J.V. Trapp, "Adapting a generic BEAMnrc model of the BrainLAB m3 micro-multileaf collimator to simulate a local collimation device," Phys Med Biol **55**, N451-463 (2010).

[17] T. Kairn, J. Kenny, S.B. Crowe, A.L. Fielding, R.D. Franich, P.N. Johnston, R.T. Knight, C.M. Langton, D. Schlect, J.V. Trapp, "Technical Note: Modeling a complex micro-multileaf collimator using the standard BEAMnrc distribution," Medical Physics **37**, 1761 (2010).

[18] G. Cranmer-Sargison, S. Weston, J.A. Evans, N.P. Sidhu, D.I. Thwaites, "Implementing a newly proposed Monte Carlo based small field dosimetry formalism for a comprehensive set of diode detectors," Medical Physics **38**, 6592-6602 (2011).

[19] P. Francescon, S. Cora, N. Satariano, "Calculation of k(Q(clin),Q(msr)) (f(clin),f(msr)) for several small detectors and for two linear accelerators using Monte Carlo simulations," Medical Physics **38**, 6513-6527 (2011).

[20] J.R. Kerns, S.F. Kry, N. Sahoo, D.S. Followill, G.S. Ibbott, "Angular dependence of the nanoDot OSL dosimeter," Medical Physics **38**, 3955 (2011).

[21] C.M. Ma, D.W.O. Rogers, Report No. NRCC Report PIRS-0509(C)revA, 2009.

[22] B. Walters, I. Kawrakow, D.W.O. Rogers, Report No. NRCC Report PIRS-794revB, 2011.

Chapter 5: Monte Carlo-base diode design for correction-less small field dosimetry

P H Charles[1], S B Crowe[1], T Kairn[1,2], R T Knight[2], B Hill[2], J Kenny[3,4], C M Langton[1] and J V Trapp[1].

[1] School of Chemistry, Physics and Mechanical Engineering, Queensland University of Technology, Brisbane, Australia

[2] Premion, The Wesley Medical Centre, Auchenflower, Qld, Australia

[3] The Australian Clinical Dosimetry Service, Australian Radiation Protection and Nuclear Safety Agency, Yallambie, Vic, Australia

[4] Radiation Oncology Queensland, St Andrew's Toowoomba Hospital, Toowoomba, Qld, Australia

Journal: Physics in Medicine and Biology

Status: Published June 2013

Citations to date: 7

STATEMENT OF JOINT AUTHORSHIP

Title: Monte Carlo-based diode design for correction-less small field dosimetry

Authors: Paul Charles; Scott Crowe; Tanya Kairn; Richard Knight; Brendan Hill; John Kenny; Christian Langton; Jamie Trapp;

Paul Charles (candidate)
Project concept, direction and design. Performed all Monte Carlo simulations. Analysed an interpreted all results. Wrote the manuscript.

Scott Crowe
Supplied Monte Carlo model of linac. General advice and supervision as required. Edited manuscript.

Tanya Kairn
Supplied Monte Carlo model of linac. General advice and supervision as required. Edited manuscript

Richard Knight
General advice and supervision as required.

Brendan Hill
General advice and supervision as required.

John Kenny
General advice and supervision as required.

Christian Langton
General advice and supervision as required.

Jamie Trapp
General advice and supervision as required. Edited manuscript.

ABSTRACT

Due to their small collecting volume diodes are commonly used in small field dosimetry. However the relative sensitivity of a diode increases with decreasing small field size. Conversely, small air gaps have been shown to cause a significant decrease in the sensitivity of a detector as the field size is decreased. Therefore this study uses Monte Carlo simulations to look at introducing air upstream to diodes such that they measure with a constant sensitivity across all field sizes in small field dosimetry.

Varying thicknesses of air were introduced onto the upstream end of two commercial diodes (PTW 60016 photon diode and PTW 60017 electron diode), as well as a theoretical unenclosed silicon chip using field sizes as small as 5 mm × 5 mm . The metric $\frac{D_{w,Q}}{D_{Det,Q}}$ used in this study represents the ratio of the dose to a point of water to the dose to the diode active volume, for a particular field size and location. The optimal thickness of air required to provide a constant sensitivity across all small field sizes was found by plotting $\frac{D_{w,Q}}{D_{Det,Q}}$ as a function of introduced air gap size for various field sizes, and finding the intersection point of these plots. That is, the point at which $\frac{D_{w,Q}}{D_{Det,Q}}$ was constant for all field sizes was found.

The optimal thickness of air was calculated to be 3.3 mm, 1.15 mm and 0.10 mm for the photon diode, electron diode and unenclosed silicon chip respectively. The variation in these results was due to the different design of each detector. When calculated with the new diode design incorporating the upstream air gap, $k_{Q_{clin},Q_{msr}}^{f_{clin},f_{msr}}$ was equal to unity to within statistical uncertainty (0.5 %) for all three diodes. Cross-axis profile measurements were also improved with the new detector design.

The upstream air gap could be implanted on the commercial diodes via a cap consisting of the air cavity surrounded by water equivalent material. The results for the unclosed silicon chip show that an ideal small field dosimetry diode could be created by using a silicon chip with a small amount of air above it.

5.1 INTRODUCTION

Diodes provide a good alternative to ion chambers for relative dosimetry for radiotherapy because they generally have very small collecting volumes (<0.1 mm^3). However, at very small field sizes even diode measurements are affected by perturbations due to the diodes' relatively dense collecting medium (silicon) [1, 2]. This study uses Monte Carlo simulations to investigate a simple modification to commercial diode designs, which could negate the variation of this perturbation effect with field size. This would allow diodes to be used in small field dosimetry without the need to calculate field size specific correction factors.

The increased sensitivity in small fields caused by the silicon is predominantly due to its increased density relative to water [2]. Further to this, some diodes contain other high density media which causes a further increase in dose in small fields compared to standard fields [3]. Therefore, the exact correction factor required depends on each individual detector design. Cranmer-Sarginson *et al* [4] used Monte Carlo simulations to show that for a 5 mm field size, the sensitivity correction factors required were 0.961, 0.939 and 0.906 for a stereotactic diode, an electron diode and a photon diode respectively. This represented a range of sensitivity changes between 4 % and nearly 10 % between the different diodes. In another study Cranmer-Sarginson *et al* [3] demonstrated that differences between the responses were due to the fact that the electron diode contained a thin metal filter plate above the active volume, and the photon diode active volume was completely surrounded by metal shielding.

By contrast, recent work by Charles *et al* [5] has shown that optically stimulated luminescence dosimeters (OSLDs) can be made to preferentially under-respond to small-field radiation doses by the introduction of small volumes of air upstream to their active volumes.

5.1.1 Compensating diode correction factors with the presence of air gaps

Dose to water as measured by a diode can be defined by the following equation:

$$D_{w,Q} = D_{Det,Q}(s_{w,St})_Q p_Q \quad (5.1)$$

D_W is the dose to a volume of water at the location of the detector active volume, and D_{Det} is the dose to the active volume of the detector. $(s_{w,St})_Q$ is the stopping power ratio of water to silicon and p_Q is the total perturbation correction factor of the diode. The subscript Q refers to the beam quality being measured. At the field sizes encountered in small field dosimetry, p_Q is dependent on field size, thus a correction factor is required when measuring total scatter factors [6]. The field size dependent sensitivity correction is denoted in Alfonso *et al* [6] as $k_{Q_{clin},Q_{msr}}^{f_{clin},f_{msr}}$. The subscript 'msr' refers to the machine specific reference field size (which was 50 mm in this study). The subscript 'clin' refers to the clinical field sizes (which were the varying test field sizes in this study). Essentially $k_{Q_{clin},Q_{msr}}^{f_{clin},f_{msr}} = p_{Q,clin} / p_{Q,ref}$. Equating this with equation 1 yields:

$$k_{Q_{clin},Q_{msr}}^{f_{clin},f_{msr}} = \left[\frac{D_{w,Q_{clin}}^{f_{clin}} / D_{Det,Q_{clin}}^{f_{clin}}}{D_{w,Q_{msr}}^{f_{msr}} / D_{Det,Q_{msr}}^{f_{msr}}}\right] \quad (5.2)$$

The deliberate introduction of air into the diodes causes an additional perturbation to the electron fluence. This will be denoted as p_{gap} in this study. Equation 1 then becomes:

$$D_{w,Q} = D_{Det,Q}(s_{w,St})_Q p_Q p_{gap} \quad (5.3)$$

The main aim of this study is to introduce a thickness of air above the diodes such that the value $p_Q p_{gap}$ is constant across all fields sizes. This removes the need to apply $k_{Q_{clin},Q_{msr}}^{f_{clin},f_{msr}}$. If $p_Q p_{gap}$ was constant across all field sizes, then according to equation 3 the ratio $\frac{D_{w,Q}}{D_{Det,Q}}$ would also be constant at all field sizes. Thus $\frac{D_{w,Q}}{D_{Det,Q}}$ is the metric used in this study.

The resulting data allows the concept of deliberately implanting small air gaps on or into the diodes to remove their dependence on field size to be introduced and

investigated. This study identifies and then evaluates a set of three diode designs, which each incorporate an optimized volume of air, for accurate small field dosimetry.

5.2 METHODOLOGY

5.2.1 Monte Carlo simulation overview

All linear accelerator simulations were performed with the BEAMnrc Monte Carlo user code [7], using an established model of the Varian 21iX (Varian Medical Systems, Palo Alto, USA) with the Brainlab M3 μMLC attachment (Brainlab, AG, Feldkirchen, Germany) [8, 9]. For small field simulations the focal spot size is highly important [10, 11] and in the present work it was verified using a procedure similar to that proposed by Cranmer-Sargison *et al* [4].

All diode simulations were performed in the EGSnrc C++ user code cavity [12]. The diode construction details were obtained from the manufacturer. The diode geometry was simulated in full for this study, with the exception of the coaxial cabling. The diode simulation accuracy was verified against measurements on the linear accelerator down to a field size of 5 mm.

In the phantom material, the electron and photon cut off energies were chosen to be 521 and 10 keV respectively. Inside the volume of the simulated diode they were reduced to 512 and 1 keV respectively for increased accuracy within the detector volume and air gaps. Sufficient histories were simulated so that the statistical uncertainty of the Monte Carlo calculated correction factors was maintained at less than 0.5%.

A select number of simulations involving each detector, both with and without an air gap, were repeated with the entire simulation geometry set with cut off values of 512 keV for electrons and 1 keV for photons. This made no difference to the resultant dose to the cavity, so it was deemed that potential interface effects that may occur

when changing between media with different cut off values did not affect any results in this study.

All simulations were performed at a nominal energy of 6 MV. In all simulations (with the exception of testing for measurement location) the location of the modeled diodes was constant. They were positioned with their active volume on the central axis of the beam, at a depth in water of 5 cm, with a source to surface distance (SSD) of 95 cm.

5.2.2 Diodes investigated

Commerical diodes.

Two commercially available diodes were simulated in this study: the PTW 60016 photon diode, and the PTW 60017 electron diode (PTW, Freiburg, Germany). The photon diode has a high density shielding material which limits its suitability for small field dosimetry. The electron diode on the other hand has much less shielding. Further discussion on the construction of these diodes and their influence on small field dosimetry can be found in Cranmer-Sargison *et al* [3]. In this same study Cranmer-Sarginson *et al* introduce the concept of simplified detector geometry. However the full detector geometry was used in this study because the rapid re-establishment of electronic equilibrium beyond an air gap meant that detector design would be particularly important [5]. A summary of the commercial diodes is displayed in table 1.

Theoretical unenclosed silicon chip.

The construction of the two diodes above is quite different, except for the geometry of the silicon chip contained within. It was expected that the construction of the material would heavily influence the results. Therefore an unenclosed silicon chip was also simulated, to eliminate the effects of the specific construction of the

commercial detectors and give insight into how diode design may be optimized for small field dosimetry.

Table 5.1. Summary of commercial diodes used in this study.

Property	PTW T60016	PTW T60017
Reference point location	2 mm from tip	0.6 mm from tip
Nominal sensitive volume	0.03 mm^3	0.03 mm^3
Nominal sensitive radius	0.6 mm	0.6 mm
Photon shielding	Yes	No

5.2.3 The addition of air onto the diodes

An air gap was introduced immediately upstream of the detector (i.e. touching the end of the detector that faced the source). The size and the shape of this air gap in the perpendicular to beam direction was the same as the diode (circular with a diameter of 6.9 mm). In the beam direction the thickness was varied in 0.2 mm increments from 0.0 – 2.0 mm. This was performed for all three detectors in Section 5.2.2, for various square field sizes ranging from 5 mm to 50 mm side length. The air gap thickness was incrementally increased up to 5 mm for 60016 photon diode, as 2 mm was not sufficiently thick to eliminate the dependence on field size of this diode. For the 60016 photon diode, the width of the air gap was also iteratively changed to give the best results.

Figure 5.1 is a schematic representation of the location and sizes of the air gaps with respect to the detectors as simulated in this study.

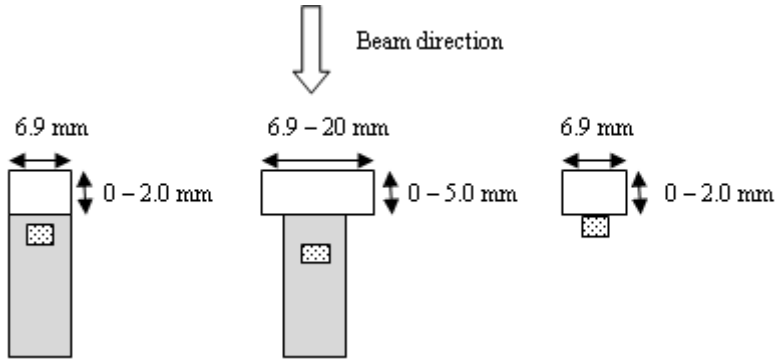

Figure 5.1. Schematic of the placement of the air gap proximal to the diode detector. The grey represents the body of the detector, the dotted area is the silicon chip, and the white is the air gap. From left to right are schematics of the PTW60017 diode, PTW60016 diode and the unenclosed silicon chip respectively. The geometry of both the air gap and the detector is cylindrical in the perpendicular to beam direction. The diagram is not to scale.

5.2.4 Finding the optimal air thickness for correction-less small field dosimetry

Equation 5.2 was used to calculate $k_{Q_{clin},Q_{msr}}^{f_{clin},f_{msr}}$ for the field sizes and detectors in this study. In order to evaluate $D_{W,}$ calculations of dose in a small volume of water within the total water volume were required to calculate the output factors in the absence of the detector.

To calculate the thickness of air required to eliminate the dependence on field size of the diodes, $\frac{D_{w,Q}}{D_{Det,Q}}$ was plotted as a function of air gap thickness for various field sizes. The optimal air gap was then obtained by using the best intersection point of the plots. The intersection point represented the point where $\frac{D_{w,Q}}{D_{Det,Q}}$ was constant across all field sizes. This was performed for each diode for an air gap width of 6.9 mm. For the 60016 photon diode, the width had to be optimized to obtain an intersection point.

5.2.5 Testing the modified detector designs under various conditions

The air gap thickness required to eliminate the diode dependence on field size was obtained under particular conditions. It was therefore pertinent to check that these modified detector designs still responded well under various conditions important to

small field dosimetry. The simulations in this section were performed for all three new detector designs. These dose calculations were also made in water, without detectors present. Unless otherwise mentioned, all simulations in this section were performed with a field size of 5 mm as the smallest field size is most affected by measurement and simulation conditions.

Measurement location.

The simulations (originally at 5 cm depth) were repeated at several depths from 1.5 cm to 21 cm, keeping source to surface distance (95 cm) constant, to evaluate the reliability of the modified diodes when used at different depths. Additionally, cross axis profiles were simulated to evaluate the consistency of the modified diodes when used to measure the varying dose across the field. These tests were used to establish the feasibility of using diodes with introduced air gaps for obtaining key beam characterization measurements; off-axis ratios and percentage depth doses. The results of these tests could also be important for quantifying the potential of geometrical set-up errors when measuring small field output factors.

For all of these calculations, the modified detector design (with the air gap) was compared directly against the existing detector design (without the air gap), and against the results from water, without the detectors present. The results for the different depths were normalized to the results at a depth of 5 cm. The cross-axis profiles were normalized to the central axis value. The results for the water (without the detectors present) cross-axis profiles were calculated using DOSXYZnrc [13]. The voxel size used to calculate dose was 0.25 mm in the direction of measurement and 1.0 mm in the other 2 dimensions.

Beam parameters.

In order to provide an indication of the validity of the modified diode models for providing measurements in small 6 MV photon beams with slightly different spectral qualities from the beams for which they were optimized in this study, the initial electron beam characteristics used in the model linac were systematically varied.

Previous studies have found these effects to be minimal on the central axis for ionization chambers [14] and diodes [3, 15]. However the introduction of air provided a novel situation that required testing.

The electron focal spot size incident on to the photon target in the BEAMnrc simulation was radially symmetric and Gaussian in distribution. The full width half maximum (FWHM) was varied from 0.7 mm to 2.2 mm FWHM. $\frac{D_{w,Q}}{D_{Det,Q}}$ was calculated with each FWHM and plotted for direct comparison.

Additionally, the incident electron energy on to the photon target used in this study was monoenergetic and 5.8 MeV. This value was changed to values between 5.5 MeV and 7.0 MeV. $\frac{D_{w,Q}}{D_{Det,Q}}$was calculated with each energy and plotted for direct comparison.

5.3 RESULTS

5.3.1 The thickness of air required to eliminate the dependence of the diode on field size

Table 5.2 displays the calculated values of $k_{Q_{clin},Q_{msr}}^{f_{clin},f_{msr}}$ for each detector as a function of nominal field size.

Figure 5.2 is a plot of $\frac{D_{w,Q}}{D_{Det,Q}}$ against thickness of air for all diodes, for the following field sizes: 5 mm, 6 mm, 8 mm, 10 mm, 12 mm and 30 mm. Two different air widths (6.9 mm and 11 mm) are shown for the PTW 60016 diode. From these graphs the optimal thickness of air could be clearly identified. These values are displayed in table 5.3.

The new values of $k_{Q_{clin},Q_{msr}}^{f_{clin},f_{msr}}$, after the application of the thicknesses of air listed in table 5.3 are displayed in table 5.2. The thicknesses of air displayed in table 5.3 were

used for all field sizes. These data show that when recalculated with the new diode design incorporating the upstream air gap, $k_{Q_{clin},Q_{msr}}^{f_{clin},f_{msr}}$ is equal to unity to within statistical uncertainty (0.5 %) for all three diodes.

Table 5.2. $k_{Q_{clin},Q_{msr}}^{f_{clin},f_{msr}}$ for the three diodes simulated in this study as a function of square field size. These values are normalized to the field size of 50 mm. Shown is the unmodified detector design (without the air gap) as well as the modified detector design which includes the air gap. Note that the Monte Carlo statistical uncertainty in each value is approximately 0.5 %.

Field size (mm)	PTW 60016		PTW 60017		Unenclosed silicon chip	
	No air	Air	No air	Air	No air	Air
5	0.900	0.995	0.922	1.001	0.975	1.004
6	0.911	0.997	0.938	1.004	0.985	1.004
7	0.921	0.999	0.944	1.000	0.984	1.000
8	0.931	1.005	0.957	1.001	0.995	0.999
9	0.945	1.004	0.966	0.997	0.989	1.003
10	0.948	0.999	0.969	0.998	0.996	0.995
12	0.966	1.000	0.983	0.995	0.995	0.998
18	0.991	0.995	0.997	1.000	1.004	1.005
30	0.995	0.995	1.000	0.999	0.997	1.001
50	1.000	0.999	1.000	1.000	1.000	1.000

Table 5.3. The thickness of air required to offset the dependence on field size of the diodes. The error indicates a thickness of air that would result in an error of up to 1 % in the calculated $k_{Q_{clin},Q_{msr}}^{f_{clin},f_{msr}}$ value.

Diode	Thickness of air required (mm)	Diameter of air used (mm)
PTW T60016	3.3 ± 0.4	11.0
PTW T60017	1.15 ± 0.15	6.9
Silicon chip only	0.10 ± 0.04	6.9

5.3.2 Testing the modified detector designs

Measurement location.

The output at several depths for each modified detector, as well as water without the detectors present is shown in figure 3. The modifications to the detectors have no effect on the accuracy of the percentage depth dose curve, with all detectors (modified and unmodified) agreeing well with water. The agreement is such that all but 3 measurement points in figure 3 are within 1 % of the corresponding water value and all measurement points are with 1.4 %. The only systematic difference observed was slight under-response shown by the 60017 and unenclosed chip diodes at depths deeper than 17 cm.

The cross axis profile at a depth of 5 cm is displayed for each detector (modified and unmodified) as well as water without the detectors present in figure 4. The modified commercial diodes reproduced the water profile more accurately than the unmodified diodes, particularly in the penumbra region.

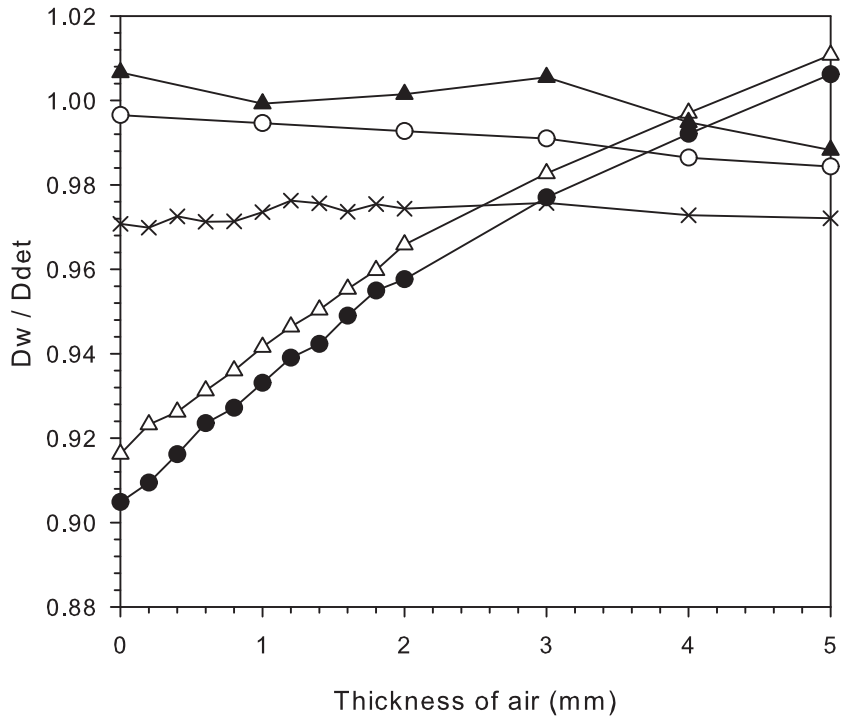

(a)

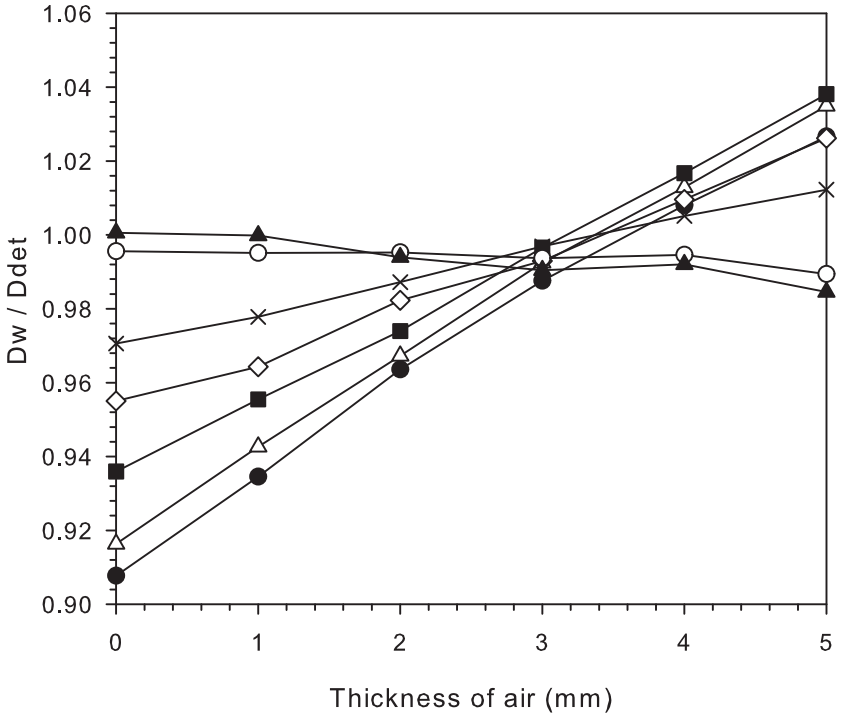
1.06
1.04
1.02
1.00
0.98
0.96
0.94
0.92
0.90
Dw / Ddet
0
1
2
3
4
5
Thickness of air (mm)

(b)

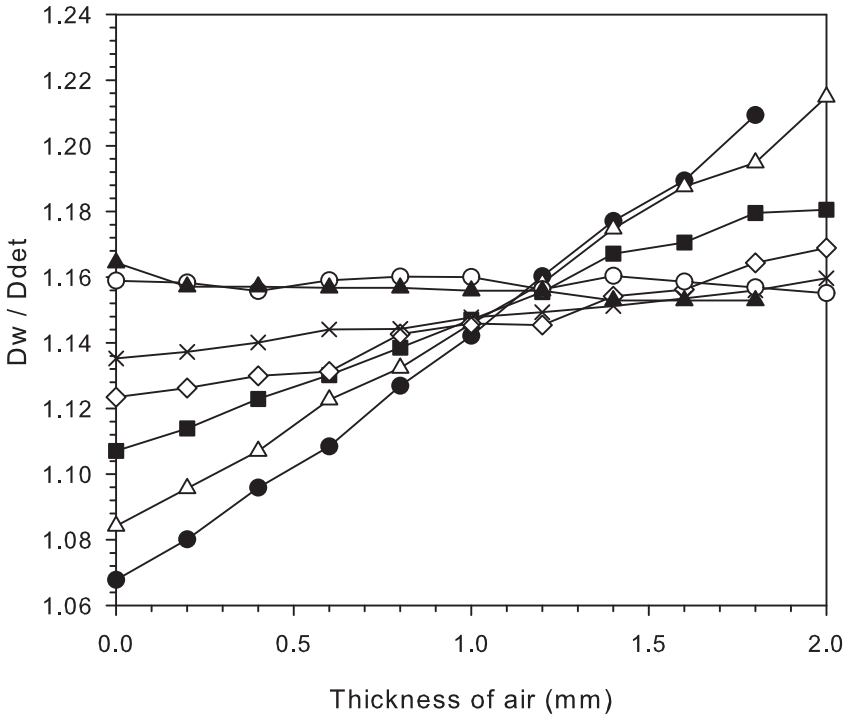
1.24
1.22
1.20
1.18
1.16
1.14
1.12
1.10
1.08
1.06
Dw / Ddet
0.0
0.5
1.0
1.5
2.0
Thickness of air (mm)

(c)

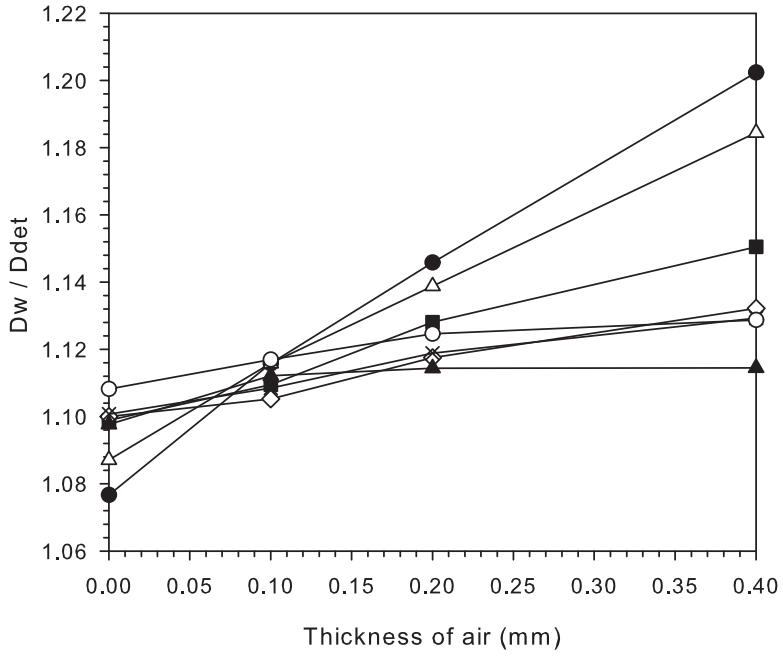

(d)

Figure 5.2. D_w / D_{Det} as a function of upstream air gap size for the (a) PTW 60016 diode (air gap width = 6.9 mm); (b) PTW 60016 diode (air gap width = 11 mm); (c) PTW60017 diode (air gap width = 6.9 mm; (d) unenclosed silicon chip (air gap width = 6.9 mm). Plotted are the following field sizes: 5 mm (black circles), 6 mm (white triangles), 8 mm (squares), 10 mm (diamonds), 12 mm (crosses), 18 mm (white circles), and 30 mm (black triangles).

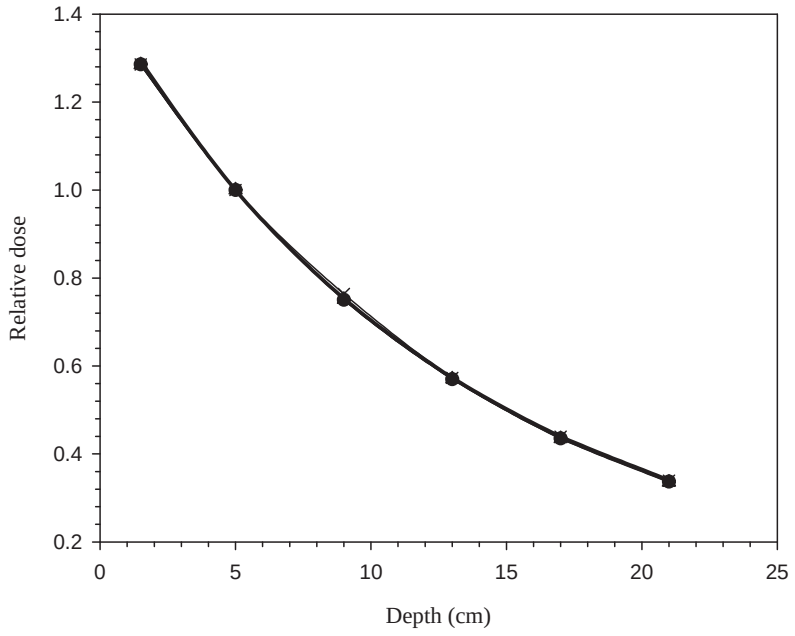

Figure 5.3. Percentage depth dose profiles for all three detectors using the modified design: 60016 photon diode (crosses); 60017 electron diode (circles); unenclosed silicon chip (triangles). Also included are the results to water without the detectors present (thick black line). All results are for the 5 mm field size and are normalized to a depth of 5 cm.

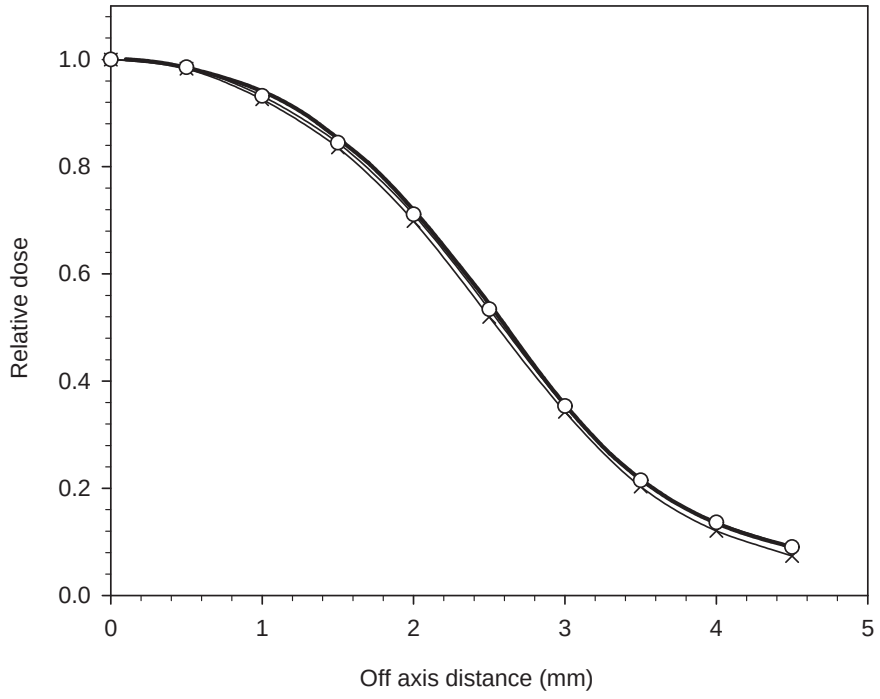
Relative dose
1.0
0.8
0.6
0.4
0.2
0.0
0
1
2
3
4
5
Off axis distance (mm)

(a)

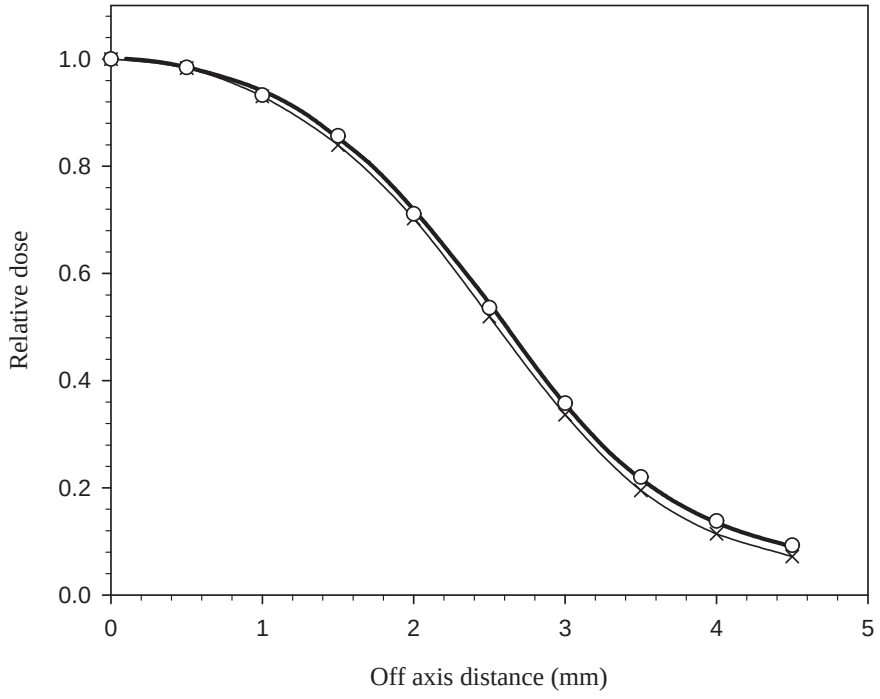
Relative dose
1.0
0.8
0.6
0.4
0.2
0.0
0
1
2
3
4
5
Off axis distance (mm)

(b)

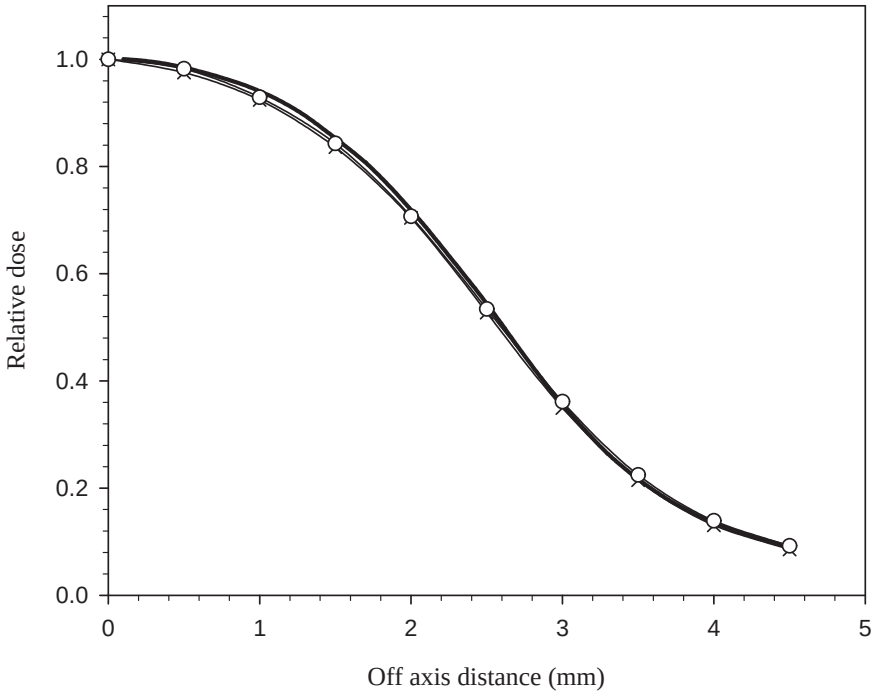

(c)

Figure 5.4. Cross axis profiles for all three detectors using the original design (black crosses) and the modified design (white circles). The 60016 photon diode is shown is (a); the 60017 electron diode is shown in (b); and the unenclosed chip is shown in (c). Also included in each graph are the results to water without the detectors present (thick black line). All results are for the 5 mm field size at a depth of 5 cm in water.

The modified version of the unenclosed silicon chip generally measured the cross axis profiles accurately, although a slight discrepancy is visible in the shoulder region.

Beam parameters.

Figure 5.5 shows the variation in $\frac{D_{w,Q}}{D_{Det,Q}}$ as a function of FWHM for each detector. In figure 5.6, $\frac{D_{w,Q}}{D_{Det,Q}}$ as a function of incident electron energy is displayed. Across all detectors, there is no substantial difference as a function of FWHM or energy. This could be because the total perturbation in all cases was less than 16 %, meaning it would take a very large change in beam parameters to alter this by more than 2 %, as this example would equate to a 12.5 % relative change.

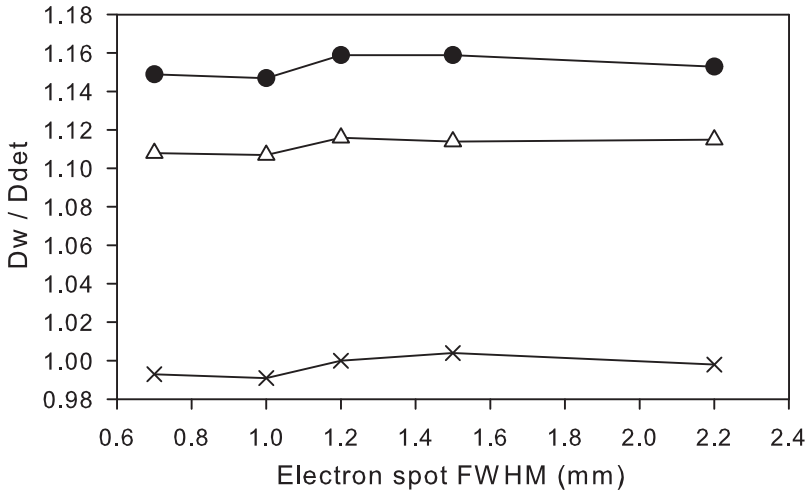

Figure 5.5. Simulated $\frac{D_{w,Q}}{D_{Det,Q}}$ for a 5 mm field size as a function of the full-width-half-maximum (FWHM) of the incident electron beam for all three detectors using the modified design: 60016 photon diode (crosses); 60017 electron diode (circles); unenclosed silicon chip (triangles). The Monte Carlo statistical uncertainty in each value is approximately 0.3 %.

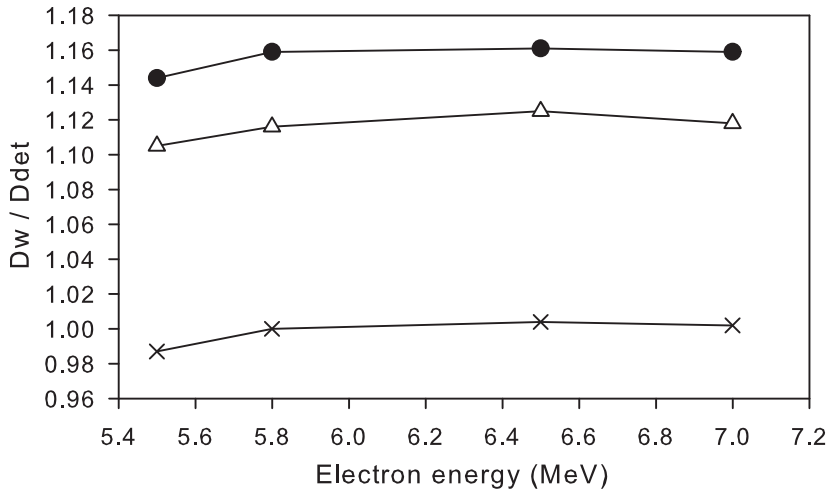

Figure 5.6. Simulated $\frac{D_{w,Q}}{D_{Det,Q}}$ for a 5 mm field size as a function of the energy of the incident electron beam for all three detectors using the modified design: 60016 photon diode (crosses); 60017 electron diode (circles); unenclosed silicon chip (triangles). The Monte Carlo statistical uncertainty in each value is approximately 0.3 %.

5.4 DISCUSSION

5.4.1 The effect of air gaps on different diodes

Figures 5.2 shows that the effect of air on small field dosimetry strongly depends on the detector design. For example the decrease in dose to the diode active volume caused by 1 mm of air for a 6 mm field was 2.5 %, 5.4 % and 18.2 % for the 60016 shielded diode, 60017 unshielded diode, and unenclosed silicon chip respsectively, despite all three detectors containing identical silicon chips. The difference is due to the rapid re-establishment of lateral electronic equilibrium after the air gap. The shielded diode contained 2.0 mm of material between the end of the detector and the silicon chip while the unshielded diode contained 0.6 mm and the silicon chip only detector obviously had no material between the chip and the air gap.

In terms of potential error that small air gaps would introduce, this also means that the shielded diode is least affected. However this diode has by far the largest sensitivity change in small fields (see table 5.2). The electron diode is less affected by air gaps than the OSLD based results published by Charles *et al* [5] (11.5 % / mm of air for the 6 mm field size). However the effect is still large enough to come to the same conclusion: very small air gaps can affect the results of small field dosimetry, and unintentional air gaps should therefore be avoided during measurements. It is recommended that liquid water should always be used for small field dosimetry, and the detector surface should be checked for the presence of air bubbles, when immersed in water.

5.4.2 Modified diode design

By calculating $\frac{D_{w,Q}}{D_{Det,Q}}$ for each diode at various field sizes it was possible to calculate how much air was required to eliminate the dependence of the diodes' sensitivity on field size. The optimal thickness of air was calculated to be 3.3 mm, 1.15 mm and 0.10 mm for the 60016 photon diode, 60017 electron diode and unenclosed chip respectively. The 60016 photon diode also required the width of the air gap to be

increased to 11 mm. Note that even though the shielded diode had an increased sensitivity at a field size of 12 mm (due to the metal shielding present), the 6.9 mm wide air-gap could not offset this.

Results shown in table 5.2 indicate that deliberately introducing these air gaps upstream to the detector successfully eliminated the dependence of the diodes on field size, for field sizes between 5 mm and 30 mm. This resulted in detectors that had $k_{Q_{clin},Q_{msr}}^{f_{clin},f_{msr}}$ = 1.000 within the statistical uncertainty 0.5 % (1 standard deviation) for all three diodes.

It has been shown that the output factors can be obtained at a range of different depths, without the need for a field size dependent correction factor (see figure 5.3). Therefore percentage depth dose curve (beyond the depth of maximum dose) will not be affected by the air. The modified detector designs also improve the accuracy of profile measurements, particularly in the penumbra region (see figure 5.4). The discrepancy between the unmodified 60017 electron diode and the water profiles was as high as 0.2 mm in the penumbra region. The modified diode design effectively eliminated this error.

The initial source parameters of the electron beam had minimal bearing on the results of this study (see figures 5.5 and 5.6). Therefore the modified diode designs will be able to be used with confidence on other nominally 6 MV photon beams. It has also been shown that these parameters have minimal influence on $k_{Q_{clin},Q_{msr}}^{f_{clin},f_{msr}}$ [2, 3, 16]. One can therefore possibly extend this concept to say that the relative dose perturbations caused by different detector designs are not affected by the small changes to beam quality or intensity caused by variations in initial electron beam parameters.

Evidently, deliberate use of the air gaps identified in this study could allow reliable and consistent small field dose measurements to be obtained directly, without the need to use Monte Carlo simulations (or other methods) to calculate the field size specific correction factors. For existing diodes, a ‘cap’ could be created consisting of an air cavity within a water equivalent material. This also has the advantage of the detector becoming dual purpose. For example the electron diode could still be used

for electron dosimetry without the cap; while adding the cap would create a very good small field dosimeter.

Alternatively, a new detector could be created with a small amount of air above a silicon active volume, effectively negating the sensitivity changes caused by the high density of silicon.

5.5 CONCLUSIONS

The effect on measured dose to two existing diodes caused by very small air gaps were quantified as 2.5 % / mm of air for the PTW 60016 shielded diode, and 5.4 % / mm for the PTW 60017 unshielded diode, for a 6 mm field size. This confirms that small volumes of air can substantially alter the results of small field dosimetry and that the unintentional introduction of air gaps adjacent to dosimeters should be avoided as much as possible. It is recommended that liquid water should always be used for small field dosimetry, and the detector surface should be checked for the presence of air bubbles, when immersed in water.

However, this work has also demonstrated that air could be introduced deliberately to the upstream end of these diodes to eliminate their dependence on field size in small field dosimetry. The thickness of the air required strongly depends on the design of the detector. 1.15 mm of air, placed at the end of PTW 60017 unshielded diode would eliminate the need to apply a field size specific sensitivity correction factor ($k_{Q_{clin},Q_{msr}}^{f_{clin},f_{msr}}$). The thickness of air required for the PTW 60016 shielded diode was 3.3 mm. The addition of these optimized air gaps also improved the accuracy of small field profiles.

Simulations of a theoretical unenclosed silicon chip showed that an ideal small field dosimeter that does not require sensitivity correction factors could be created by placing a small amount of air above the active volume. For a silicon chip with dimensions the same as the two PTW diodes, the thickness of air required would be 0.10 mm. The width of the air in the non-beam direction was shown to be an important factor.

This study provides a methodology by which manufacturers or designers might investigate the deliberate introduction of air or other low-density materials into the encapsulation of diodes, in order to achieve accurate and consistent small field dosimetry measurements.

5.6 ACKNOWLEDGEMENTS

This work was funded by the Australian Research Council in partnership with the Queensland University of Technology (QUT), the Wesley Research Institute and Premion (Linkage Grant No. LP110100401). Computational resources and services used in this work were provided by the High Performance Computing and Research Support Unit, (QUT), Brisbane, Australia.

5.7 REFERENCES

1 G. Cranmer-Sargison, S. Weston, N.P. Sidhu, D.I. Thwaites, "Experimental small field 6MV output ratio analysis for various diode detector and accelerator combinations," Radiother Oncol **100**, 429-435 (2011).

2 A.J. Scott, S. Kumar, A.E. Nahum, J.D. Fenwick, "Characterizing the influence of detector density on dosimeter response in non-equilibrium small photon fields," Phys Med Biol **57**, 4461-4476 (2012).

3 G. Cranmer-Sargison, S. Weston, J.A. Evans, N.P. Sidhu, D.I. Thwaites, "Monte Carlo modelling of diode detectors for small field MV photon dosimetry: detector model simplification and the sensitivity of correction factors to source parameterization," Phys Med Biol **57**, 5141-5153 (2012).

4 G. Cranmer-Sargison, S. Weston, J.A. Evans, N.P. Sidhu, D.I. Thwaites, "Implementing a newly proposed Monte Carlo based small field dosimetry formalism for a comprehensive set of diode detectors," Medical Physics **38**, 6592-6602 (2011).

[5] P.H. Charles, S.B. Crowe, T. Kairn, J. Kenny, J. Lehmann, J. Lye, L. Dunn, B. Hill, R.T. Knight, C.M. Langton, J.V. Trapp, "The effect of very small air gaps on small field dosimetry," Phys Med Biol **57**, 6947-6960 (2012).

[6] R. Alfonso, P. Andreo, R. Capote, M.S. Huq, W. Kilby, P. Kjäll, T.R. Mackie, H. Palmans, K. Rosser, J. Seuntjens, W. Ullrich, S. Vatnitsky, "A new formalism for reference dosimetry of small and nonstandard fields," Medical Physics **35**, 5179 (2008).

[7] D.W.O. Rogers, B.A. Faddegon, G.X. Ding, C.M. Ma, J. We, "BEAM: A Monte Carlo code to simulate radiotherapy treatment units," Medical Physics **22**, 503 - 524 (1995).

[8] T. Kairn, T. Aland, R.D. Franich, P.N. Johnston, M.B. Kakakhel, J. Kenny, R.T. Knight, C.M. Langton, D. Schlect, M.L. Taylor, J.V. Trapp, "Adapting a generic BEAMnrc model of the BrainLAB m3 micro-multileaf collimator to simulate a local collimation device," Phys Med Biol **55**, N451-463 (2010).

[9] T. Kairn, J. Kenny, S.B. Crowe, A.L. Fielding, R.D. Franich, P.N. Johnston, R.T. Knight, C.M. Langton, D. Schlect, J.V. Trapp, "Technical Note: Modeling a complex micro-multileaf collimator using the standard BEAMnrc distribution," Medical Physics **37**, 1761 (2010).

[10] A.J.D. Scott, A.E. Nahum, J.D. Fenwick, "Using a Monte Carlo model to predict dosimetric properties of small radiotherapy photon fields," Medical Physics **35**, 4671 (2008).

[11] A.J.D. Scott, A.E. Nahum, J.D. Fenwick, "Monte Carlo modeling of small photon fields: Quantifying the impact of focal spot size on source occlusion and output factors, and exploring miniphantom design for small-field measurements," Medical Physics **36**, 3132 (2009).

[12] I. Kawrakow, E. Mainegra-Hing, F. Tessier, B.R.B. Walters, "The EGSnrc C++ class library, ," NRC Report PIRS-898 (rev A)2009).

[13] B. Walters, I. Kawrakow, D.W.O. Rogers, Report No. NRCC Report PIRS-794revB, 2011.

[14] F. Crop, N. Reynaert, G. Pittomvils, L. Paelinck, C. De Wagter, L. Vakaet, H. Thierens, "The influence of small field sizes, penumbra, spot size and measurement depth on perturbation factors for microionization chambers," Phys Med Biol **54**, 2951-2969 (2009).

[15] P. Francescon, W. Kilby, N. Satariano, S. Cora, "Monte Carlo simulated correction factors for machine specific reference field dose calibration and output factor measurement using fixed and iris collimators on the CyberKnife system," Phys Med Biol **57**, 3741-3758 (2012).

[16] P. Francescon, S. Cora, N. Satariano, "Calculation of k(Q(clin),Q(msr)) (f(clin),f(msr)) for several small detectors and for two linear accelerators using Monte Carlo simulations," Medical Physics **38**, 6513-6527 (2011).

Chapter 6: The influence of Monte Carlo source parameters on detector design and dose perturbation in small field dosimetry

P H Charles[1], S B Crowe[1], T Kairn[1,2], R T Knight[2], B Hill[2], J Kenny[3,4], C M Langton[1] and J V Trapp[1].

[1] School of Chemistry, Physics and Mechanical Engineering, Queensland University of Technology, Brisbane, Australia

[2] Premion, The Wesley Medical Centre, Auchenflower, Qld, Australia

[3] The Australian Clinical Dosimetry Service, Australian Radiation Protection and Nuclear Safety Agency, Yallambie, Vic, Australia

[4] Radiation Oncology Queensland, St Andrew's Toowoomba Hospital, Toowoomba, Qld, Australia

Journal: Journal of Physics Conference Series

Status: Published March 2014

STATEMENT OF JOINT AUTHORSHIP

Title: Monte Carlo-based diode design for correction-less small field dosimetry

Authors: Paul Charles; Scott Crowe; Tanya Kairn; Richard Knight; Brendan Hill; John Kenny; Christian Langton; Jamie Trapp;

Paul Charles (candidate)
Project concept, direction and design. Performed all Monte Carlo simulations. Analysed an interpreted all results. Wrote the manuscript.

Scott Crowe
Supplied Monte Carlo model of linac. General advice and supervision as required. Edited manuscript.

Tanya Kairn
Supplied Monte Carlo model of linac. General advice and supervision as required. Edited manuscript

Richard Knight
General advice and supervision as required.

Brendan Hill
General advice and supervision as required.

John Kenny
General advice and supervision as required.

Christian Langton
General advice and supervision as required.

Jamie Trapp
General advice and supervision as required. Edited manuscript.

ABSTRACT

To obtain accurate Monte Carlo simulations of small radiation fields, it is important to model the initial source parameters (electron energy and spot size) accurately. However recent studies have shown that small field dosimetry correction factors are insensitive to these parameters. The aim of this work is to extend this concept to test if these parameters affect dose perturbations in general, which is important for detector design and calculating perturbation correction factors.

The EGSnrc C++ user code cavity was used for all simulations. Varying amounts of air between 0 and 2 mm were deliberately introduced upstream to a diode and the dose perturbation caused by the air was quantified. These simulations were then repeated using a range of initial electron energies (5.5 to 7.0 MeV) and electron spot sizes (0.7 to 2.2 mm FWHM).

The resultant dose perturbations were large. For example 2 mm of air caused a dose reduction of up to 31% when simulated with a 6 mm field size. However these values did not vary by more than 2 % when simulated across the full range of source parameters tested.

If a detector is modified by the introduction of air, one can be confident that the response of the detector will be the same across all similar linear accelerators and the Monte Carlo modelling of each machine is not required.

6.1 INTRODUCTION AND AIM

Small air gaps upstream to a diode active volume heavily perturb small photon fields causing a large reduction in dose to the active volume[1, 2]. Therefore air can be deliberately introduced into diode designs to negate the inherent over-response of diodes in small photon fields[2]. The amount of air required to produce a diode which responds uniformly at all field sizes depends on the diode design[2].

The aim of this work is to study the dependence of the dose reduction caused by controlled amounts of air on the Monte Carlo initial source parameters (incident electron spot size and energy) of a linear accelerator. Hence this study reveals if a new diode design involving any amount of air can be used with confidence across a population of similar linear accelerators.

6.2 BACKGROUND

Dosimetry of small photon fields presents many challenges, one of the largest being the perturbation of the beam by the detector used[3-5]. Traditional radiation detectors such as ionization chambers and diodes become relatively large compared to the size of the field, and therefore the composition of these detectors becomes important when calculating the response of the detector in a small field.

Alfonso *et al*[4] proposed a formalism where the change in sensitivity of a detector as a function of small field size is accounted for by applying an additional factor $k_{Q_{clin},Q_{msr}}^{f_{clin},f_{msr}}$ to standard output factor measurements.

$k_{Q_{clin},Q_{msr}}^{f_{clin},f_{msr}}$ has been systematically calculated for diodes using Monte Carlo modelling[6-9] and its value depends strongly on the composition of the detector[10]. Diodes have been shown to have increased sensitivity in small fields due to the high density of the silicon active volume[11, 12] as well as high density metals which may be upstream to the active volume[10]. It has been shown that $k_{Q_{clin},Q_{msr}}^{f_{clin},f_{msr}}$ values calculated via Monte Carlo simulations for diodes are independent of the initial source

parameters used to model the linear accelerator (incident electron energy and focal spot size)[8-10]. However in each case the exact composition of the detector has been modelled, so the results are very specific to those detectors.

In a recent study Charles *et al*[2] used Monte Carlo simulations to study the effect of deliberately introducing air into diodes such that the dose reduction caused by the air eliminated the field size dependence of the diode. The authors successfully calculated the amount of air that would be required for a shielded diode, an unshielded diode and a theoretical unenclosed silicon chip to respond uniformly at all field sizes. In each case the air was simulated to be on the upstream end on the diode.

6.3 METHODOLOGY

6.3.1 Monte Carlo simulation overview

All linear accelerator Monte Carlo simulations were performed using the user code BEAMnrc[13] and a previously modeled Varian iX (Varian Medical Systems, Palo Alto, CA)[2, 14, 15]. The field size used throughout this study was a 6 mm × 6 mm square.

All diode simulations were performed using the EGSnrc C++ user code cavity[16]. The unmodified diode used in this study was a simple cylindrical silicon chip (see figure 1). All detector simulations were performed in water at a depth of 5 cm and source to detector distance of 100 cm. All dose calculations were performed on the central axis of the beam.

In the phantom material, the electron and photon cut off energies were chosen to be 521 and 10 keV respectively. Inside the volume of the simulated diode they were reduced to 512 and 1 keV respectively for increased accuracy within the detector volume and air gaps. Sufficient histories were simulated so that the statistical uncertainty of the Monte Carlo calculated correction factors was maintained at less than 0.5%.

6.3.2 Modification of the diode with air

Air was introduced immediately upstream to the silicon active volume (see figure 6.1). For each case the dose to active volume of the diode was calculated, as was the dose reduction caused by the air gap. Here dose reduction refers to the percent change in dose when compared to the dose to the detector with no air present. That is:

Dose reduction (x) = $[(D_{Det,air(x)} - D_{Det,air(0)}) / D_{Det,air(0)}]$ x 100

$D_{Det,air(x)}$ is the dose to the detector with x mm thickness of air placed upstream.
The simulations were initially performed with an incident electron energy onto the target of 5.8 MeV and a focal spot size of 1.2 mm. The simulations were repeated for an incident electron energy of 7.0 MeV (the focal spot size remained 1.2 mm) and the dose differences caused by the air were compared.

Keeping the energy constant at 5.8 MeV, the simulations were then repeated using the following focal spot sizes: 0.4, 0.7, and 2.2 mm. Once again the dose reduction caused by the air was compared across the different focal spot sizes.

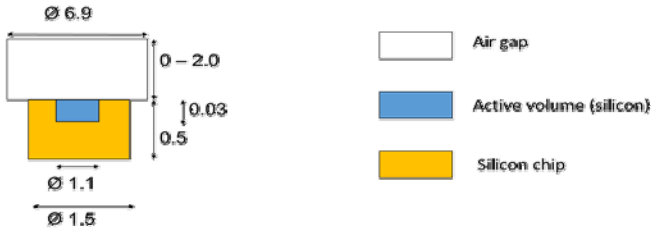

Figure 6.1. The simulation geometry of the detector used in this study (a basic silicon chip) and the upstream air gap. The dimensions are shown in mm. The diagram is not to scale.

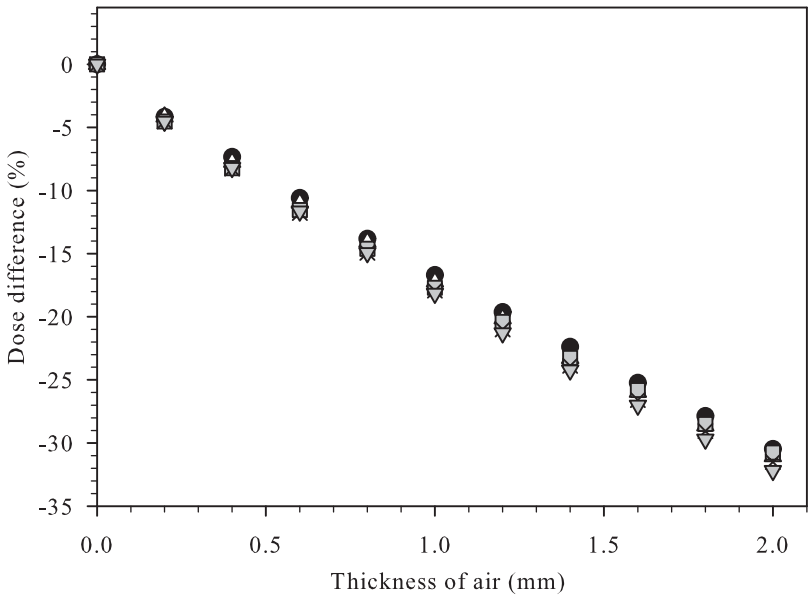

Figure 6.2. The dose reduction as a function of upstream air thickness. Dose reduction refers to the change in dose relative to a simulation with no air gap. Shown here are the results using an incident electron energy of 5.8 MeV and an incident electron spot size of 0.4 mm (black circles), 0.7 mm (white triangles), 1.2 mm (grey squares) and 2.2 mm (crosses). Also shown is the results for an incident electron energy of 7.0 MeV (grey upside-down triangles) (spot size = 1.2 mm).

6.4 RESULTS AND DISCUSSION

The dose difference as a function of air gap thickness is presented in figure 6.2 for the two different incident electron energies and for the various focal spot sizes. It can be seen that while the air strongly perturbs the dose to the detector, this dose difference does not vary greatly with the initial source parameters.

Air causes a large dose reduction to the active volume due to the filtering of electrons with a high angle of incidence[1]. However the dose reduction results were consistent across all input parameter variations. The consistency of these results suggests that the incident source parameters do not significantly affect the subsequent angular distribution of the dose depositing electrons in water. One can therefore be confident that introducing any amount of air into a detector design will result in a consistent effect across multiple linear accelerators.

6.5 CONCLUSIONS

This study showed the influence on initial source parameters on the dose perturbation caused by air placed immediately upstream to a silicon active volume at the central axis of the beam. If a detector is modified by the introduction of air, one can be confident that the response of the detector will be the same across all similar linear accelerators and the Monte Carlo modeling of each machine is not required.

6.6 ACKNOWLEDGEMENTS

This work was funded by the Australian Research Council in partnership with the Queensland University of Technology, the Wesley Research Institute and Premion (Linkage Grant No. LP110100401). Computational resources and services used in this work were provided by the High Performance Computing and Research Support Unit, Queensland University of Technology (QUT), Brisbane, Australia.

6.7 REFERENCES

1 P.H. Charles, S.B. Crowe, T. Kairn, J. Kenny, J. Lehmann, J. Lye, L. Dunn, B. Hill, R.T. Knight, C.M. Langton, J.V. Trapp, "The effect of very small air gaps on small field dosimetry," Phys Med Biol **57**, 6947-6960 (2012).

2 P.H. Charles, S.B. Crowe, T. Kairn, R.T. Knight, B. Hill, J. Kenny, C.M. Langton, J.V. Trapp, "Monte Carlo-based diode design for correction-less small field dosimetry," Phys Med Biol **58**, 4501-4512 (2013).

3 I.J. Das, G.X. Ding, A. Ahnesjö, "Small fields: Nonequilibrium radiation dosimetry," Medical Physics **35**, 206 (2008).

4 R. Alfonso, P. Andreo, R. Capote, M.S. Huq, W. Kilby, P. Kjäll, T.R. Mackie, H. Palmans, K. Rosser, J. Seuntjens, W. Ullrich, S. Vatnitsky, "A new formalism for reference dosimetry of small and nonstandard fields," Medical Physics **35**, 5179 (2008).

[5] M.L. Taylor, T. Kron, R.D. Franich, "A contemporary review of stereotactic radiotherapy: inherent dosimetric complexities and the potential for detriment," Acta Oncol **50**, 483-508 (2011).

[6] G. Cranmer-Sargison, S. Weston, J.A. Evans, N.P. Sidhu, D.I. Thwaites, "Implementing a newly proposed Monte Carlo based small field dosimetry formalism for a comprehensive set of diode detectors," Medical Physics **38**, 6592-6602 (2011).

[7] P. Francescon, S. Cora, N. Satariano, "Calculation of k(Q(clin),Q(msr)) (f(clin),f(msr)) for several small detectors and for two linear accelerators using Monte Carlo simulations," Medical Physics **38**, 6513-6527 (2011).

[8] P. Francescon, W. Kilby, N. Satariano, S. Cora, "Monte Carlo simulated correction factors for machine specific reference field dose calibration and output factor measurement using fixed and iris collimators on the CyberKnife system," Phys Med Biol **57**, 3741-3758 (2012).

[9] D. Czarnecki, K. Zink, "Monte Carlo calculated correction factors for diodes and ion chambers in small photon fields," Phys Med Biol **58**, 2431-2444 (2013).

[10] G. Cranmer-Sargison, S. Weston, J.A. Evans, N.P. Sidhu, D.I. Thwaites, "Monte Carlo modelling of diode detectors for small field MV photon dosimetry: detector model simplification and the sensitivity of correction factors to source parameterization," Phys Med Biol **57**, 5141-5153 (2012).

[11] A.J. Scott, S. Kumar, A.E. Nahum, J.D. Fenwick, "Characterizing the influence of detector density on dosimeter response in non-equilibrium small photon fields," Phys Med Biol **57**, 4461-4476 (2012).

[12] J.D. Fenwick, S. Kumar, A.J. Scott, A.E. Nahum, "Using cavity theory to describe the dependence on detector density of dosimeter response in non-equilibrium small fields," Phys Med Biol **58**, 2901-2923 (2013).

[13] D.W.O. Rogers, B.A. Faddegon, G.X. Ding, C.M. Ma, J. We, "BEAM: A Monte Carlo code to simulate radiotherapy treatment units," Medical Physics **22**, 503 - 524 (1995).

[14] T. Kairn, T. Aland, R.D. Franich, P.N. Johnston, M.B. Kakakhel, J. Kenny, R.T. Knight, C.M. Langton, D. Schlect, M.L. Taylor, J.V. Trapp, "Adapting a generic BEAMnrc model of the BrainLAB m3 micro-multileaf collimator to simulate a local collimation device," Phys Med Biol **55**, N451-463 (2010).

[15] T. Kairn, J. Kenny, S.B. Crowe, A.L. Fielding, R.D. Franich, P.N. Johnston, R.T. Knight, C.M. Langton, D. Schlect, J.V. Trapp, "Technical Note: Modeling a complex micro-multileaf collimator using the standard BEAMnrc distribution," Medical Physics **37**, 1761 (2010).

[16] I. Kawrakow, E. Mainegra-Hing, F. Tessier, B.R.B. Walters, "The EGSnrc C++ class library, ," NRC Report PIRS-898 (rev A)2009).

Chapter 7: Design and experimental testing of air slab caps which convert commercial electron diodes into dual purpose, correction-free diodes for small field dosimetry

P H Charles[1,2], G Cranmer-Sargison[3,4], D I Thwaites[5], T Kairn[2,6], S B Crowe[2], G Pedrazzini[6], T Aland[7], J Kenny[7], C M Langton[2], J V Trapp[2]

[1]Radiation Oncology, Princess Alexandra Hospital, Brisbane, Australia

[2]School of Chemistry, Physics and Mechanical Engineering, Queensland University of Technology, Brisbane, Australia

[3]Department of Medical Physics, Saskatchewan Cancer Agency, Saskatoon, Canada

[4]College of Medicine, University of Saskatchewan, Saskatoon, Canada

[5]Institute of Medical Physics, School of Physics, University of Sydney, Australia

[6]Premion, The Wesley Medical Centre, Brisbane, Australia

[7]Epworth Radiation Oncology, Richmond, Vic, Australia

Journal: Medical Physics

Status: Accepted July 2014

STATEMENT OF JOINT AUTHORSHIP

Title: Design and experimental testing of correction-free diodes for small field dosimetry

Authors: Paul Charles; Gavin Cranmer-Sargison; David Thwaites; Scott Crowe; Tanya Kairn; Richard Knight; John Kenny; Christian Langton; Jamie Trapp;

Paul Charles (candidate)
Project concept, direction and design. Performed all Monte Carlo simulations. Performed all measurements with the PTWe diode. Analysed an interpreted all results. Wrote the manuscript.

Gavin Cranmer-Sargison
Contributed to the design and direction of project. Performed all measurements using the Sun-Nuclear EDGEe diode. Wrote some of manuscript. Edited of manuscript.

David Thwaites
Provided discussion and advice as required. Edited of manuscript.

Tanya Kairn
Assisted with measurements using the PTWe diode. Supplied Monte Carlo model of linac. General advice and supervision as required. Edited manuscript.

Scott Crowe
Supplied Monte Carlo model of linac. General advice and supervision as required. Edited manuscript.

Greg Pedrazzini
Designed and manufactured the air cap for PTW electron diode.

Trent Aland
Assisted with measurements, including the functional use of the air cap. Edited manuscript.

John Kenny

General advice and supervision as required.

Christian Langton

General advice and supervision as required.

Jamie Trapp

Provided advice and supervision as required. Edited manuscript.

ABSTRACT

Purpose: Two diodes which do not require correction factors for small field relative output measurements are designed and validated using experimental methodology. This was achieved by adding an air layer above the active volume of the diode detectors, which cancelled out the increase in response of the diodes in small fields relative to standard field sizes.

Methods: Due to the increased density of silicon and other components within a diode, additional electrons are created. In very small fields, a very small air gap acts as an effective filter of electrons with a high angle of incidence. The aim was to design a diode that balanced these perturbations to give a response similar to a water only geometry.

Three thicknesses of air were placed at the proximal end of a PTW 60017 electron diode (PTWe) using an adjustable 'air cap'. A set of output ratios (OR_{Det}) for square field sizes of side length down to 5 mm were measured using each air thickness and compared to OR_{Det} measured using an IBA stereotactic field diode (SFD). $k_{Q_{clin},Q_{msr}}^{f_{clin},f_{msr}}$ was transferred from the SFD to the PTWe diode and plotted as a function of air gap thickness for each field size. This enabled the optimal air gap thickness to be obtained by observing which thickness of air was required such that $k_{Q_{clin},Q_{msr}}^{f_{clin},f_{msr}}$ was equal to 1.00 at all field sizes. A similar procedure was used to find the optimal air thickness required to make a modified Sun Nuclear EDGE detector (EDGEe) which is "correction-free" in small field relative dosimetry. In addition, the feasibility of experimentally transferring $k_{Q_{clin},Q_{msr}}^{f_{clin},f_{msr}}$ values from the SFD to unknown diodes, was tested by comparing the experimentally transferred $k_{Q_{clin},Q_{msr}}^{f_{clin},f_{msr}}$ values for unmodified PTWe and EDGEe diodes to Monte Carlo simulated values.

Results: 1.0 mm of air was required to make the PTWe diode correction-free. This modified diode ($PTWe_{air}$) produced output factors equivalent to those in water at all field sizes (5 mm to 50 mm). The optimal air thickness required for the EDGEe diode was found to be 0.6 mm. The modified diode ($EDGEe_{air}$) produced output factors equivalent to those in water, except at field sizes of 8 mm and 10 mm where

it measured approximately 2 % greater than the relative dose to water. The experimentally calculated $k_{Q_{clin},Q_{msr}}^{f_{clin},f_{msr}}$ for the both the PTWe and the EDGEe diodes (without air) matched Monte Carlo simulated results; thus proving that it is feasible to transfer $k_{Q_{clin},Q_{msr}}^{f_{clin},f_{msr}}$ from one commercially available detector to another using experimental methods, and the recommended experimental setup.

Conclusions: It is possible to create a diode which does not require corrections for small field output factor measurements. This has been performed and verified experimentally. The ability of a detector to be "correction-free" depends strongly on its design and composition. A non-water-equivalent detector can only be "correction-free" if competing perturbations of the beam cancel out at all field sizes. This should not be confused with true water equivalency of a detector.

7.1 INTRODUCTION

With a small active volume, diode detectors are often used for small field relative dosimetry. However, the higher density of the silicon active volume relative to that of water is problematic at small field sizes[1-3] - with measured relative output ratios being greater than those applicable to a water-only situation, and also a function of field size. Scott *et al*[1] have demonstrated through Monte Carlo simulation that the diode detector over-response is a silicon density effect relative to that of water. Fenwick *et al*[2] has shown that when compared to water the diode detector over-response is the result of an increased number of internally generated electrons that do not escape from the active volume.

In addition to the active volume, other non-water equivalent components used in diode detectors will also perturb the beam[4-8]. For example, the active volume of a diode is a thin layer of silicon placed on top of a thicker layer of silicon that causes additional backscatter. Cranmer-Sargison[4] et al found that scatter from the steel shielding found in the PTW60016 diode increased the dose to the active volume by 7 % at a field size of 5 mm. Francescon et al[8] showed that the uncertainty of the density of the epoxy material used in diodes will cause an uncertainty in the over-all response of the detector. As such, the sensitivity of a diode detector in small fields is very dependent on the construction of the diode and is a function of field size.

Alfonso *et al* has presented a framework whereby the change in the detector response can be corrected for by applying a field size dependent correction factor $k_{\frac{f_{clin}f_{msr}}{Q_{clin}Q_{msr}}}$ [9]. However, this correction factor needs to be determined for each detector and field size combination and therefore the motivation to fabricate a diode based detector that does not require a correction becomes clear. The recent Monte Carlo work of Charles *et al*[6] has shown that an air volume placed upstream of the active silicon volume will perturb the small field in such a way as to cancel out the over-response of a diode detector for field sizes as small as 5 mm. Underwood *et al*[7] showed how air can be used to produce a theoretical correction-free diamond detector at small field sizes. The current study experimentally verifies the Monte Carlo results from Charles *et al*[6] for the PTW 60017 electron diode (PTWe); thus constructing the first correction-free

diode for small field dosimetry. The concept of combining Monte Carlo simulation with experimental measurements to design a modified Sun Nuclear Edge diode is also explored in detail, leading to general recommendations for detector design for small field dosimetry.

7.2 METHOD

7.2.1 Monte Carlo modelling of the custom Sun Nuclear EDGE ("EDGEe") diode

Monte Carlo overview

All linear accelerator simulations were performed with the BEAMnrc Monte Carlo user code[10] , using a model of the Varian 21iX (Varian Medical Systems, Palo Alto, USA) that had previously been commissioned in other studies for field sizes as small as 5 mm[6, 11, 12]. The incident electron fluence onto the target of this linear accelerator was modeled as centrally symmetric with a Gaussian distribution with a full-width-half-maximum (FWHM) equal to 1.2 mm. The electron spot size was tuned using the methodology of Cranmer-Sargison *et al*[13]. All phantom simulations were performed using the EGSnrc C++ user code cavity[14]. Unless otherwise stated, all simulations had an ECUT value of 512 keV and a PCUT value of 1 keV. All simulations were performed at a nominal energy of 6 MV at a depth in water of 5 cm, and a source-to-measurement distance of 100 cm.

Simulation of $\frac{D_{w,Q}}{D_{Det,Q}}$ and $k_{Q_{clin},Q_{msr}}^{f_{clin},f_{msr}}$

In this study, $D_{w,Q}$ denotes the dose to a point in a 100 % water geometry (no detector present); while $D_{Det,Q}$ represents the dose to a detector active volume within water. Unless a detector is made out of water, these values will be different. The dose ratio $\frac{D_{w,Q}}{D_{Det,Q}}$, was the primary metric used in the Monte Carlo-based study by Charles *et al*[6] and is used again in this study for consistency. This ratio effectively gives the

relative response of a detector, compared to an ideal water geometry. The dose per incident particle to the detector active volume was scored for a particular field size ($D_{Det,Q}$) . Under the same conditions, the dose per incident particle scored to a cylindrical volume of water 0.5 mm in diameter (perpendicular-to-beam direction) and 2 mm deep (beam direction), in place of the detector ($D_{W,Q}$) . The ratio of these two simulation results ($\frac{D_{W,Q}}{D_{Det,Q}}$) was calculated for various square field sizes with side lengths ranging from 5 mm to 30 mm.

$k_{Q_{clin},Q_{msr}}^{f_{clin},f_{msr}}$ was then calculated as follows[9].

$$k_{Q_{clin},Q_{msr}}^{f_{clin},f_{msr}} = \left[\frac{D_{W,Q_{clin}}^{f_{clin}} / D_{Det,Q_{clin}}^{f_{clin}}}{D_{W,Q_{msr}}^{f_{msr}} / D_{Det,Q_{msr}}^{f_{msr}}}\right] \qquad (7.1)$$

In this study the machine specific reference field size (f_{msr}) was 30 mm; while f_{clin} represents each test field size.

The influence of diode components on measured dose

Figure 7.1 displays the geometry and materials used to model the Sun Nuclear EDGE diode. The Sun Nuclear Edge detector was modeled with four different designs; each sequentially removing a high density component:

1. The Sun Nuclear EDGE detector as commercially available (i.e. in full)
2. As the EDGEe detector used experimentally in this study (i.e. with the copper backscatter shielding removed and replaced with acrylic).
3. The EDGEe with the brass external shielding removed
4. The EDGEe with the brass external shielding removed and the Epoxy set to a water equivalent density instead of 1.5 g/cm^3.

The response of the diode in each configuration above was compared to the dose simulated in water using the following equation:

$$R_{Det,w} = \left[\frac{D^{f\,clin}_{Det,Q_{clin}} / D^{f\,msr}_{Det,Q_{msr}}}{D^{f\,clin}_{w,Q_{clin}} / D^{f\,msr}_{w,Q_{msr}}} - 1 \right] \times 100 \qquad (7.2)$$

Where $R_{Det,w}$ is defined as the 'response error' of the detector relative to dose to water calculated for each field size.

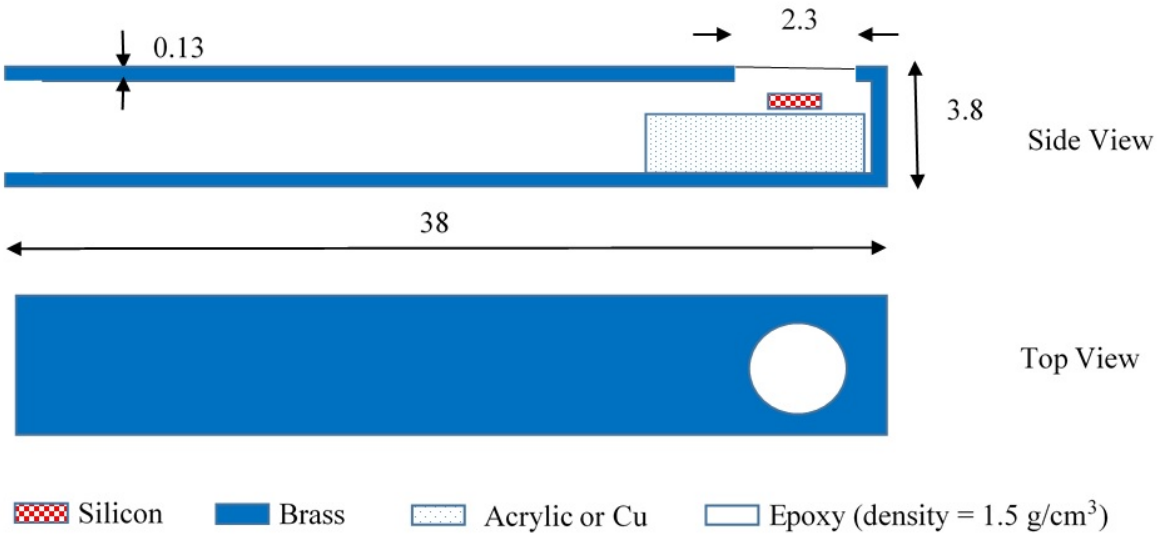

Figure 7.1. The A Schematic diagram of the Sun Nuclear EDGE diode geometry used for Monte Carlo simulations. All dimensions are shown in mm. The silicon chip is 0.4 mm x 1.3 mm x 1.3 mm and is 0.3 mm from the top of the diode. The active volume is 0.03 mm x 0.8 mm x 0.8 mm and is 0.1 mm from the top of the chip. Note that the diagram is not to scale.

Initial optimisation of air gap size for correction-free EDGEe

The optimal air gap thickness required to convert the EDGEe diode was calculated using the methodology set out in Charles *et al*[6]. The response ratio of the dose in water without a detector, relative to the dose calculated in the detector active volume ($\frac{D_{w,Q}}{D_{Det,Q}}$), was simulated as a function of upstream air gap thickness for field sizes of 5, 6, 8, 10, 12, 20 and 30 mm. Each data set was plotted on the same graph and the intersection point of the data, that is where $\frac{D_{w,Q}}{D_{Det,Q}}$ was the same for all field sizes, was found - which represents the optimal air gap thickness required to correct for the detector over-response. For these simulations the air gap width used was set to 6.9 mm, consistent with the width used for the majority of the simulations in Charles *et al*[6]. The resultant optimal air thickness found through the Monte Carlo simulations was used as an approximate baseline for the experimental optimization process.

7.2.2 Experimental optimisation of correction-free diodes

Output ratios (OR_{Det}) were measured using the stereotactic field diode (SFD), PTW T60017 electron diode (PTWe) and the modified Sun Nuclear EDGE diode (EDGEe) at nominal field sizes of 5, 6, 8, 10, 20 and 30 mm. Each OR_{Det} was calculated by normalising the measured signal for each field size in question back to the signal measured in the 30 mm field size. The measurement depth was 5 cm in water with a 100 cm source-to-detector distance (SDD). The extremely careful experimental methodology set out by Cranmer-Sargison *et al*[15] was used for the field sizes smaller than 15 mm[16], including the measurement of field size at the same time as the OR_{Det} measurement. A benchmark set of field size measurements were performed using the SFD and validated during each subsequent experimental set-up.

Experimental transfer of $k_{Q_{clin},Q_{msr}}$

An experimental transfer of $k_{Q_{clin},Q_{msr}}$ was performed from the previously benchmarked SFD to either of the other detectors using the following equation:

$$k_{Q_{clin},Q_{msr}}^{DET_{clin},DET_{msr}} = k_{Q_{clin},Q_{msr}}^{SFD_{clin},SFD_{msr}} \frac{OR_{SFD}}{OR_{DET}} \qquad (7.3)$$

Where $k_{Q_{clin},Q_{msr}}^{SFD_{clin},SFD_{msr}}$ was taken to be that of Cranmer-Sargison *et al*[13] calculated using Monte Carlo simulations. The total uncertainty expected using this technique was evaluated using the reported uncertainty on $k_{Q_{clin},Q_{msr}}^{SFD_{clin},SFD_{msr}}$ at ±1.0 %[13] added in quadrature with the experimental uncertainty in OR_{Det} at very small field sizes (±0.2 – ±0.7 % depending on field size).

Air gap optimization for the PTW T60017

A custom made 'air-cap' (see figure 7.2) was placed over the end of the PTWe diode. This air tight cap consisted of a cylindrical cavity, 7 mm in diameter, formed by a

thin (< 1 mm) piece of delrin plastic. The cap could be fastened at any point on the stem of the PTWe using a screw. Thus an air gap of any thickness could be created at the proximal end of the diode detector. In all cases the OR_{PTWe} data was re-measured at each field size with air gap thickness of 0.5, 1.0 and 1.5 mm. These air gap thicknesses were set using Vernier callipers with an uncertainty of < ±0.1 mm. Another set of data was measured with the cap on but the air gap set to 0.0 mm. This was done to show that the cap had no beam perturbing effects.

$k_{Q_{clin},Q_{msr}}^{PTWe_{clin},PTWe_{msr}}$ was calculated for each air gap thickness and field size. Each data set was plotted on the same graph and the intersection point of the functions showed the optimal air gap thickness required. This intersection point represented where $k_{Q_{clin},Q_{msr}}^{PTWe_{clin},PTWe_{msr}}$ was the same at all field sizes (and by definition equal to 1).

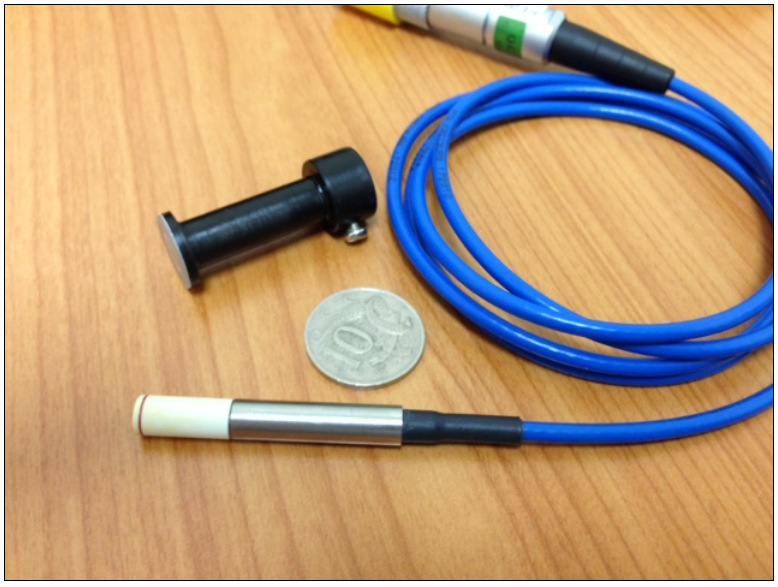

Figure 7.2. The PTWe diode along with the custom made 'air cap'. Shown for scale is a coin with a diameter of 24 mm.

Air gap optimization for the EDGEe

A series of Solid Water 'air tops' which locked on top of the EDGEe detector were fabricated (see figure 7.3) with the following air gap thickness: 0.0, 0.3, 0.6 and 0.9 mm. Three different sets of the four tops were created to investigate the effect of air gap width on the response of the EDGEe. The three sets had air gap widths equal to

3.06, 4.53 and 6.19 mm. This approach was taken to test if experimental results alone could be used to optimize the required air top. The optimal air gap thickness was found in an identical manner as for the PTWe for each of the three different air gap widths.

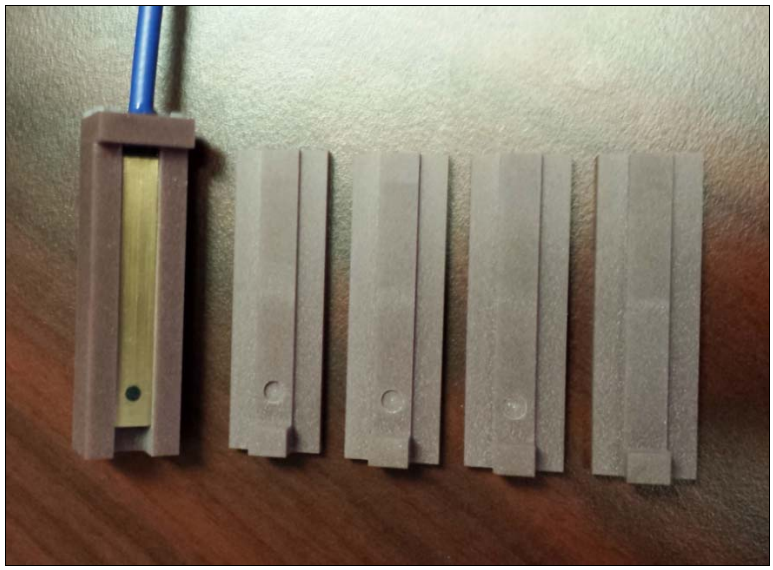

Figure 7.3.The 'air tops' used in conjunction with the EDGEe diode. Shown here is the set of tops with a width of 3.03 mm.

7.2.3 Uncertainty analysis

The uncertainty in the $k_{Q_{clin},Q_{msr}}^{EDGEe_{clin},EDGEe_{msr}}$ values calculated by Monte Carlo simulations (see section 2.1.2) was found by adding the reported statistical uncertainty of each component of equation 7.1 in quadrature. The uncertainty in the Monte Carlo calculated values of $k_{Q_{clin},Q_{msr}}^{PTWe_{clin},PTWe_{msr}}$ was taken directly from Charles *et al*[6], and was equal to 0.5 % at all field sizes. The uncertainty in the Monte Carlo calculated values of $k_{Q_{clin},Q_{msr}}^{SFD_{clin},SFD_{msr}}$ was taken directly from Cranmer-Sargison *et al*[13], and was equal to 1.0 % at all field sizes.

The experimental uncertainty of the output ratio measurements was estimated from the results of Cranmer-Sargison *et al*[15], where the authors measured output ratios using the PTWe diode in three independent experimental sessions. The standard error of the mean output ratio was calculated for each field size across the three

experimental sessions. This was performed on five different linear accelerators. The average standard error on the mean output ratio across the five linear accelerators was used as the experimental uncertainty of the measurement in the current study.

Table 7.1. Average standard error of mean for each field size used.

Nominal Field size (mm)	Average standard error of mean (%)[15]
5	0.7
6	0.6
8	0.4
10	0.2
20	0.5
30	0.1

The uncertainty in the experimentally derived $k_{Q_{cltn},Q_{msr}}^{DET_{cltn},DET_{msr}}$ values were calculated by combining in quadrature the uncertainties in $k_{Q_{cltn},Q_{msr}}^{SFD_{cltn},SFD_{msr}}$ and two sets of experimental output ratio results (see equation 7.3, and table 7.2).

7.3 RESULTS

7.3.1 Monte Carlo modelling of the custom EDGEe diode

The over-response of various designs of the EDGE detector, as a function of field size, is shown in figure 7.4. It can clearly be seen that each high density component of the EDGE detector contributes to the over-response, as the iterative removal of each component reduces the over-response. The near optimal air gap thickness for

the EDGEe detector, found through Monte Carlo simulation, was approximately 0.5 mm and was used as a baseline for experimental optimization.

7.3.2 Experimental optimisation of correction-free diode

Transfer of $k_{Q_{clin},Q_{msr}}$

The $k_{Q_{clin},Q_{msr}}^{PTWe_{clin},PTWe_{msr}}$ values calculated by transfer from the SFD are shown in table 7.2. Also shown for comparison are the Monte Carlo calculated values from Charles *et al*[6]. The transferred and Monte Carlo calculated values agree to within 0.9%, with most agreeing to within 0.5%. These differences compare favorably with the uncertainties in $k_{Q_{clin},Q_{msr}}^{PTWe_{clin},PTWe_{msr}}$ (also shown in table 7.2) proving that the experimental transfer of $k_{Q_{clin},Q_{msr}}$ to the PTWe diode is feasible.

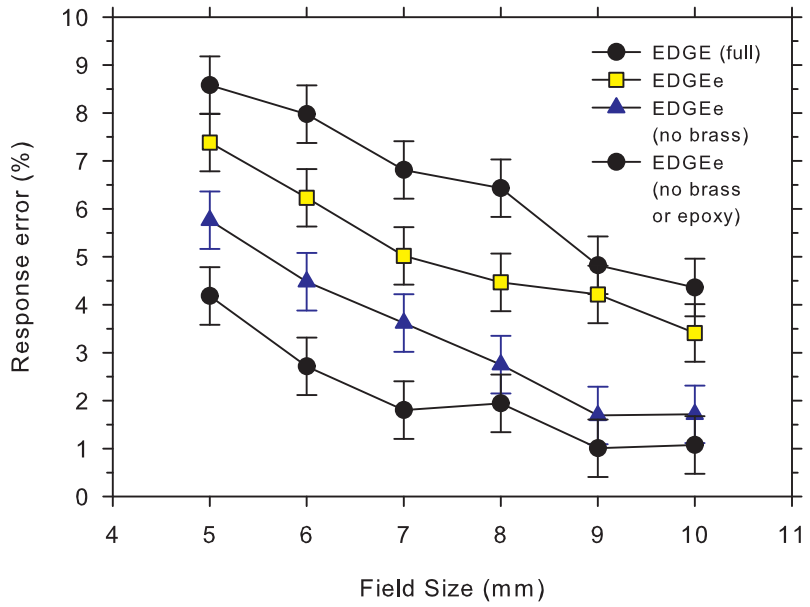

Figure 7.4. The response error (see equation 2) of modifications of the Sun-Nuclear Edge diode.

Table 7.2. Comparison of $k_{Q_{clin},Q_{msr}}^{PTWe_{clin},PTWe_{msr}}$ calculated using experimental and Monte Carlo methods. The uncertainty in the PTWe (Monte Carlo) results is equal to 0.5 % at all field sizes.

Field size (mm)	SFD	PTWe (measured)	PTWe (Monte Carlo)[6]	% Difference (measured/MC)	Methodological uncertainty
5.3	0.966	0.936	0.931	0.5	1.4
6.2	0.975	0.949	0.941	0.9	1.3
8.1	0.987	0.961	0.958	0.3	1.2
10	0.996	0.974	0.969	0.5	1.1
20	0.999	0.994	1.000	-0.6	1.2
30	1.000	1.000	1.000	0.0	1.0

$k_{Q_{clin},Q_{msr}}^{EDGEe_{clin},EDGEe_{msr}}$ values calculated by transfer from the SFD are shown in table 7.3. Also shown for comparison are the Monte Carlo calculated values. The transferred and Monte Carlo calculated values agree to within 0.7 %. These differences compare favorably with the uncertainty (see table 7.3) showing that the experimental transfer of $k_{Q_{clin},Q_{msr}}$ to the EDGEe diode is also feasible.

Table 7.3. Comparison of $k_{Q_{clin},Q_{msr}}^{EDGEe_{clin},EDGEe_{msr}}$ calculated using experimental and Monte Carlo methods. The uncertainty in the EDGEe (Monte Carlo) results is equal to 0.5 % at all field sizes.

Field size (mm)	SFD	EDGEe (measured)	EDGEe (Monte Carlo)	% Difference (measured/MC)	Methodological uncertainty
5.3	0.961	0.931	0.931	0.5%	1.4
6.2	0.973	0.942	0.941	0.6%	1.3
8.1	0.987	0.952	0.957	0.0%	1.2
10.0	0.996	0.967	0.967	0.5%	1.1

20	0.999	0.988	1.000	-0.7%	1.2
30	1.000	0.995	1.000	0.0%	1.0

Optimisation of PTWe air gap size

Figure 7.5 shows $k_{Q_{clin},Q_{msr}}^{PTWe_{clin},PTWe_{msr}}$ as a function of air gap thicknesses for all field sizes measured. An intersection point is observed at 1.0 mm. Therefore the optimal air thickness for the modified detector is 1.0 mm, which is similar to the Monte Carlo calculated value of 1.15 mm[6]. In figure 7.6, OR_{Det} is displayed as measured by the PTWe, the PTWe modified with 1 mm of air ($PTWe_{air}$) and the SFD (corrected using Monte Carlo calculated $k_{Q_{clin},Q_{msr}}^{SFD_{clin},SFD_{msr}}$ values). Whilst the known over-response of the unmodified PTWe diode is apparent, OR_{Det} measured using the $PTWe_{air}$ diode closely match the corrected SFD values.

Optimisation of EDGEe air gap size

Figure 7.7 shows the experimentally calculated $k_{Q_{clin},Q_{msr}}^{EDGEe_{clin},EDGEe_{msr}}$ values as a function of air gap thickness for all field sizes measured. Increasing the width of the air gap from 3.06 mm to 4.59 mm slightly enhances the dose reduction caused by the air gap. However a further increase to 6.13 mm appears to have little additional effect. Because of this, the optimal air gap thickness placed on top of the EDGEe detector can be obtained from either figure 7b or 7c and is equal to 0.6 mm, as this is the air thickness that results in the detector responding most similarly at each field size. Figure 7.8 shows the output ratios measured with EDGEe diode, the modified EDGEe diode (EDGEeair), the SFD (corrected), as well as detector-free MC calculated output factors from Cranmer-Sargison *et al*[13] for comparison. It can be seen

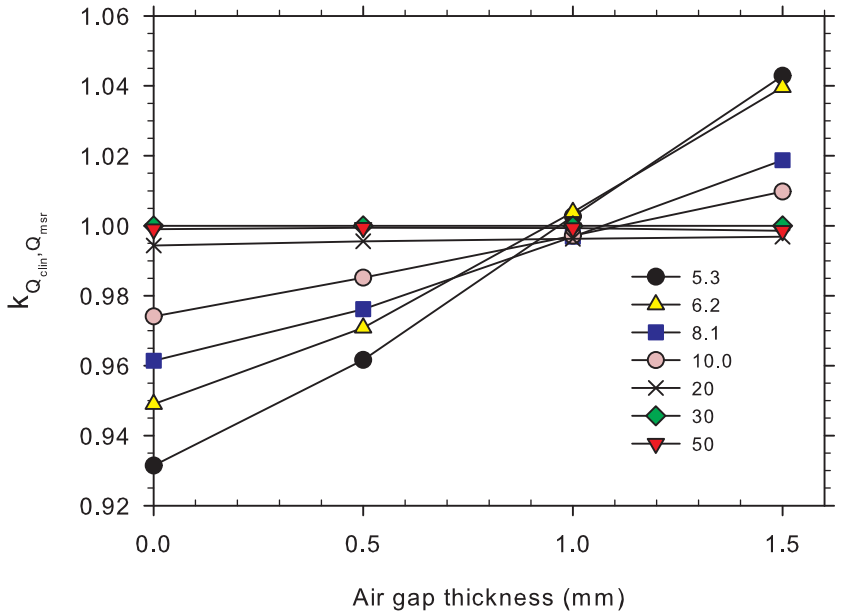

Figure 7.5. $k_{Q_{clin},Q_{msr}}^{PTWe_{clin},PTWe_{msr}}$ as a function of air gap thickness for various square field sizes (see legend, field sizes shown in mm).

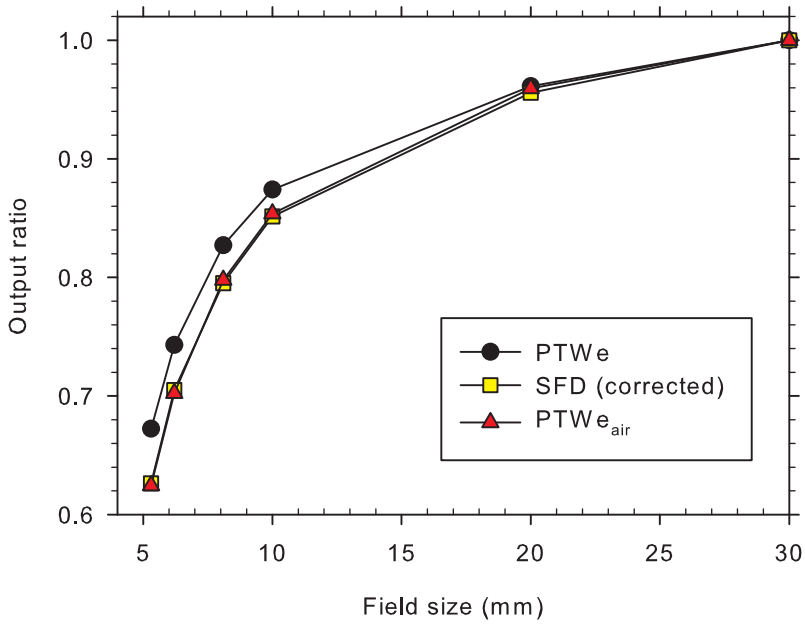

Figure 7.6. OR_{Det} measured using three diodes (see legend). The SFD results have been corrected with $k_{Q_{clin},Q_{msr}}^{SFD_{clin},SFD_{msr}}$, whereas PTWe and PTWe$_{air}$ results are not corrected. The experimental uncertainty (up to 0.7 %) is smaller than the marker size.

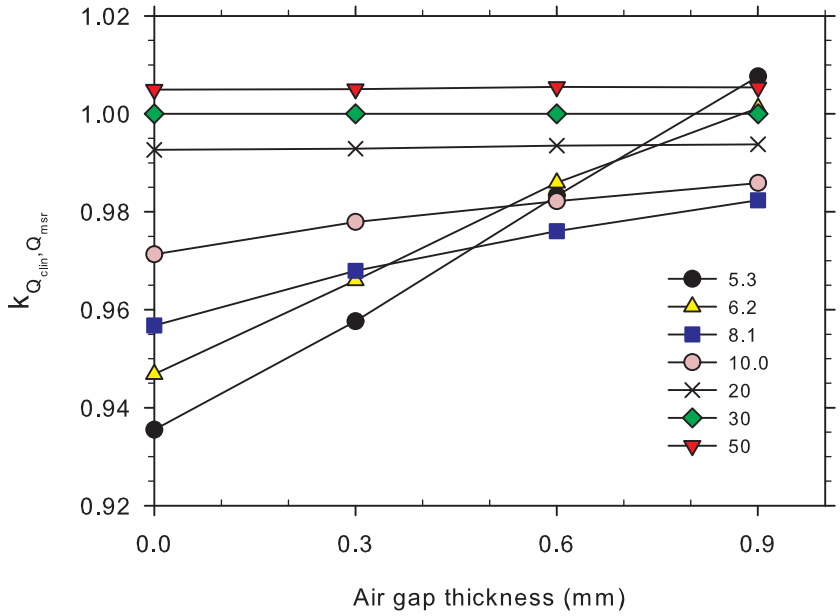
1.02
1.00
0.98
0.96
0.94
0.92
0.0
0.3
0.6
0.9
Air gap thickness (mm)
$k_{Q_{clin},Q_{msr}}$
5.3
6.2
8.1
10.0
20
30
50

(a)

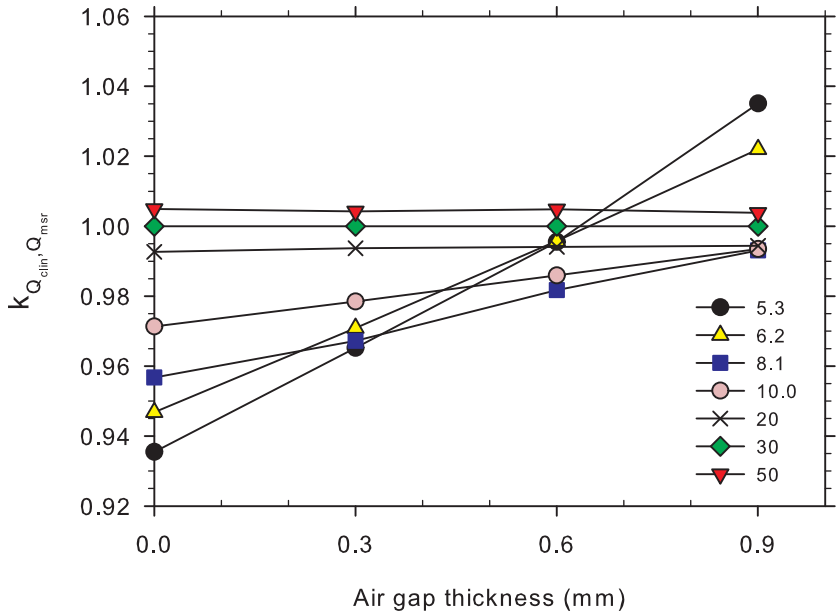
1.06
1.04
1.02
1.00
0.98
0.96
0.94
0.92
0.0
0.3
0.6
0.9
Air gap thickness (mm)
$k_{Q_{clin},Q_{msr}}$
5.3
6.2
8.1
10.0
20
30
50

(b)

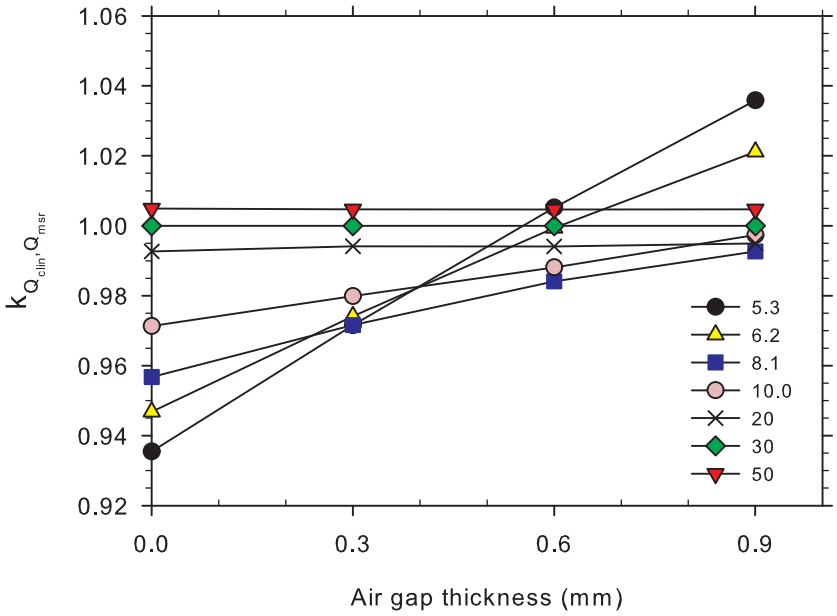

(c)

Figure 7.7. $k_{Q_{clin},Q_{msr}}^{EDGEe_{clin},EDGEe_{msr}}$ as a function of air gap thickness for various square field sizes (see legend, field sizes shown in mm). The results are shown for an air gap width of 3.06 mm (a), 4.59 mm (b) and 6.13 mm (c).

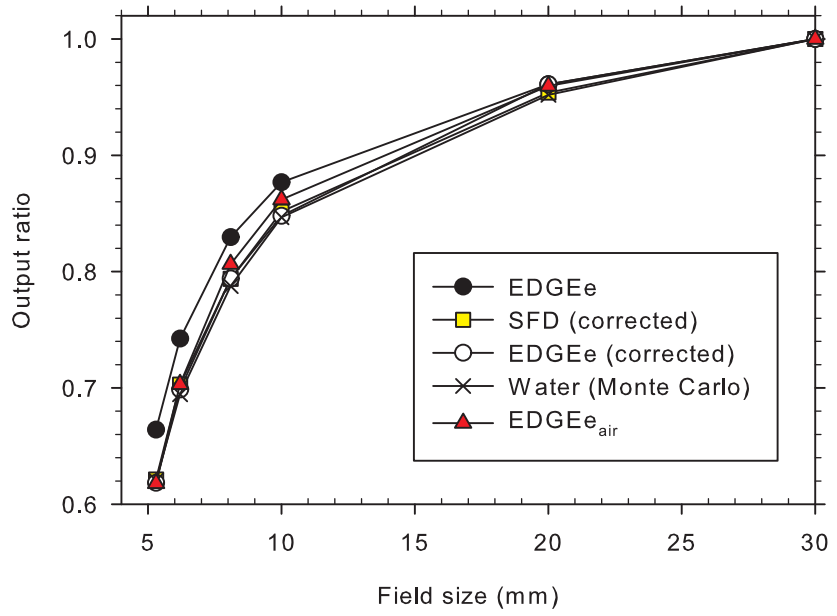

Figure 7.8. OR_{Det} measured using three diodes (see legend). The SFD results have been corrected with $k_{Q_{clin},Q_{msr}}^{SFD_{clin},SFD_{msr}}$. The EDGEe OPFs are shown both uncorrected and corrected. The $EDGEe_{air}$ results are not corrected. Also shown are the Monte Carlo calculated OPFs in a detector-free water geometry[13]. The uncertainty (up to 0.7 %) is smaller than the marker size.

that the $EDGEe_{air}$ is a vast improvement on the original EDGEe output ratio results; however $OR_{EDGEe_{air}}$ at field sizes of 8 mm and 10 mm are approximately 2 % higher than the desired water equivalence.

7.4 DISCUSSION

The PTW 60017 (PTWe) diode has successfully been modified, creating a diode which can be used for output factor measurements at small and very small field sizes - without the need to apply additional corrections. This was achieved by using a removable cap to position 1.0 mm of air onto the proximal end of the diode. The experimentally calculated optimal thickness of air was close to the Monte Carlo calculated value predicted by Charles *et al* of 1.15 mm[6]. The removable cap design is advantageous because it enables the detector to become dual purpose. In one instance the detector is performing as a correction-free small field dosimeter (with the cap on) and in another instance performing as a standard electron diode (with the cap off).

The results of this study show that it is possible to experimentally optimize the air gap thickness and width for design of a correction-free diode. It has been shown that increasing the air gap width from ~ 4 mm to ~ 6 mm had little effect on the sensitivity of the EDGEe detector. Conversely, the Monte Carlo based results from Charles *et al*[6], for the PTW 60016 shielded diode, showed that increasing the air gap width from 6.9 mm to 11.0 mm resulted in a significant decrease in detector response from a 12 mm field size. This is likely due to interplay between the width of the air gap and the thickness of the air gap. The air gap thicknesses investigated in this study using the EDGEe diode ranged from 0.3 to 0.9 mm; while the air gap thicknesses investigated by Charles *et al* using the PTW 60016 shielded diode ranged from 1.0 to 5.0 mm.

The PTW 60016 shielded diode was modelled in the study by Charles *et al*[6], but was not considered in the current work for the following reasons. The composition of 60016 diode is identical to the PTWe used in this study, except that it has an additional steel housing surrounding the silicon chip[4]. This only serves as an

additional perturbation material in small field output factor measurements, causing additional over-response. Furthermore, the active volume is 2.0 mm from the tip of the PTW 60016 diode, as compared to 0.6 mm from the tip in the PTWe diode. Charles *et al*[5] showed that there is an extremely rapid re-establishment of lateral electronic equilibrium following a very small air gap, thus the more material between the tip of the detector and the active volume the more air is required to cause a dose reduction at the active volume. Finally, the optimal air width simulated by Charles *et al* for the PTWe diode was 6.9 mm and for the PTW 60016 diode was 11.0 mm[6]. The width of the detector and stem of both diodes is 6.9 mm, thus the construction of the PTWe air cap was relatively simple, whereas the PTW 60016 air cap would be required to be 4 mm wider than the detector, making construction more difficult. All these effects combine to give more significant perturbations that would need to cancel each other out in order to make the PTW 60016 diode correction-free. In general, the amount of materials in the detector should be minimized to remove as many perturbations as possible when designing a correction-free diode. This has been shown experimentally in the current study, as the PTWe was successfully redesigned to be correction-free, whereas the more geometrically complicated EDGEe detector was not as successfully converted into a correction-free small field detector.

The nearly optimized EDGEe detector produced output factors that were equivalent to those in water for all but the 8 mm and 10 mm field sizes, where the results were ~ 2 % higher than the all water relative response (see figure 7.8). The lack of a discrete intersection point in figure 7.7 suggests that the geometry of the EDGEe detector is not ideal for optimization. Figure 7.4 reveals that the over-response of this detector could be reduced further by removing the brass. The dense epoxy (density = 1.5 g/cm^3) also causes an over response. Removing the brass and using a water equivalent epoxy would make the response of EDGEe very similar to the SFD, which has been shown to over-respond by only 1.5 % and 0.5 % for the 8 mm and 10 mm field sizes respectively[13].

This study, along with previous studies[4, 5, 7, 15], have shown that there is a very complex relationship between the response of a detector in very small fields and the density and geometry of the detector. This study and others[6, 7] have been focused on

making a detector 'correction-free', even though it has an active volume, and various other non-active materials, with densities different to water. This should not be confused with true water equivalency, because in essence the detectors in these studies are being redesigned such that competing perturbations cancel out, which produces measurement results equivalent to the relative response in water. As discussed in the introduction, the over-response of a diode in small fields is due to the creation of additional electrons in high density components in or near the detector active volume. As studied in detail by Charles *et al*[5], very small air gaps cause a reduction in dose beyond the air gap by filtering electrons with a high angle of incidence. Charles et al also showed that the re-establishment of electronic equilibrium beyond an air gap is very rapid, hence the effect of the air gap will depend strongly on its location with respect to the active volume. A non-water-equivalent detector can only be correction-free if all these perturbations happen to cancel out at all field sizes. Thus it is reasonable to recommend that the number of perturbations should be minimized by limiting the amount of non-water equivalent materials in a diode. Also, because of the highly complex interplay between the perturbations it is difficult to avoid the empirical approach to finding the overall sensitivity of the diode, as used in this study.

It is also important to note here that the very small air gaps introduced into the design of these diodes have no effect on field sizes larger than 3 cm[5]. Thus all limitations that exist in the unshielded diodes at field sizes larger than those used in this study (such as the over response of diodes at larger field sizes) remain. It also must be noted that the interplay between the competing perturbations may cause a shift of the effective point of measurement in the modified detectors. Monte Carlo simulations by Charles *et al*[6] showed that the relative response of the modified detectors did not change as a function of depth (beyond the depth of dose maximum). However, the precise location of an effective point of measurement has yet to be investigated, and is beyond the scope of the current study.

This study has also proved that it is feasible to transfer $k_{Q_{clin},Q_{msr}}$ experimentally from one diode to another. Experimental methods have previously been used to directly calculate $k_{Q_{clin},Q_{msr}}$, [17-20] but in this study the experimental transfer of a previously

calculated $k_{Q_{clin},Q_{msr}}$ value has been performed. The SFD is good choice for this purpose as it has $k_{Q_{clin},Q_{msr}}$ values closer to unity than other diodes, owing to the fact that it contains little high density material other than the silicon chip itself. This methodology also enables the use of a diode with well published $k_{Q_{clin},Q_{msr}}$ values in experimental design of new detectors.

7.5 CONCLUSIONS

Two correction-free diodes have been designed using an experimental methodology. The PTWe$_{air}$ diode was created by placing 1.0 mm of air on to the proximal end of a PTW 60017 electron diode using a removable cap. The PTWe$_{air}$ diode measured output factors are equivalent to those in water for field sizes as small as 5 mm. The EDGEe diode had a geometry less amenable to optimization, due to remaining high density components. However the designed EDGEe$_{air}$ was only 2 % from being correction-free at all field sizes. All air caps and tops created in this project were fabricated in house, and not in conjunction with a commercial partner. In principle the design should be able to be replicated within any clinical department.

Creating a correction-free detector by using competing perturbations should never be confused with true water equivalency of a detector. A non-water-equivalent detector will only give results equivalent to those in water if all competing perturbations cancel out at each field size. It is recommended that Monte Carlo simulations and careful experimental methods be combined when designing detectors for small field dosimetry.

7.6 ACKNOWLEDGEMENTS

This work was funded by the Australian Research Council in partnership with the Queensland University of Technology (QUT), the Wesley Research Institute and Premion (Linkage Grant No. LP110100401). Computational resources and services

used in this work were provided by the High Performance Computing and Research Support Unit, (QUT), Brisbane, Australia.

7.7 REFERENCES

[1] A.J. Scott, S. Kumar, A.E. Nahum, J.D. Fenwick, "Characterizing the influence of detector density on dosimeter response in non-equilibrium small photon fields," Phys Med Biol **57**, 4461-4476 (2012).

[2] J.D. Fenwick, S. Kumar, A.J. Scott, A.E. Nahum, "Using cavity theory to describe the dependence on detector density of dosimeter response in non-equilibrium small fields," Phys Med Biol **58**, 2901-2923 (2013).

[3] T.S. Underwood, H.C. Winter, M.A. Hill, J.D. Fenwick, "Detector density and small field dosimetry: Integral versus point dose measurement schemes," Medical Physics **40**, 082102 (2013).

[4] G. Cranmer-Sargison, S. Weston, J.A. Evans, N.P. Sidhu, D.I. Thwaites, "Monte Carlo modelling of diode detectors for small field MV photon dosimetry: detector model simplification and the sensitivity of correction factors to source parameterization," Phys Med Biol **57**, 5141-5153 (2012).

[5] P.H. Charles, S.B. Crowe, T. Kairn, J. Kenny, J. Lehmann, J. Lye, L. Dunn, B. Hill, R.T. Knight, C.M. Langton, J.V. Trapp, "The effect of very small air gaps on small field dosimetry," Phys Med Biol **57**, 6947-6960 (2012).

[6] P.H. Charles, S.B. Crowe, T. Kairn, R.T. Knight, B. Hill, J. Kenny, C.M. Langton, J.V. Trapp, "Monte Carlo-based diode design for correction-less small field dosimetry," Phys Med Biol **58**, 4501-4512 (2013).

[7] T.S. Underwood, H.C. Winter, M.A. Hill, J.D. Fenwick, "Mass-density compensation can improve the performance of a range of different detectors under non-equilibrium conditions," Phys Med Biol **58**, 8295-8310 (2013).

[8] P. Francescon, W. Kilby, N. Satariano, S. Cora, "Monte Carlo simulated correction factors for machine specific reference field dose calibration and output factor measurement using fixed and iris collimators on the CyberKnife system," Phys Med Biol **57**, 3741-3758 (2012).

[9] R. Alfonso, P. Andreo, R. Capote, M.S. Huq, W. Kilby, P. Kjäll, T.R. Mackie, H. Palmans, K. Rosser, J. Seuntjens, W. Ullrich, S. Vatnitsky, "A

new formalism for reference dosimetry of small and nonstandard fields," Medical Physics **35**, 5179 (2008).

[10] D.W.O. Rogers, B.A. Faddegon, G.X. Ding, C.M. Ma, J. We, "BEAM: A Monte Carlo code to simulate radiotherapy treatment units," Medical Physics **22**, 503 - 524 (1995).

[11] T. Kairn, T. Aland, R.D. Franich, P.N. Johnston, M.B. Kakakhel, J. Kenny, R.T. Knight, C.M. Langton, D. Schlect, M.L. Taylor, J.V. Trapp, "Adapting a generic BEAMnrc model of the BrainLAB m3 micro-multileaf collimator to simulate a local collimation device," Phys Med Biol **55**, N451-463 (2010).

[12] T. Kairn, J. Kenny, S.B. Crowe, A.L. Fielding, R.D. Franich, P.N. Johnston, R.T. Knight, C.M. Langton, D. Schlect, J.V. Trapp, "Technical Note: Modeling a complex micro-multileaf collimator using the standard BEAMnrc distribution," Medical Physics **37**, 1761 (2010).

[13] G. Cranmer-Sargison, S. Weston, J.A. Evans, N.P. Sidhu, D.I. Thwaites, "Implementing a newly proposed Monte Carlo based small field dosimetry formalism for a comprehensive set of diode detectors," Medical Physics **38**, 6592-6602 (2011).

[14] I. Kawrakow, E. Mainegra-Hing, F. Tessier, B.R.B. Walters, "The EGSnrc C++ class library, ," NRC Report PIRS-898 (rev A)2009).

[15] G. Cranmer-Sargison, P.H. Charles, J.V. Trapp, D.I. Thwaites, "A methodological approach to reporting corrected small field relative outputs," Radiother Oncol **109**, 350-355 (2013).

[16] P.H. Charles, G. Cranmer-Sargison, D.I. Thwaites, S.B. Crowe, T. Kairn, R.T. Knight, J. Kenny, C.M. Langton, J.V. Trapp, "A practical and theoretical definition of very small field size for radiotherapy output factor measurements," Med Phys **41**, 041707 (2014).

[17] E. Pantelis, A. Moutsatsos, K. Zourari, L. Petrokokkinos, L. Sakelliou, W. Kilby, C. Antypas, P. Papagiannis, P. Karaiskos, E. Georgiou, I. Seimenis, "On the output factor measurements of the CyberKnife iris collimator small fields: Experimental determination of the k(Q(clin),Q(msr)) (f(clin),f(msr)) correction factors for microchamber and diode detectors," Medical Physics **39**, 4875-4885 (2012).

[18] C. Bassinet, C. Huet, S. Derreumaux, G. Brunet, M. Chea, M. Baumann, T. Lacornerie, S. Gaudaire-Josset, F. Trompier, P. Roch, G. Boisserie, I.

Clairand, "Small fields output factors measurements and correction factors determination for several detectors for a CyberKnife and linear accelerators equipped with microMLC and circular cones," Medical Physics **40**, 071725 (2013).

[19] A. Ralston, P. Liu, K. Warrener, D. McKenzie, N. Suchowerska, "Small field diode correction factors derived using an air core fibre optic scintillation dosimeter and EBT2 film," Phys Med Biol **57**, 2587-2602 (2012).

[20] G. Cranmer-Sargison, P.Z. Liu, S. Weston, N. Suchowerska, D.I. Thwaites, "Small field dosimetric characterization of a new 160-leaf MLC," Phys Med Biol **58**, 7343-7354 (2013).

Chapter 8: Conclusions

The aim of this research was to investigate small fields, evaluate the physics behind them in a detailed manner, and improve on the accuracy of small field dosimetry. The concept of reporting the measured dosimetric field size for each small field output factor measurement (as opposed to reporting the nominal field size) was investigated to see if inter-machine consistency could be improved. Using the dosimetric field to report small field output factor measurements significantly reduced the inter-machine variation of measured output factors (by up to 12 % for a 5 mm field size).

This work introduced the formal definition of a *very small field* and established two scientific definitions of the threshold of very small field size. The physics behind very small field dosimetry was investigated in detail, leading to a quantifiable theoretical definition of a very small field. It was found that measuring the effective field size was required for field sizes 15 mm or smaller to ensure output factors were consistent to within ±1 %. This formed the practical definition of a very small field. A detailed simulation analysis showed that electronic disequilibrium was the main reason for the large change in output factor as a function of field size. Electronic disequilibrium caused a significant change in dose below a field size of 12 mm. This was the theoretical definition of a very small field. This work gave a clear indication that careful experimental methodology, with profiles measured at the same time as output factors for each field size setting is required for field sizes $\leq$ 12 mm and more conservatively for field sizes $\leq$ 15mm.

The perturbations caused by of non-water equivalent materials in very small fields were studied in detail, with a particular focus on air. It was confirmed that very small amounts of air (up to 2 mm) did not perturb the radiation beam at normal field sizes, but did so at very small field sizes; with the size of the perturbation increasing with decreasing field size. Care should be taken to eliminate all air gaps where possible. This applies to waterproofing any detector for use in water phantoms using a sleeve as well as to inserting detectors into solid phantoms.

The subsequent detailed understanding of these air perturbations led to the simulation based design of a new diode detector which, uniquely, responded the same in very small fields as in standard fields. The introduction of air into the design of a diode successfully produced a detector that responded equivalently to water for output factors in very small fields. This was due to the under-response of the air cancelling out the over-response of the silicon in the diode at all field sizes.

These detectors were then physically constructed and found to be accurate; and general recommendations for detector design for very small field dosimetry were established. This “correction-free” diode was the first diode detector in the world that could measure very small field output factors without the need for field size dependent correction factors.

Overall, this work has introduced some significant concepts that may change the direction of future research and cause changes to clinical practice. When reporting field sizes below 15 mm, it is recommended to report the measured effective field size and not simply the nominal field size. It is important that a consistent method for

measuring effective field size (such as that outlined in chapter 2) is utilised. By introducing the concept of a very small field, and its theoretical threshold (12 mm), one can begin to see in a quantitative manner the threshold of when electronic disequilibrium plays a major role in dosimetry. On a Varian iX linear accelerator, source occlusion was found to not have a major effect on dosimetry until field sizes of 8 mm or smaller, and that electronic disequilibrium was a larger factor in the rapid change in dose. The large perturbations caused by electronic disequilibrium in very small fields were very apparent when air gaps existed, even on a sub-millimetre scale. The extent of this is such that it is recommended that dosimetry in solid phantoms is avoided and even detectors submerged in liquid water should be checked for the presence of air bubbles before commencing measurements. However it was shown that these perturbations can be controlled and used in detector design such that they cancel out. This was shown by designing a detector that measured output factors in water that did not require corrections. These detectors could be used in the clinic to perform output factor measurements without the need for field size specific correction factors, which at the moment is not common practice, and thus would be attractive to the clinical user.

Future extensions of the research is this thesis could involve investigating the input of effective field size into stereotactic treatment planning systems, as opposed to the nominal field size. Or alternatively creating a high-level QA procedure so that the effective field size was similar enough to the nominal field size at very small fields. Much of this work could also be repeated on Elekta linear accelerators to see if minor variations to the energy spectrum, as well as a different spot size affected any results.

The effects of electronic disequilibrium on other materials, such as tissues found in the body, or other non-water equivalent detectors could also be explored.